

Dynamics of Quenched Ultracold Quantum Gases

by

John P. Corson

B.S., Brigham Young University, 2009

M.S., Brigham Young University, 2011

A thesis submitted to the
Faculty of the Graduate School of the
University of Colorado in partial fulfillment
of the requirements for the degree of
Doctor of Philosophy
Department of Physics

2016

This thesis entitled:
Dynamics of Quenched Ultracold Quantum Gases
written by John P. Corson
has been approved for the Department of Physics

Prof. John Bohn

Asst. Prof. Jose D’Incao

Date _____

The final copy of this thesis has been examined by the signatories, and we find that both the content and the form meet acceptable presentation standards of scholarly work in the above mentioned discipline.

Corson, John P. (Ph.D., Physics)

Dynamics of Quenched Ultracold Quantum Gases

Thesis directed by Prof. John Bohn

Recent advances in the tunability of ultracold atomic gases have created opportunities for studying interesting quantum many-body systems. Fano-Feshbach resonances, in particular, allow experimenters to freely adjust the scattering of atoms by controlling an external magnetic field. By rapidly changing this field near a resonance, it is possible to drive systems out of equilibrium towards novel quantum states where correlations between atoms change dynamically. In this thesis, we take a wave-function-based approach to theoretically examine the response of several interesting systems to suddenly-switched, or “quenched”, interactions.

We first calculate the time evolution of a Bose-Einstein condensate that is quenched to the unitarity regime, where the scattering length a diverges. Working within the time-dependent variational formalism, we find that the condensate does not deplete as quickly as the usual Bogoliubov theory would suggest. We also make a quantitative prediction for the dynamics of short-range pair correlations, encoded in Tan’s contact. We then consider the dynamics of these correlations for quenches to small a , and we find that bound states can cause high contrast oscillations of the contact. These dynamics can be modelled quantitatively at short times by using a properly-chosen two-body model. Finally, we characterize the nonlocal correlation waves that are generated by an interaction quench in arbitrary dimensionality. Our analysis demonstrates that the large-momentum limit of the post-quench momentum distribution can sometimes include contributions from both the short range and the long range, depending on the quench protocol.

Dedication

To my one true amor.

Acknowledgements

I would first like to thank my advisor, John Bohn. I applied to CU-Boulder with a “clear” plan of exactly what research I wanted to do, and twenty minutes at a whiteboard with John changed everything. His intuition-based storytelling is almost as fun to witness as it is informative, and it quickly kindled my interest in cold quantum gases. Over the years since then, I have felt inspired by John’s creativity as a problem solver, his enthusiasm as a leader, and his patience as a mentor. I should specifically mention his rare gift for pointing out miscalculations without triggering embarrassment.

It has been a pleasure to associate with other folks from the Bohn group. In no particular order, I would like to thank Ryan, Michelle, Brandon, Andrew, James, Goulven, Michael, Lucie, and Arnaud. We’ve had good times. I would also like to thank Jose for taking time to chat about three-body physics, and for his competition at ping pong. I also acknowledge the multitude of brilliant experimentalists at JILA who have taught me lessons about real-world physics. Specifically, the KRb mixture group, the ^{85}Rb group, and the degenerate Fermi gas group.

Thanks are due also to Justin Peatross and Michael Ware, my research advisors at BYU, for helping me discover the joy and satisfaction of research. They have been valuable mentors and friends over the years.

Most of all, I would like to thank my wife Amy for her love, support, and patience. She is the wind in my sails.

Contents

Chapter	
1	Introduction 1
1.1	Outline 5
2	Short-Range Two-Body Interactions 7
2.1	Alkali-Atom Interactions 8
2.1.1	Low-Energy Behavior 10
2.1.2	Fano-Feshbach Resonances 11
2.2	Single-Channel Models 14
2.2.1	Finite-Range Models 15
2.2.2	Zero-Range Models 18
2.3	Tan's Contact 23
2.4	Summary 25
3	Weakly Interacting Bose-Einstein Condensates 27
3.1	The Phenomenon 27
3.1.1	The Importance of Indistinguishability 29
3.1.2	Experimental Observation in Dilute Alkali Gases 31
3.2	Many-body Formalism 34
3.2.1	Second Quantization 35
3.3	Weakly Interacting BECs 38

3.3.1	The Bogoliubov Approximation	38
3.3.2	Solving the Problem	41
3.3.3	The Ground State	42
4	BEC Quenched to Unitarity	46
4.1	Motivation	46
4.2	Many-Body Model	48
4.3	Post-Quench Dynamics	51
4.4	Summary and Discussion	59
5	Bound-State Signatures in Quenched BECs	61
5.1	Preliminaries	61
5.2	Many-body Phenomenon	63
5.3	Two-Body Models	67
5.3.1	Calibration	67
5.3.2	Revisiting the Quench to Unitarity	70
5.3.3	Quenching to Finite Scattering Length	73
5.4	Summary	78
6	Quench-Induced Correlation Waves	80
6.1	Background	80
6.2	Ballistic waves	82
6.3	Arbitrary Quenches	86
6.4	Lattice Transport	91
6.5	Summary	98
7	Conclusion	101

Bibliography	104
---------------------	------------

Appendix

A Two-Body Solution after a Quench	115
A.1 Solving the Problem in 1D	115
A.2 Generalizing to 3D	121
A.3 Generalizing to 2D	121

Figures

Figure

2.1	Schematic adiabatic curve	9
2.2	Schematic Feshbach Resonance	12
2.3	Square-well potentials	15
2.4	Square-well scattering states	17
2.5	Interactions as boundary conditions	19
3.1	Ballistic expansion of a BEC	33
3.2	Born Series	38
4.1	Resonant interaction potentials	52
4.2	Dynamical momentum distribution at unitarity	53
4.3	Dynamical momentum distribution at different density	55
4.4	Dynamics of a single mode	56
4.5	Depletion dynamics after the quench	57
4.6	Contact dynamics after the quench	58
5.1	Bound-state oscillations of the contact in quenched many-body model	65
5.2	Bound-state oscillations of depletion in quenched many-body model	66
5.3	Momentum distribution of two-body models	71
5.4	Contact oscillations: two-body vs many-body	74
5.5	Contact oscillations after a downward quench	76

6.1	Ballistic expansion of a bound-state wave function	83
6.2	Wigner distribution for expanded bound state	84
6.3	Wigner distribution for a weak quench	87
6.4	Quenching a bound state to repulsive interactions	88
6.5	Quenching a bound state on a lattice site	94
6.6	Lattice transport dynamics after a quench	97
A.1	Integration contour for two-body solution	118

Chapter 1

Introduction

In recent years, ultracold atomic gases have become a fertile ground for developing and testing ideas of quantum many-body physics. Typical experiments use magnetic or optical forces to trap a dilute vapor of atoms in high vacuum. To a good approximation, samples are thermally isolated from the environment and thus represent idealized quantum systems. Atoms can be further manipulated by external magnetic, electric, or optical fields to realize new and exciting states of matter that are governed by the laws quantum mechanics.

One of the most significant breakthroughs in this realm was the experimental creation of Bose-Einstein condensates (BECs) of Alkali atoms. This novel state of matter was first theorized by Einstein a century ago [56, 57] based on contemporary work by Bose [16], who had considered the statistics of photons. The statistics that describe photons apply more generally to any indistinguishable particles that do not satisfy the Pauli exclusion principle, termed “bosons”. Einstein’s insight was that, below a certain temperature, such particles preferentially occupy the exact same single-particle quantum state. This many-body ensemble, a BEC, was not observed in the controlled environment of cold atomic gases until 1995, when researchers at JILA [1] and MIT [44] successfully cooled atoms to below the transition temperature ($\sim 100\text{nK}$). This achievement came on the heels of a couple decades of progress in the realm of atomic trapping and laser cooling [134, 29, 34].

The exquisite control necessary to realize Bose-Einstein condensation in the laboratory paved the way for a wealth of other studies of quantum phenomena. Experimenters began to explore how

interactions between atoms change the character of a system. These interactions give rise to the complexity that makes a single many-body problem intrinsically different from many one-body problems. In the absence of interactions, the many-body Schrödinger equation is completely separable, and the eigenstates of the system can be described completely in terms of single-particle quantum states. This simplification is what makes the thermodynamics and phase transition of a noninteracting BEC a common textbook problem of statistical mechanics [131]. Nontrivial interactions, on the other hand, introduce particle-particle correlations that alter the many-body state in fundamental ways.

The theory of interacting BECs has been in development for several decades. Most of the early work focused on the ground state in the weakly interacting limit, where mean-field theory gives an adequate description of the many-body system [10, 7, 8, 106, 84, 74, 75, 136]. Mean-field theory makes the assumption that most of the atoms remain at rest in the ground state, despite interactions. For short-range interactions, this assumption is predicated upon the smallness of the diluteness parameter na^3 , where n is the number density and a is the s -wave scattering length for the interacting particles. The scattering length is defined in terms of the phase shift of an interacting two-body wave function, and it relates to the low-energy limit of the elastic cross section for the colliding pair via $\sigma \sim a^2$. In mean-field models, its magnitude is a measure of the interaction strength and its sign indicates repulsive ($a > 0$) or attractive ($a < 0$) character. The condition that $na^3 \ll 1$ is easily satisfied in most experimental setups, and as a result, the predictions of mean-field theory have typically agreed very well with BEC experiments [162, 130, 81, 115, 174].

The discovery and characterization of Fano-Feshbach resonances in ultracold gases [158, 86, 165, 42] has given experimenters the ability to explore exotic, strongly interacting regimes that cannot be described by the usual mean-field models. These resonances occur at specific values of the magnetic field and, in some cases, they can be several Gauss wide. Close to resonance, the scattering length a is large in magnitude, and it diverges on resonance (the “unitarity” regime). Interactions can be tuned by simply fixing an external magnetic field to a desired value close to a resonance [28]. Experimenters can therefore study the effects of interactions in a given system

by repeating experiments at various interaction strengths. This advantage is rather unique to the field of ultracold atoms. For example, the parameters of the Standard Model of particle physics (masses, couplings, etc) are fixed by Nature, and we must live with the consequences. Not so, in ultracold atoms.

Performing experiments at large scattering length does come at a cost, however. Just as a large scattering length increases the probability for a two-body collision event, it also increases the probability for three-body inelastic processes. When three atoms come together, two of them can bond chemically, and the released binding energy is transformed into the kinetic energy of the new molecule and third atom in a way that conserves momentum and energy. This extra kinetic energy is almost always greater in magnitude than the depth of the magnetic or optical trap that is confining the atoms. As a result, all three atoms are lost from the trap. Even in dilute gases, where $na^3 \ll 1$, the total number of trapped atoms always decreases if you wait long enough. It has been shown that the loss rate scales as a^4 multiplied by a species-specific constant [63, 127, 59, 167]. This unfortunate scaling of loss has hindered experimental investigations of strongly-interacting BECs in equilibrium. The splendor of large scattering lengths is, unfortunately, short lived.

The possibility of tuning interactions via Fano-Feshbach resonance has led to a resurgence of theoretical efforts to understand strongly interacting BECs, despite their short lifetimes in practice. Several studies [43, 146, 45] used constrained variational methods to calculate the ground state energy and chemical potential at strong interactions. Among the results found was that, in the $a \rightarrow \infty$ limit, these quantities scale universally with units derived from the number density n , as found for two-component Fermi gases in the analogous regime [102]. Efimovian three-body contributions [54, 55] to the dilute-gas limit were considered in Ref. [17], and Refs. [14, 177] considered the metastability of the system in the strongly interacting limit. The equilibrium states discussed in these studies are interesting in their own right, but it is unclear whether it's possible to transition to them adiabatically given the catastrophic a^4 scaling of the three-body loss rate.

The outlook on the strongly-interacting-BEC problem changed when it was discovered that, when a system is rapidly brought out of equilibrium, interesting dynamics may occur before sub-

stantial three-body loss sets in. The idea is to take a weakly interacting BEC ($na^3 \ll 1$) and rapidly change the scattering length to the unitarity regime ($a \rightarrow \infty$) by ramping the magnetic field quickly to a Fano-Feshbach resonance. This general protocol of rapidly changing a parameter of the Hamiltonian to induce nonequilibrium dynamics is often called a “quench”. The experiment reported in Ref. [112] performed a quench to unitarity and observed that, at typical densities, three-body loss occurs over the course of about 1 ms. Interestingly, their measurements of the dynamic momentum distribution indicated that their system seemed to reach some kind of steady state in about 100 μ s, with momentum-dependent saturation dynamics occurring along the way. This landmark experiment raises interesting questions about how weakly correlated states develop stronger correlations when the interaction strength is increased, and about the nature of the nonequilibrium steady state. Are there simple ways to understand the dynamics that occurs?

The nonequilibrium realm of ultracold quantum gases has become a hot topic in recent years due to the exotic nature of the excited states that can be generated. For a BEC that is quenched to unitarity, as discussed in the previous paragraph, the state is remarkably long lived. When quenching a one-dimensional BEC from strong repulsion to strong attraction, the resultant state is correlated in such a way that the attractive forces do not cause clustering [3]. This exotic state, known as the super-Tonks-Girardeau gas, was recently observed in experiment [76]. Another experiment [85] studied weak interaction quenches in two-dimensional BECs, and the authors found that the system shows oscillatory density-density correlations, called Sakharov oscillations [140], that are similar in nature to what has been famously observed in the distribution of matter in the known universe [58]. Also of interest are the results reported in Ref. [48]. They observed that a BEC undergoing a Ramsey sequence of interaction quenches can display coherence between atomic and molecular states. We also mention the “bosonovae” experiment [49], which observed the violent collapse dynamics of a three-dimensional BEC whose interactions are suddenly quenched from weak repulsion to weak attraction. These experiments, and others, serve as an inspiration for the work presented in this thesis.

1.1 Outline

This thesis represents my graduate work done on the topic of interaction quenches in ultracold atomic systems, and it does not include my studies of dipolar BECs [41, 40] and the Bose polaron [83]. Most of the presented results deal with three-dimensional Bose-Einstein condensates, although some aspects are more generally applicable. Chapter 2 describes the interactions that typically take place in ultracold atoms. Due to the low energies involved at ultralow temperatures, the scattering is predominantly *s*-wave in character and is well described by the scattering length a . Although atom-atom interactions are generally very complicated on the microscopic scale, one can often approximate these interactions with simpler short-range models that yield the correct low-energy scattering behavior. This idea leads to a universality in which the important consequences of interactions are model-independent. We introduce Tan's contact [152, 154, 153], which relates short-range pair correlations to the energetics of generic few- and many-body systems.

Chapter 3 gives a review of background concepts for BECs in the noninteracting and weakly-interacting regimes. We discuss the thermodynamics of the condensed state, demonstrating how the indistinguishability of identical bosons leads to macroscopic occupation of the single-particle ground state even at nonzero temperature. We then introduce Bogoliubov theory, which describes the low-energy collective excitations of a weakly-interacting BEC in terms of quasiparticles.

Chapter 4 presents our theoretical work on the topic of a BEC that is quenched to unitarity. Our approach uses a time-dependent variational wave function to approximate the dynamical many-body state of the system. The ansatz explicitly encodes two-body correlations, which we expect to be dominant in the early stages of evolution. The short-time dynamics that we compute is independent of the way in which we model short-range, resonant interactions. As main results, we find that the BEC does not deplete as rapidly as Bogoliubov theory would suggest, and the dynamics of the momentum distribution scale universally with units derived from the number density n . This observation is consistent with the experimental results reported in Ref. [112]. We are also able to compute the time evolution of Tan's contact after the quench. Much of this work

was published in Ref. [150]

In Chapter 5, we describe the dynamics of short-range pair correlations for BECs quenched to finite scattering length. An important result is that bound-state effects may strongly influence the dynamics when the quench is diabatic. The condensate fraction and Tan's contact oscillate at a frequency E_B/\hbar , where E_B is the binding energy of the bound state. We also find that short-range pair correlations are strongly enhanced by the bound state. Intriguingly, a diabatic decrease in the scattering length yields a net increase in short-range pair correlations. We are able to explain these results with an intuitive two-body model that yields quantitatively accurate results at short times. This work was published in Ref. [38].

In Chapter 6, we present results on the nonlocal correlation waves that are generated by an interaction quench. We investigate these waves at the level of a two-body wavefunction, where the simplicity of the system allows for an analytic representation of the correlation waves in momentum space. We find that correlations propagate ballistically and, to leading order, the amplitude of the wave relates directly to the quench parameters and the initial short-range pair correlations. Although intuition about equilibrium usually associates large-momentum asymptotics exclusively with short-range behavior, our solution to the quench problem demonstrates that the large-momentum tail of a nonequilibrium momentum distribution may also have a nonlocal, ballistic contribution. We find that a semiclassical model based on the ballistic wave function gives accurate predictions for transport over barriers, such as in an optical lattice. These results have recently been accepted for publication and can be found on the arXiv [39].

Chapter 7 provides a summary of our work and describes promising avenues for future research.

Chapter 2

Short-Range Two-Body Interactions

Given the complexity of a single many-electron atom, it may seem odd that people consider doing theoretical calculations for systems that contain thousands or millions of interacting atoms. There are too many degrees of freedom to keep track of, and modern computational resources are hopelessly out of their league. Nevertheless, a considerable simplification comes about when we work in the ultracold regime.

An analogy can be drawn to our theoretical understanding of the proton. Particle-accelerator experiments reveal that protons are composite particles made up of quarks dressed by a field of gluons. Understanding all of the nuts and bolts on a truly microscopic scale is a complicated problem, but these details are not significant at sufficiently low energy scales. It is usually a good approximation to consider the proton to be a structureless point particle that is characterized by a mass, a spin, and an electric charge. To a casual spectroscopist, the energy levels of the hydrogen atom can't seem to tell the difference.¹

A similar approximation can be made in the theoretical description of ultracold atomic gases. At sufficiently low energies, we can treat individual atoms as point particles that are defined by their mass, some quantum numbers that summarize their internal structure (such as a hyperfine or Zeeman state), and a single parameter that defines how atoms interact with each other. This interaction parameter, the scattering length a , has a complicated dependence on the internal states of the atoms and the magnetic field. The precise determination of a , as well as the location of

¹ High-precision spectroscopy reveals that the internal structure of the proton leads to slight, but measurable, changes in the hydrogenic energy levels. For an example, see Ref. [60].

Fano-Feshbach resonances, requires sophisticated calculations that are fine-tuned with experimental data. Over the years, experimental physicists have become adept at controlling the internal state of trapped Alkali atoms using coherent manipulation techniques, such as adiabatic rapid passage and RF pulses. Typical experiments usually trap an ultracold sample whose atoms occupy well-defined spin states and where an external magnetic field fixes the scattering length to a known value. The model many-body Hamiltonian is usually easy to write down and includes a just as a parameter, as will be shown in Ch. 3. The challenge, then, is to solve the many-body problem.

We now turn our attention to describing simple models for the interactions between neutral Alkali atoms, with a special focus on effects in three spatial dimensions. In what follows, we briefly review the schematics of more realistic atom-atom interactions, emphasizing the important role played by the scattering length. We then outline several useful short-range-interaction models that are used as inputs into our many-body calculations. This chapter then concludes with a discussion of Tan's contact, which has emerged as a useful concept in understanding how interactions define the short-range correlations and energetics of few- and many-body systems.

2.1 Alkali-Atom Interactions

The low-energy scattering of Alkali atoms is an intricate process that depends in detail on how the electrons in each atom respond to the presence of the other atom. The natural language for describing these interactions is given by the Born-Oppenheimer approximation, where the atomic cores are assumed to move slowly in the field produced by the valence electrons. This is justified by the orders-of-magnitude separation between the mass scales of the atomic core and the valence electrons. The general idea is to treat the separation between the atomic cores, \mathbf{r} , as a slowly changing parameter and then solve for the electronic energies as a function of \mathbf{r} . These energies define a set of adiabatic potential curves that, if the atoms are asymptotically in their electronic ground state, are approximately spherically symmetric. Figure 2.1 depicts one of these curves schematically.

The qualitative behavior of atom-atom interactions is intuitive. We would expect that when

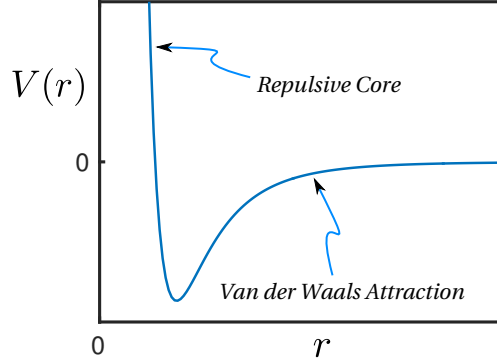


Figure 2.1: Schematic representation of an adiabatic potential curve, with van der Waals attraction in the long range and repulsion in the short range.

r is roughly the size of an atom or smaller, the electronic clouds from the two atoms should have significant overlap. This leads to repulsion at small interatomic separations on a length scale set by the Bohr radius, a_0 . On large length scales, the instantaneous polarization of one atom can create an electric field that induces opposite polarization in the other atom. This results in an attractive van der Waals force that decays as r^{-6} for large particle separations. It is typical to define a van der Waals length r_{vdW} that quantifies the approximate “range” of the interaction. This range is typically less than 5 nm for Alkali atoms [28].

At intermediate distances, the adiabatic potential smoothly interpolates between the repulsive and attractive asymptotic regimes. The depth of the well depends strongly on whether the two valence electrons have a symmetric (triplet) or antisymmetric (singlet) spin configuration, which determines if covalent bonding is likely to occur. When the atoms are more than a few nanometers apart, their individual hyperfine or Zeeman energies dominate the physics and define the scattering channels of the problem. Colliding atoms that are initially in well-defined hyperfine/Zee-man states project nontrivially onto the electron spin basis that governs interactions at smaller r . This leads to coupling between the different scattering channels of the problem. An interesting result of this coupling is that Fano-Feshbach resonances can occur in ultracold Alkali-atom systems. We discuss the phenomenology of these resonances in Sec. 2.1.2.

2.1.1 Low-Energy Behavior

Scattering events take on a particularly simple description in the low-energy limit. One can make a partial-wave expansion of the scattering amplitude and exploit the fact that high angular momentum requires high kinetic energy and/or a large impact parameter. For short-ranged interactions and low energies, we therefore expect that higher partial waves should not contribute appreciably to the scattering. This expectation is verified in the Wigner threshold laws, which state the following: For an interaction potential that decays as $r^{-\nu}$ in the long range, the contribution of the ℓ^{th} partial wave to the total cross section σ vanishes at least as quickly as $\sigma_\ell \sim E^{\min\{\nu-3, 2\ell\}}$ in the $E \rightarrow 0$ limit, where E is the kinetic energy [155]. For van der Waals interactions, where $\nu = 6$, only s -wave ($\ell = 0$) scattering occurs at ultralow temperatures.

The results of s -wave scattering are easy to write down in the low-energy limit. In the absence of interactions, isotropic waves in 3D take the form

$$\psi(r) \propto \frac{\sin(kr)}{r} \quad (2.1)$$

where $k = \sqrt{2\mu E/\hbar}$ is the wave number and μ is the reduced mass for the noninteracting atoms. When scattering occurs in the presence of interactions, this wave experiences an energy-dependent phase shift $\delta_0(k)$ for $r \gg r_{\text{vdW}}$:

$$\psi(r) \sim \frac{\sin(kr + \delta_0(k))}{r}. \quad (2.2)$$

It can be shown that the low-energy behavior of $\delta_0(k)$ satisfies the effective range expansion [155]

$$k \cot(\delta_0(k)) = -\frac{1}{a} + \frac{1}{2}r_{\text{eff}}k^2 + \mathcal{O}(k^4), \quad (2.3)$$

where a is the s -wave scattering length and r_{eff} is the so-called “effective range” of the interaction. It is often (but not always!) the case that the effective range r_{eff} is similar in magnitude to the short range r_{vdW} . Such cases are universal in the sense that, for low energies satisfying $kr_{\text{eff}} \ll 1$, the s -wave phase shift is determined only by the energy and the scattering length a . Despite the complicated physics occurring in the short range, scattered wave functions are remarkably easy to

characterize in the low-energy limit once the scattering length is known. As an added bonus, the total cross section has a simple energy dependence in this regime:²

$$\sigma \approx \frac{4\pi a^2}{1 + k^2 a^2}. \quad (2.4)$$

The magnitude of the scattering length therefore describes the apparent size of interacting atoms from a low-energy collisional standpoint.

For attractive short-range interactions, the scattering length can be either positive or negative depending on the behavior of the scattering phase shift. It is easy to show from Eq. (2.3) that $\delta_0(k) \approx -ka$ for $k|a| \ll 1$. Positive scattering length thus corresponds to waves being phase shifted to larger particle separations, as occurs for purely repulsive potentials. Despite the seeming repulsion for scattering states, however, attractive short-range interactions always admit a shallow bound state when $a > 0$, and the binding energy behaves as

$$E_B = -\frac{\hbar^2}{2\mu a^2} \quad (2.5)$$

in the limit of large a , where μ is the reduced mass of the interacting atoms. This counterintuitive fact will be demonstrated for a simple case in Sec. 2.2.1. We will see in Chapter 3 that, within typical mean-field theories, small positive (negative) scattering length corresponds to repulsive (attractive) interactions because the interaction energy is proportional to a .

2.1.2 Fano-Feshbach Resonances

The multichannel nature of atomic collisions leads to the useful phenomenon of Fano-Feshbach resonances. These resonances are typically manifested in the fact that, for atoms in a given scattering channel j , the scattering length exhibits a resonance profile

$$a_j(B) = a_{\text{bg},j} \left(1 - \frac{\Delta_j}{B - B_{0,j}} \right) \quad (2.6)$$

as a function of the magnetic field B . The parameter $B_{0,j}$ describes the location of a given resonance (of which there might be many), Δ_j defines the width of the resonance, and $a_{\text{bg},j}$ is the background

² For identical bosons, symmetrization requires that we multiply this formula by a factor of 2

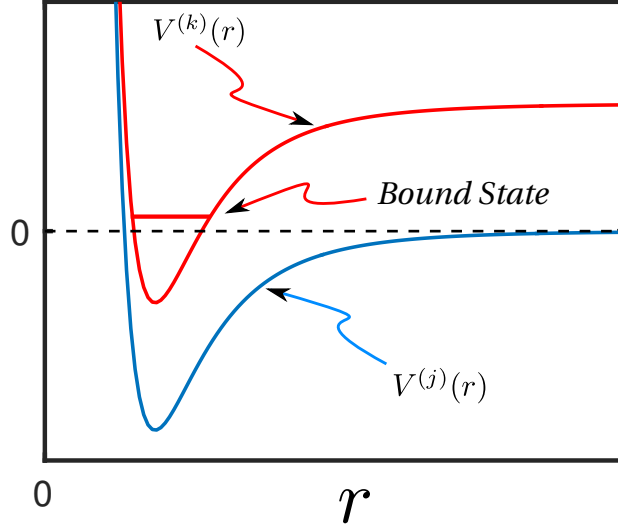


Figure 2.2: Schematic representation of a Fano-Feshbach resonance. The cyan curve is the adiabatic potential for the scattering channel j , the red curve is the potential for some higher-energy channel k , and the horizontal dashed line represents the low energy of the scattering atoms.

scattering length at magnetic fields far away from any resonance. We have made explicit the dependence of the resonance parameters on the scattering channel j .

The basic phenomenology of a Fano-Feshbach resonance can be understood from a two-channel model. We will consider the coupled channels to represent different Zeeman states whose magnetic moments are different by an amount $\delta\mu$, and we assume that the atoms scatter in channel j , which we define to have the lower energy in the $r \rightarrow \infty$ limit. The adiabatic curves are shown schematically in Fig. 2.2. The channel k is termed “closed” because energy conservation prevents atoms from exiting in this channel. Channel j is analogously termed “open”. A Fano-Feshbach resonance occurs when atoms colliding in the open channel have approximately the same energy as a bound state in the closed channel, as shown. Due to the magnetic-moment differential $\delta\mu$ between the two channels, their energy difference, and hence the detuning of the bound state relative to the scattering energy, is sensitive to the magnetic field B in accordance with the Zeeman effect. The resonance position $B_{0,j}$ is the magnetic field at which the bound-state detuning approximately vanishes, and its precise location depends on the coupling between the channels. The width of the resonance, Δ_j , relates to the strength of the channel coupling, where strong coupling usually results

in a broad resonance. The background scattering length, $a_{\text{bg},j}$, is determined by the scattering that occurs in the potential $V^{(j)}(r)$, ignoring channel coupling [28].

The idea of exploiting magnetic Fano-Feshbach resonances to tune interactions in ultracold gases was first suggested in 1993 [158], and it was demonstrated experimentally in 1998 [86]. The experimental protocol was to measure the loss of an ultracold sample of trapped ^{23}Na atoms as a function of magnetic field. It is predicted that the loss rate should scale as a^4 multiplied by a constant [63, 127]. Hence, loss should be strongly enhanced in the vicinity of a Fano-Feshbach resonance. By scanning the magnetic field along a range of about 1000 G, experimenters were able to identify two loss resonances whose locations agreed with theoretical predictions. They were then able to infer the scattering length near these resonances by measuring the interaction energy of a Bose-Einstein condensate, which is predicted to scale linearly with the scattering length (see Sec. 3.3.3). Near the loss resonances, the magnetic-field profile of the scattering length matched the predicted profile of Eq. (2.6).

Although most experiments utilize magnetic Fano-Feshbach resonances to tune interactions, we also mention the possibility of using optical Feshbach resonances. The underlying physics is nearly identical to that already described, where scattering states from one channel are coupled to the bound state of another channel. The distinguishing feature in optical Feshbach resonances is that the coupling is provided by an external laser field that couples scattering states to an excited quasibound state via an optical transition. Rather than tune the magnetic field B , one can tune both the intensity I and frequency ω of the off-resonant laser beam to alter the scattering length of collisions [62, 11, 12]. Soon after its prediction, this effect was confirmed in experiments [61, 156]. This scheme suffers the disadvantage of having extra loss when the excited state decays spontaneously, and the laser field may also induce unwanted dipole forces to the system under observation. However, recent progress has been made to mitigate these drawbacks [30]. Optical Feshbach resonances offer the possibility of spatially modulating interactions. Additionally, they allow experimenters to dynamically tune interactions on shorter timescales than are feasible with magnetic Fano-Feshbach resonances. This improves the prospects for measuring the nonequilibrium

results that we present in Chapters 4-6.

2.2 Single-Channel Models

The discussion in Sec. 2.1.1 shows that the phase shifts and cross sections of ultracold Alkali collisions can be reduced to a simple form that depends only on the scattering length, a , and the effective range, r_{eff} . The description continues to simplify if we narrow our consideration to the regime where $|a| \gg |r_{\text{eff}}|$. In this limit, the low-energy condition $kr_{\text{eff}} \ll 1$ is sufficient to keep only the scattering length term on the right-hand side of the effective-range expansion, Eq. (2.3). This approximation, in which all scattering is determined by a only, is a valid description of ultracold gases near entrance-channel-dominated resonances. The scattering and bound wave functions associated with these resonances are composed mainly of the open-channel component, with relatively little contribution from the closed-channel bound state despite the coupling [96]. These resonances are often wider than 1 G and are commonly referred to as “broad” resonances [28]. In the remainder of this thesis, we will only consider interactions that are governed by this class of Feshbach resonance. The scattering length a therefore uniquely determines all scattered wave functions according to Eqs. (2.2)-(2.3), where we ignore the effective range and higher-order terms.

In our quest to describe the physics of interacting many-body systems, we can exploit the diluteness of typical experimental Alkali-atom samples in the ultracold regime. The nearest-neighbor spacing is usually a few orders of magnitude larger than the interaction range r_{vdW} , and this suggests that only a tiny fraction of the wave function exists within the interaction region. We therefore expect that all of the interesting physics in such interacting systems is determined by the part of the wave function that is phase shifted. The scattering length governs this phase shift and, as a result, should uniquely dictate how interactions affect a dilute many-body system in the ultracold limit. To simplify the many-body problem, we represent the microscopically-complicated atom-atom interactions with simplified models that reproduce the desired scattering length. The only errors introduced by this approximation occur at small particle separations ($r \lesssim r_{\text{vdW}}$) and at

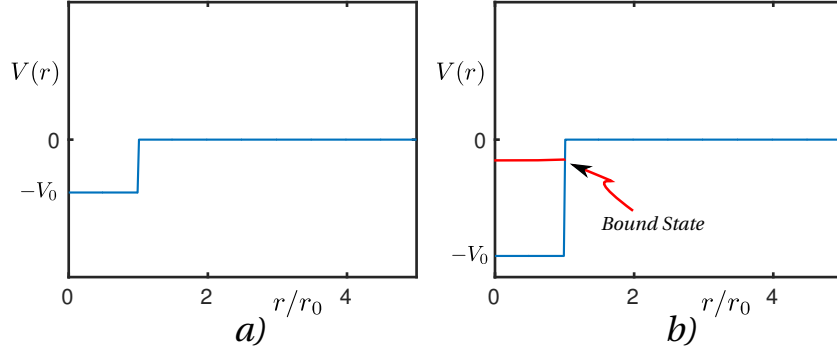


Figure 2.3: Attractive square-well potentials. In (a), the well is shallow. In (b), the well is deep and admits a bound state, as shown.

large momentum ($kr_{\text{eff}} \sim 1$), both of which compose only a negligible fraction of the wave function for ultracold, dilute, Alkali gases.

This section describes several useful short-range interaction models. The first class of models uses a finite-range attractive well whose depth and range are chosen to reproduce the correct scattering length. The second class invokes the zero-range approximation, where interactions are replaced with a scattering-length-dependent boundary condition on the wave function at vanishing particle separation.

2.2.1 Finite-Range Models

The simplest interaction potentials for which the Schrödinger equation can be solved analytically are those that are piecewise constant. The solutions are either real or complex exponentials, depending on how the energy compares to the local potential height. The piecewise wave functions can then be joined by assuming continuity and smoothness. As our first example, we solve for the scattering and bound solutions in an attractive square-well potential

$$V(r) = -V_0\Theta(r_0 - r), \quad (2.7)$$

where $V_0 > 0$ is the depth of the well, r_0 is its range, and Θ is the Heaviside step function. This potential is depicted in Fig. 2.3.

We confine our analysis to solutions that are spherically symmetric, representing the s partial wave that dominates at ultralow temperatures. In three dimensions, it is easiest to solve for the quantity $u(r) \equiv r\psi(r)$, where ψ is the relative wave function. The radial Schrödinger equation is then given by

$$Eu = -\frac{\hbar^2}{2\mu} \frac{d^2u}{dr^2} + Vu \quad (2.8)$$

where μ is the reduced mass for the atoms and E is the energy. Hermiticity requires that $u(r)|_{r \rightarrow 0} = 0$ [118]. We will first consider scattering solutions where $E = \hbar^2 k^2 / 2\mu$ is the relative kinetic energy. For $r > r_0$, the potential vanishes and the solution is given by

$$u_k(r) = A \sin(kr + \delta), \quad (2.9)$$

where A is a normalization constant and δ is the yet-to-be-determined phase shift. For $r < r_0$, the solution is

$$u_k(r) = B \sin(k'r) \quad (2.10)$$

where B is a normalization constant, and the wavenumber is shifted to $k' = \sqrt{2\mu(E + V_0)}/\hbar$ due to the excess kinetic energy inside the well. We can solve for the phase shift δ by matching the log derivative u'/u at r_0 . After a small amount of algebra, one finds that

$$\delta = \tan^{-1} \left(\frac{k}{k'} \tan(k'r_0) \right) - kr_0. \quad (2.11)$$

The low-energy limit of this phase shift should be $\delta \rightarrow -ka$ according to the effective range expansion, and this fixes the scattering length to be

$$a = r_0 - \frac{\hbar}{\sqrt{2\mu V_0}} \tan \left(\sqrt{2\mu V_0} r_0 / \hbar \right). \quad (2.12)$$

Two sample scattering solutions are shown in Fig. 2.4 for a well whose range and depth are chosen to yield a scattering length of $a = 10r_0$. In the long range, they show the usual oscillatory behavior with a phase shift. This extra phase is acquired in the short range, as shown in the left-hand plot. As a consistency check of Eqs. (2.11)-(2.12), we see that both the phase shift and the scattering length vanish in the $V_0 \rightarrow 0$ limit. The scattering length in Eq. (2.12) diverges whenever $\sqrt{2\mu V_0} r_0 / \hbar =$

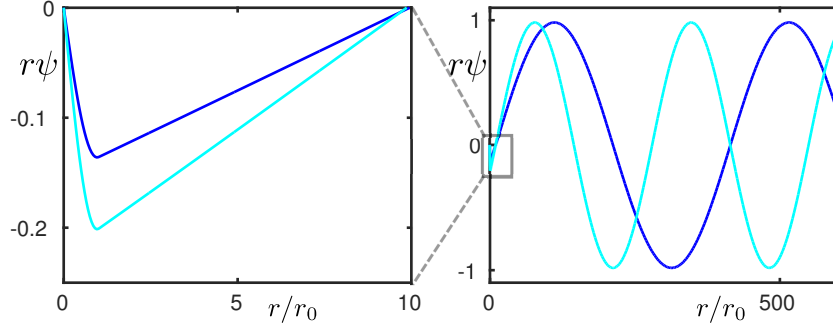


Figure 2.4: Two scattering states at different energies for a square well whose range and depth are chosen to yield a scattering length of $a = 10r_0$. We constrain the depth such that $\sqrt{2\mu V_0}r_0/\hbar < 3\pi/2$, where at most one bound state is allowed. Deeper wells lead to more short-range nodes of the wave function. The left-hand plot shows a short-range zoom of the wave functions. The plotted functions are normalized to behave as $\sin(kr + \delta)$ for $r > r_0$

$(n + 1/2)\pi$, where n is a non-negative integer. As we will see below, this resonant behavior occurs whenever the well deepens sufficiently to include another bound state.

The bound-state solutions can be calculated in much the same way as already shown, except that we assume the energy satisfies $-V_0 < E < 0$. The solution outside of the well must decay exponentially as

$$u_E(r) = Ae^{-\sqrt{-2\mu E}r/\hbar}. \quad (2.13)$$

The solution inside the well is unchanged. Matching log derivatives at r_0 , we find that the energy must satisfy

$$\sqrt{-E} = -\sqrt{E + V_0} \cot\left(\sqrt{2\mu(E + V_0)}r_0/\hbar\right). \quad (2.14)$$

No solution exists for $\sqrt{2\mu V_0}r_0/\hbar < \pi/2$, as the well is not deep enough to support a bound state in this regime. It is easy to verify that this equation has a zero-energy solution when $\sqrt{2\mu V_0}r_0/\hbar = (n + 1/2)\pi$ for non-negative integer n . There is a shallow bound state when $\sqrt{2\mu V_0}/\hbar$ is slightly greater than $(n + 1/2)\pi$, and this regime corresponds also to large positive scattering length as evidenced by Eq. (2.12). For a weakly-bound state satisfying $|E| \ll V_0$, one can approximate

Eq. (2.16) as

$$\begin{aligned}\sqrt{-E} &\approx -\sqrt{V_0} \cot\left(\sqrt{2\mu V_0} r_0/\hbar\right) \\ &\approx \frac{\hbar}{\sqrt{2\mu a}},\end{aligned}\tag{2.15}$$

where we have used the large- a limit of Eq. (2.12). For large positive scattering length ($a \gg r_0$), the shallow bound state is given by

$$\psi_B(r) \approx \frac{e^{-r/a}}{r\sqrt{2\pi a}}, \quad E_B \approx -\frac{\hbar^2}{2\mu a^2}\tag{2.16}$$

for $r \gg r_0$. This asymptotic relation between the scattering length and the shallow bound state is valid more generally [28], as mentioned in connection with Eq. (2.5).

One can simulate short-range interactions with other single-channel potentials besides the square well. The square well offers the simplicity of being transparent and analytically solvable, and the scattering length relation Eq. (2.12) allows one to conveniently choose the two model parameters V_0 and r_0 to achieve any desired scattering length. One can also add a repulsive barrier to the square well [88]. Analytic solutions are also available for a pure van der Waals interaction with a hard core [71, 66], whose free parameters are the C_6 coefficient and the core radius. The low-energy scattering in a Morse potential can also be solved analytically [123, 94, 93]. Another simple interaction model is the attractive Gaussian well, although the relation between the scattering length and its depth and range must be found numerically [157]. The common thread of these models is that they are essentially short ranged and can be tuned to give the correct low-energy scattering.

2.2.2 Zero-Range Models

From a theoretical standpoint, we are free to choose the interaction range of our model to be as small in magnitude as we wish. The parameter r_0 in the square well, for example, could take an arbitrarily small value. One would simply have to adjust the depth V_0 to yield the desired scattering length a according to Eq. (2.12). As we allow r_0 to approach zero for fixed scattering length, the scattering wave function (2.9) and bound wave function (2.16), valid for particle separations

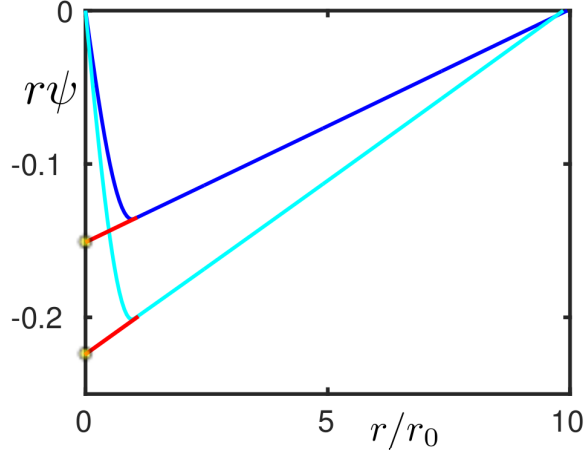


Figure 2.5: Short-range part of the scattered wave functions for a square-well potential chosen to yield $a = 10r_0$, with the phase shifts extrapolated back to vanishing particle separation. Compare with the left-hand plot in Fig. 2.4.

satisfying $r > r_0$, eventually become valid for all $r > 0$. This is shown schematically in Fig. 2.5, which should be compared with the left-hand plot in Fig. 2.4. It is in this limiting sense that we introduce the idea of a zero-range interaction.

The zero-range approximation stipulates that the relative wave function for a pair of interacting atoms satisfies the noninteracting Schrödinger equation, albeit with a rigged boundary condition at vanishing particle separation. For three-dimensional systems, this boundary condition is given by

$$\left. \frac{\partial [r\psi] / \partial r}{r\psi} \right|_{r \rightarrow 0^+} = -\frac{1}{a}, \quad (2.17)$$

as discussed in a famous paper by Bethe and Peierls [9]. (The basic idea was also presented in earlier work by Fermi [64].) The quantity on the left-hand side is often called the “logarithmic derivative”, as it can be expressed as $\partial [\ln(r\psi)] / \partial r$. The Bethe-Peierls boundary condition enforces a scattering-length-dependent relation between the value of the wave function and its slope in the $r \rightarrow 0^+$ limit. For small particle separations, the wave function must behave linearly as

$$r\psi(r) = [r\psi]_{r \rightarrow 0^+} \left[1 - \frac{r}{a} + \mathcal{O}(r^2) \right]. \quad (2.18)$$

The scattering length evidently has the following meaning in the zero-range approximation: If you

fit a line to the short-range behavior of $r\psi$, it intercepts the horizontal axis at $r = a$. This same geometric interpretation is valid for interactions with a finite range in the limit that $|a| \gg r_0$, although it is only robust in the low-energy regime ($kr_0 \ll 1$) and the line must be fit outside the interaction region. This behavior is readily visible in the square-well eigenstates depicted in Fig. 2.5, and one can easily verify its validity for the bound-state solution (2.16).

It is easy to find the eigenstates of the Schrödinger equation within the zero-range approximation. For $r > 0$, the scattering solution must be a superposition of $\sin(kr)$ and $\cos(kr)$, and the only superposition that satisfies the log-derivative boundary condition (2.17) is

$$r\psi_k(r) = A [\sin(kr) - ka \cos(kr)] \quad , \quad E_k = \frac{\hbar^2 k^2}{2\mu} \quad (2.19)$$

where A is a normalization constant. After a simple trigonometric manipulation, one can show that this is proportional to $\sin(kr + \delta)$, where the phase shift must satisfy

$$k \cot(\delta) = -\frac{1}{a} \quad (2.20)$$

for all k . On comparing this with the effective range expansion (2.3), we see that the zero-range approximation sets $r_{\text{eff}} \rightarrow 0$ and defines all phase shifts in terms of the scattering length only. A bound-state solution only exists for $a > 0$, and it is given by

$$r\psi_B(r) = \frac{e^{-r/a}}{r\sqrt{2\pi a}} \quad , \quad E_B = -\frac{\hbar^2}{2\mu a^2}. \quad (2.21)$$

These solutions are useful in that they are simple to write down, and they give a remarkably accurate description of ultracold scattering in the limit that $|a| \gg r_{\text{vdW}}$ near a broad Feshbach resonance.

Zero-range interactions are often cast in the language of the Fermi pseudopotential [65, 84]. Within this framework, the relative wavefunction for a pair of interacting particles in three dimensions must satisfy

$$E\psi = -\frac{\hbar^2}{2\mu} \nabla^2 \psi + \frac{2\pi\hbar^2 a}{\mu} \delta^{(3)}(\mathbf{r}) \frac{\partial(r\psi)}{\partial r}, \quad (2.22)$$

where the last term represents the operation of the Fermi pseudopotential on the wave function. Integrating Eq. (2.22) over a small sphere of radius $\epsilon > 0$ about the origin, we find that the left-hand

side vanishes in the $\epsilon \rightarrow 0$ limit. What remains is

$$0 = -\frac{\hbar^2}{2\mu} \int_{r<\epsilon} d^3r \nabla^2 \psi + \frac{2\pi\hbar^2 a}{\mu} \left. \frac{\partial(r\psi)}{\partial r} \right|_{r \rightarrow 0} \quad (2.23)$$

If we assume that $\psi(r) = (r\psi)|_{r \rightarrow 0} (\frac{1}{r} + \mathcal{O}(r^0))$ for small r , we can exploit the relation $\nabla^2 \frac{1}{r} = -4\pi\delta^{(3)}(\mathbf{r})$ to evaluate the integral. The result is that

$$0 = \frac{2\pi\hbar^2}{\mu} (r\psi)|_{r \rightarrow 0} + \frac{2\pi\hbar^2 a}{\mu} \left. \frac{\partial(r\psi)}{\partial r} \right|_{r \rightarrow 0}, \quad (2.24)$$

which is identical to the Bethe-Peierls boundary condition (2.17). The two formulations are therefore equivalent.

Representing short-range interactions with a delta function is obviously a nontrivial task, as evidenced by the unusual partial differentiation that appears in the Fermi pseudopotential (2.22). It raises the question of whether one can use a delta function without the derivative. Can we represent interactions with a potential that is constant in momentum space, as would befit the Fourier transform of a delta function? It turns out that this is possible in a limiting sense, but it requires a careful renormalization procedure in which the strength of the delta function must depend on its width (which is nonzero for a nascent delta function). We begin by defining the Fourier transform of a function

$$\tilde{f}(\mathbf{k}) = \int d^3r e^{-i\mathbf{k}\cdot\mathbf{r}} f(\mathbf{r}) \quad (2.25)$$

and its inverse transform

$$f(\mathbf{r}) = \int \frac{d^3k}{(2\pi)^3} e^{i\mathbf{k}\cdot\mathbf{r}} \tilde{f}(\mathbf{k}). \quad (2.26)$$

Rather than use a strict delta function for the interaction, whose Fourier transform equals 1 for all \mathbf{k} , we consider the analogous quantity up to a momentum-space cutoff Λ :

$$\delta_\Lambda^{(3)}(\mathbf{r}) \equiv \int \frac{d^3k}{(2\pi)^3} e^{i\mathbf{k}\cdot\mathbf{r}} \Theta(\Lambda - k) \quad (2.27)$$

where Θ is the Heaviside function. The quantity Λ^{-1} can be understood as the range of the interaction. We will define the interaction potential to be

$$V_{\text{int}}(\mathbf{r}) = U_\Lambda \delta_\Lambda^{(3)}(\mathbf{r}), \quad (2.28)$$

where U_Λ is a scattering-length-dependent coupling constant required to give the correct short-range physics.

The functional form of U_Λ can be demonstrated simply by solving the bound-state problem in momentum space. The momentum-space Schrödinger equation can be written as [117]

$$\begin{aligned} E_B \tilde{\psi}_B(\mathbf{k}) &= \frac{\hbar^2 k^2}{2\mu} \tilde{\psi}_B(\mathbf{k}) + U_\Lambda \int d^3 r e^{-i\mathbf{k}\cdot\mathbf{r}} \delta_\Lambda^{(3)}(\mathbf{r}) \psi_B(\mathbf{r}) \\ &= \frac{\hbar^2 k^2}{2\mu} \tilde{\psi}_B(\mathbf{k}) + U_\Lambda \int \frac{d^3 k'}{(2\pi)^3} \tilde{\psi}_B(\mathbf{k}' - \mathbf{k}) \Theta(\Lambda - k') \\ &\approx \frac{\hbar^2 k^2}{2\mu} \tilde{\psi}_B(\mathbf{k}) + U_\Lambda \int_{k' < \Lambda} \frac{d^3 k'}{(2\pi)^3} \tilde{\psi}_B(\mathbf{k}') \end{aligned} \quad (2.29)$$

where we have invoked the convolution theorem and assumed that Λ is much larger than both k and a^{-1} . In momentum space, the bound-state solution shown in Eq. (2.21) becomes

$$\tilde{\psi}_B(\mathbf{k}) = \frac{2\sqrt{2\pi a^3}}{1 + k^2 a^2} \quad , \quad E_B = -\frac{\hbar^2}{2\mu a^2} \quad (2.30)$$

If we substitute this solution into Eq. (2.29), all of the \mathbf{k} dependence vanishes, and we can solve directly for U_Λ . When the smoke clears, we find that

$$U_\Lambda = \frac{2\pi\hbar^2 a/\mu}{1 - \frac{2}{\pi}\Lambda a} \quad (2.31)$$

in the $\Lambda a \gg 1$ limit. This is the coupling constant required to give the correct short-range physics. It is valid more generally for any value of a and even for $\Lambda a \ll 1$ (where no bound state occurs), as can be proved with Green function techniques [19].

It is interesting that, for fixed scattering length, U_Λ decays as Λ^{-1} in the $\Lambda \rightarrow \infty$ limit. This behavior may seem surprising at first, but it is analogous to what occurs in the $r_0 \rightarrow 0$ limit of the square well calculation at fixed scattering length. In that case, the “volume” of the well ($\sim V_0 r_0^3$, analogous to U_Λ) decays as $\mathcal{O}(r_0)$ as the range is reduced.³ Given our interpretation of Λ^{-1} as the range of $\delta_\Lambda^{(3)}(\mathbf{r})$, we see that the scalings are identical in the zero-range limit. In fact, the two model potentials are not particularly different, except that one is a Heaviside function in position space

³ This is immediately obvious from Eq. (2.12) in the case of infinite scattering length, where we can fix $\sqrt{2\mu V_0} r_0 / \hbar = \pi/2$. It can be shown that this scaling is also valid for arbitrary nonzero scattering length in the $r_0 \rightarrow 0$ limit.

and the other is a Heaviside function in momentum space. Both models are broad in momentum space up to an effective cutoff $\Lambda \sim r_0^{-1}$.

2.3 Tan's Contact

There is considerable power in the idea that, once you know the scattering length for a pair of particles with short-range interactions, you can make universally valid statements about the scattering and bound wave functions to within a good approximation. We have discussed this paradigm in the two previous sections. The necessary assumption is that relative momenta be low enough to satisfy $kr_{\text{eff}} \ll 1$, which can be fulfilled in most cold-atom experiments near a broad Feshbach resonance. It turns out that, in this regime describable by the zero-range approximation, one can make even stronger statements about system observables based purely on the short-range nature of the interactions. These statements, called the Tan relations, were introduced by Shina Tan about a decade ago [152, 154, 153]. They hold true for all equilibrium states in the ultracold regime, both few-body and many-body, both in the ground state and at finite temperature, whether we know how to solve the problem or not.

Central to the Tan relations is the idea that global interaction effects should scale with the probability that atoms are close enough to interact. As an obvious example, the interaction energy for a pair of atoms is zero if their relative wave function vanishes inside the interaction region, and it should be large in magnitude if the wave function has a significant component in the short range. Within the framework of the zero-range approximation, the relative wave function behaves as $\psi(r) \approx (r\psi)|_{r \rightarrow 0} \frac{1}{r}$ in the short range, as written in Eq. (2.18). The operative quantity $(r\psi)|_{r \rightarrow 0}$ is not determined by the log-derivative boundary condition (2.17), but rather by the specific state of the system. Its magnitude-squared encodes the probability that the atoms are close enough to interact or, in other words, are in “contact” with each other. This contact probability should determine the interaction energy and the extent to which the pair will notice a change in the interactions. By properties of the Fourier transform, it should also determine the large- k behavior of the momentum distribution via $n_k \sim |\tilde{\psi}(k)|^2 \sim |(r\psi)|_{r \rightarrow 0} \frac{4\pi}{k^2}|^2$. Such a probability is well defined

for an arbitrary system of two or more interacting particles, and Tan’s crucial development was to establish quantitatively the universal ways in which it relates to the observables of any equilibrium system for which the zero-range approximation is valid.

The key parameter that appears in the Tan relations is the “contact” C , and it is proportional to the short-range pair probability of the system. The short-range r^{-2} behavior of the interacting two-body probability $|\psi(r)|^2$ carries over to the many-body pair distribution function $g^{(2)}(r)$, whose short-range behavior defines the contact via

$$g^{(2)}(r) = \frac{C}{(4\pi n)^2 r^2} + \mathcal{O}\left(\frac{1}{r}\right) \quad (2.32)$$

where n is the many-body number density of the system. The pair distribution function quantifies the relative likelihood of measuring other particles a distance r from any particle of interest.⁴ In the absence of correlations, $g^{(2)}(r) = 1$. Similar to the two-body case, the short-range behavior of the pair probability also determines the large- k tail of the momentum distribution according to

$$n_k = \frac{C}{k^4} + \mathcal{O}\left(\frac{1}{k^5}\right), \quad (2.33)$$

where n_k is assumed to be normalized to the density as $n = \int \frac{d^3k}{(2\pi)^3} n_k$. As written so far, the contact is a volume-averaged intensive quantity. If we were to normalize the density distribution to the particle number N instead of the density, then the definition (2.33) would imply that C is an extensive quantity. There are several conventions in the literature. When addressing many-body problems in this thesis, we will normalize momentum distributions to the number density n ; therefore, we consider C to be intensive.

We now briefly state some of the Tan relations as they apply to identical bosons of mass m in the absence of three-body effects.⁵ Relevant derivations can be found in Refs. [152, 154, 153, 20, 18]. The first relations can be considered to be Eqs. (2.32)-(2.33), either of which can define the contact. The contact relates intimately to the total energy density \mathcal{E} of a homogenous gas in equilibrium

⁴ This likelihood is compared to an uncorrelated gas, where the probability of measuring a particle in a volume element d^3r is given simply by $n \times d^3r$.

⁵ Three-body effects will be discussed in Ch. 7

according to

$$\mathcal{E} = \int \frac{d^3k}{(2\pi)^3} \frac{\hbar^2 k^2}{2m} \left[n_k - \frac{C}{k^4} \right] + \frac{\hbar^2}{8\pi m a} C, \quad (2.34)$$

where both the contact and the momentum distribution depend implicitly on a . The contact also determines how this energy density evolves as the scattering length is changed adiabatically:

$$\frac{d\mathcal{E}}{d(1/a)} = -\frac{\hbar^2}{8\pi m} C. \quad (2.35)$$

Similarly, diabatic changes in the scattering length lead to a contact-dependent change in the energy density

$$\mathcal{E}_f - \mathcal{E}_i = -\frac{\hbar^2}{8\pi m} C \left(\frac{1}{a_f} - \frac{1}{a_i} \right), \quad (2.36)$$

where it is assumed that the change occurs quickly enough that the short-range behavior of the initial quantum state, characterized by C , does not evolve appreciably while the interactions are switched. Similar relations have been derived for the large-detuning limit of the RF spectrum, the short-range limit of the one-body density matrix, the pressure, and the virial theorem. It is important to note that these results provide constraints on system observables, but they do not directly predict what these observables are unless the parameter C is known.

Tan's relations have been verified experimentally in a variety of systems. Several of these relations were measured in a gas of ultracold two-component fermions across the BCS-BEC crossover, and agreement was found for both weak and strong interactions [147]. Soon afterwards, Tan's predictions were seen in a weakly-interacting Bose-Einstein condensate [174]. The contact has recently gained significant interest in the context of nuclear-physics experiments, which appear to display asymptotic k^{-4} behavior in the momentum distribution [169, 168, 77]. It is significant that the contact is relevant to such disparate systems despite the fact that their densities differ by about a factor of 10^{20} .

2.4 Summary

In this chapter, we have given a basic description of Alkali-atom interactions and emphasized the important simplifications that occur in the ultracold regime. Due to the short range of

interactions, low-energy physics for both scattering and binding is determined universally by the scattering length. We can use simple models to represent these interactions, including the zero-range approximation, and this leads to a significant reduction in complexity over the multi-channel representation of true atom-atom interactions. We introduced Tan's contact, which helps bridge the conceptual gap to the many-body problem, demonstrating the important role played by short-range pair probabilities even in a many-body context.

Chapter 3

Weakly Interacting Bose-Einstein Condensates

In this chapter, we review the basic phenomenology and theoretical treatment of weakly interacting Bose-Einstein condensates in equilibrium. Two-body interactions, as described in the previous chapter, complicate the many-body picture somewhat; at the same time, however, they deeply enrich the physics, and we will see that the scattering length plays an important role in determining the properties of a BEC. This is a precursor to our studies of strongly interacting condensates out of equilibrium, which will be presented in the later chapters of this thesis.

3.1 The Phenomenon

Bose-Einstein condensation is the abrupt macroscopic occupation of the single-particle ground-state wave function that occurs when a many-boson sample is cooled below a critical temperature. Those atoms that occupy the ground state constitute the Bose-Einstein condensate (BEC). This phase of matter was first predicted for noninteracting systems by Einstein almost a century ago [56, 57], and its existence can be intuited from the Bose-Einstein distribution function for identical noninteracting bosons:

$$N(E_j, \mu, T) = \frac{1}{e^{(E_j - \mu)/k_B T} - 1}, \quad (3.1)$$

where E_j is the energy of a single-particle state, k_B is Boltzmann's constant, and T is the temperature of the system. If we measure energies with respect to the single-particle ground state, the chemical potential μ must satisfy $\mu < 0$ so that the occupation numbers are nonnegative and finite.

The chemical potential is fixed by the total particle number N according to

$$N = \sum_j N(E_j, \mu, T). \quad (3.2)$$

Equation (3.1) suggests that the single-particle ground state can be macroscopically occupied [that is, $N(0, \mu, T) = \mathcal{O}(N)$] if and only if $|\mu|$ is much smaller than the spacing between single-particle energy levels. When this is the case, all excited single-particle states satisfy $E_j \gg |\mu|$, and we can therefore approximate $\mu \approx 0$ in calculating their thermal populations via (3.1).

We can identify the conditions for Bose-Einstein condensation by investigating when $\mu \approx 0$ leads to a consistent solution of Eqs. (3.1)-(3.2). Inasmuch as the ground state may be macroscopically occupied, we can separate it out explicitly and approximate the remaining sum in Eq. (3.2) in the $\mu \rightarrow 0^-$ limit as an integral over energies:

$$\begin{aligned} N &= N(0, 0, T) + \sum_{j>0} N(E_j, 0, T) \\ &\approx N(0, 0, T) + \int_0^\infty dE g(E) N(E, 0, T), \\ &\approx N(0, 0, T) + \int_0^\infty dE \frac{g(E)}{e^{E/k_B T} - 1} \end{aligned} \quad (3.3)$$

where $g(E)$ is the system-dependent density of states.¹ For systems in which the integral in Eq. (3.3) is greater than N , the ansatz $\mu \approx 0$ is clearly wrong because it violates number conservation [Eq. (3.2)]; such systems are therefore uncondensed. When that integral is less than N , however, there is a macroscopic ground-state occupation $N(0, 0, T) > 0$ for which Eqs. (3.1)-(3.3) are satisfied, and the system is Bose condensed. The onset of condensation in such cases is determined by the temperature T_C for which

$$N = \int_0^\infty dE \frac{g(E)}{e^{E/k_B T_C} - 1}, \quad (3.4)$$

and there is a nontrivial BEC fraction for $T < T_C$ that is determined by number conservation

¹ The density of states encodes the degeneracy of single-particle states, and it is defined such that its integral $\int_0^{E'} dE g(E)$ gives the number of states below energy E' .

according to Eq. (3.3). This fraction increases continuously from zero as the temperature is lowered below T_C .

There are a few useful examples for which the condensation temperature and condensate fraction can be calculated analytically. Here, we simply state the results and refer the reader to Ref. [131] for the derivations. For a homogenous gas of N bosons in volume V , the condensation temperature has been evaluated analytically as

$$T_C = \frac{2\pi\hbar^2}{mk_B} \left[\frac{N}{V\zeta(3/2)} \right]^{2/3} \quad (\text{Homogenous Gas}), \quad (3.5)$$

where m is the mass and $\zeta(z)$ is the Riemann zeta function. We can similarly find the condensate fraction to be

$$\frac{N(0,0,T)}{N} = 1 - \left(\frac{T}{T_C} \right)^{3/2} \quad (\text{Homogenous Gas}) \quad (3.6)$$

for $T < T_C$. If the bosons are in a harmonic trap of mean frequency $\bar{\omega} = (\omega_x\omega_y\omega_z)^{1/3}$, then the condensation temperature evaluates to

$$T_C = \frac{\hbar\bar{\omega}}{k_B} \left[\frac{N}{\zeta(3)} \right]^{1/3} \quad (\text{Trapped Gas}), \quad (3.7)$$

and the condensate fraction is given by

$$\frac{N(0,0,T)}{N} = 1 - \left(\frac{T}{T_C} \right)^3 \quad (\text{Trapped Gas}) \quad (3.8)$$

when $T < T_C$. For homogenous gases in 2D and 1D, the energy integrals in Eqs. (3.3)-(3.4) diverge and no condensation occurs for $T > 0$.

3.1.1 The Importance of Indistinguishability

It may, at first glance, seem odd that thermodynamics would allow most of the particles to occupy the ground-state even when the temperature is larger than the spacing between single-particle energy levels. Consider the case of N particles in a spherically-symmetric harmonic oscillator of frequency ω . For sufficiently large N , Eqs. (3.7)-(3.8) show that it is possible to have an almost pure BEC of ground-state particles ($T \ll T_C$) at a temperature where many oscillator states are

thermally accessible to each particle ($k_B T \gg \hbar\omega$). Why do condensed bosons avoid these excited states despite their accessibility? The resolution of this seeming paradox comes from the different counting statistics that apply to distinguishable and indistinguishable particles. We will illustrate this heuristically.

For the case of distinguishable particles, we can apply Boltzmann statistics separately to each particle. Occupation probabilities are then proportional to the Boltzmann factor $e^{-E/k_B T}$. In the regime where $k_B T \gg \hbar\omega$, a large number q of modes are thermally accessible, and the probability of an atom occupying any of these states (including the ground state) is of order $1/q$. We conclude on these grounds that only a tiny fraction of particles can occupy the ground state at this temperature. We could alternatively arrive at this conclusion by applying Boltzmann statistics to the eigenstates of the many-body ensemble. From this perspective, each system state has its own energy and Boltzmann factor. The many-body ground state contributes a Boltzmann factor of unity to the partition function $Z = \sum_j e^{-E_j/k_B T}$. States with energy $\sim Nk_B T$ (that is, $\sim k_B T$ per particle) each contribute a tiny Boltzmann factor of approximately e^{-N} ; however, there should be about q^N of these states, and this more than makes up for the miniscule scale of their Boltzmann factors. These excited states, taken together, are exponentially probable for large N compared to the ground state. Again, we conclude that only a tiny fraction of particles should occupy the ground state.

When the particles are indistinguishable, we must count excited states differently. For example, suppose we take the many-body ground state and excite a single particle to a specific orbital. This configuration corresponds to only one unique eigenstate in the indistinguishable case, whereas there are N such eigenstates if the particles are distinguishable. There is, generally speaking, a dramatic suppression of entropy when we are dealing with the low-energy eigenstates of indistinguishable particles. Returning to the states of total energy $\sim Nk_B T$, the Boltzmann factors remain approximately e^{-N} . We can estimate the total number of such states by counting the number of

ways we can arrange N identical particles among q single-particle states:

$$\text{Number of States} = \binom{N+q-1}{N} = \frac{(N+q-1)!}{N!(q-1)!}. \quad (3.9)$$

Exploiting Sterling's approximation [2] and the fact that both N and q are large numbers, we can write this approximately as

$$\text{Number of States} \approx \begin{cases} \left(\frac{qe}{N}\right)^N & \text{if } 1 \ll N \ll q \\ \left(\frac{Ne}{q}\right)^q & \text{if } 1 \ll q \ll N \end{cases}. \quad (3.10)$$

At high temperatures ($N \ll q$), the number of states scales exponentially with particle number as $\sim q^N$, and the combinatoric factor again causes many-body states of energy $\sim Nk_B T$ to dominate the partition function. In contrast, the low-temperature limit ($q \ll N$) shows only polynomial scaling with particle number $\sim N^q$, and this gets trumped by the exponential decay of the Boltzmann factors e^{-N} . At low temperatures, the collection of states with energy $\sim k_B T$ per particle is thus exponentially improbable. The net result is that configurations similar to the many-body ground state have an increased relative weighting in the partition function and, consequently, the thermodynamics [142].

3.1.2 Experimental Observation in Dilute Alkali Gases

Typical cold-atom experiments operate at low number density ($n \lesssim 10^{14} \text{ cm}^{-3}$) in order to minimize chemically reactive processes, and this leads to low condensation temperatures on the order of about 100 nK. With reference to absolute zero, that is about 10 million times colder than deep space. Reaching such low temperatures is a technical challenge, and it took several decades to develop the tools necessary to trap and cool atoms just to the sub-mK regime. For a review of laser cooling and trapping, see Refs. [134, 29, 34].

The big breakthrough of Bose-Einstein condensation came when evaporative cooling was applied to laser-cooled Alkali atoms. The general idea is to selectively remove the most energetic atoms from a sample, thereby lowering the temperature of the remaining atoms. This is the same

process that occurs in a bowl of hot soup: the hottest soup molecules escape as steam, and the remaining soup cools as a result. In a liquid, the work function determines which molecules are hot enough to escape. In a cold-atom system, the depth of the confining potential discriminates hot particles, and one can cool a system by slowly lowering the trap depth [78]. One can also use an RF resonance condition, where photons are detuned in such a way that only energetic atoms can make the Zeeman or hyperfine transition [113]. (This is often called an RF “knife”.) For either method to work well, it is necessary that the thermalization timescale be short compared to the lifetime of the sample [91]. Under proper conditions, Alkali-atom systems can be evaporatively cooled from hundreds of μK to several nK, well below the threshold for the BEC transition. This technique led to the observations of Bose-Einstein condensation at JILA [1] and MIT [44] in 1995, and it has since become the standard method for creating degenerate quantum gases.

The first experimental evidence for reaching the Bose-condensed state in cold-atom systems was seen in ballistic-expansion measurements. The general protocol is to turn off the trap, wait several dozen milliseconds, and then take a picture via absorption imaging. If the gas has expanded freely during the wait time, the fastest atoms travel the furthest, and the image represents a momentum distribution. For a gas of uncondensed atoms, this distribution is fixed by the temperature *T* à la Boltzmann according to

$$n(p) \propto e^{-\frac{p^2}{2mk_B T}}, \quad (3.11)$$

where m is the atom mass. In the zero-temperature limit, however, the momentum distribution should be determined by the momentum-space wave function of the harmonic-oscillator ground state, shared mutually by all condensed atoms. For nonzero temperatures below T_C , Eq. (3.3) suggests that the distribution should be a sum of the classical and quantum predictions with the relative weighting determined by the condensate fraction (see Ref. [110] for a less hand-wavy analysis). Figure 3.1 shows this transition from a thermal gas to a BEC for a system of ^{87}Rb atoms that is evaporatively cooled across T_C [37].

Once this transition was observed, it became possible to investigate systematically how inter-

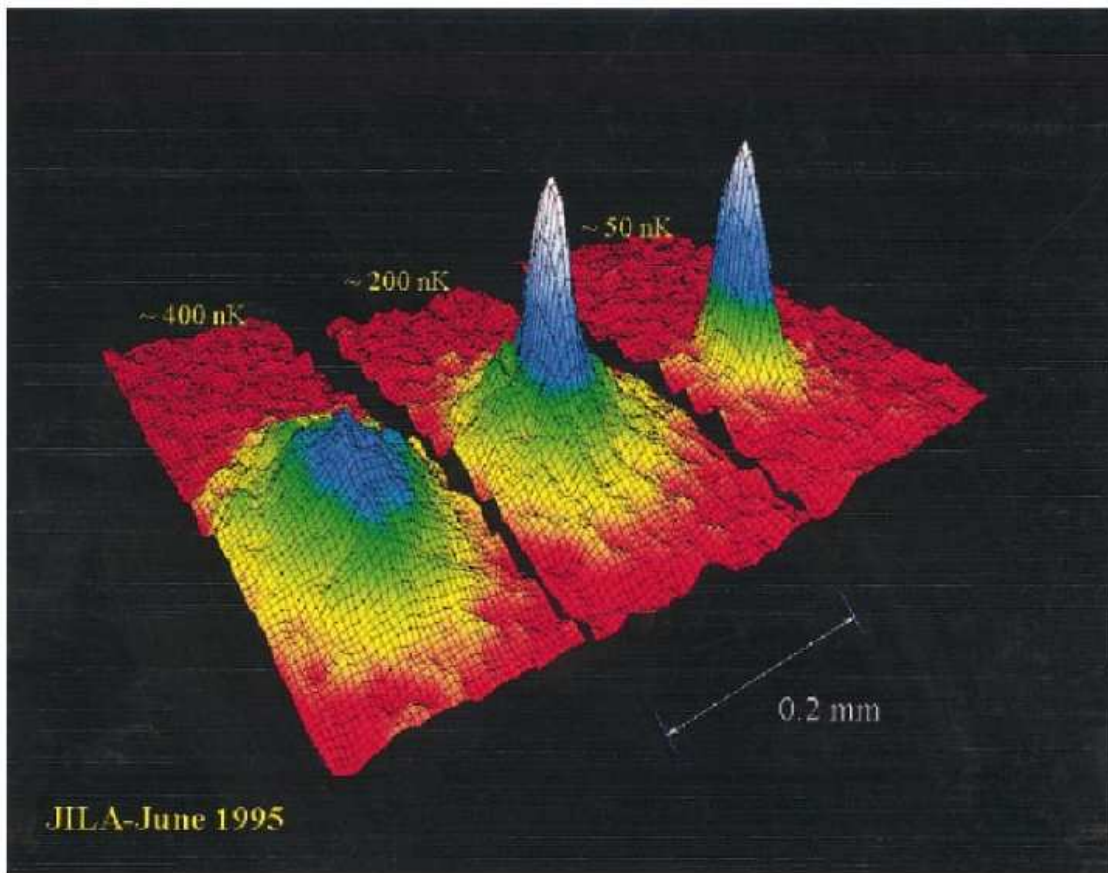


Figure 3.1: (Color online) Velocity distribution for a ballistically expanded Bose gas of ^{87}Rb atoms, as it is cooled across the BEC transition temperature. From left to right, the temperatures are 400 nK, 200 nK, and 50 nK. Used with permission from Ref. [37].

actions alter the condensed state, both in and out of equilibrium. These systems have turned into a proving ground for condensed matter theories, with Fano-Feshbach resonances opening the door to study strongly correlated systems. Before we delve into resonant interactions, we first review the present understanding of weakly interacting BECs. This will set the stage for later chapters.

3.2 Many-body Formalism

In this thesis, we will assume that systems are cold enough that thermal effects are negligible and the system can be described by a pure quantum state instead of a density matrix [131]. For a many-body system of identical bosons, this occurs at temperatures well below the condensation temperature, as suggested by Eqs. (3.6) and (3.8). We will also consider the atoms to be spin polarized such that we can suppress all indices relating to internal structure. In this regime, one can completely describe the state of an N -body system by the wave function $\Psi(\mathbf{r}_1, \mathbf{r}_2, \dots, \mathbf{r}_N, t)$. The wave function must satisfy the Schrödinger equation

$$i \frac{\partial \Psi}{\partial t} = \sum_{j=1}^N \left[-\frac{\hbar^2}{2m} \nabla_j^2 + V_{\text{ext}}(\mathbf{r}_j) \right] \Psi + \sum_{i < j}^N V_{\text{int}}(\mathbf{r}_i - \mathbf{r}_j) \Psi, \quad (3.12)$$

where m is the particle mass, V_{ext} is an external potential, and V_{int} is the interaction potential. The magnitude squared of this wave function represents the probability density of measuring the particles at positions $\{\mathbf{r}_1, \dots, \mathbf{r}_N\}$. For identical bosons, this wave function must be symmetric under particle exchange.

It is useful to reformulate the many-body problem in the language of second quantization. One chief advantage of this formulation is that it allows us to easily represent many-body states in the abstract “ket” space, as opposed to the position-space representation implied by Eq. (3.12). We enforce symmetrization by simply stating commutation relations for the operators that compose the theory.² This streamlines calculations considerably, as we will see shortly.

² The formulation for fermions is nearly identical, except that anticommutators are used [117].

3.2.1 Second Quantization

To understand second-quantized operators, we must first make sense of the Hilbert space in which they operate. Basis elements in this space, called “Fock states”, are defined by occupation numbers of single-particle states. Consider a complete, orthonormal set of states $\{\phi_j(\mathbf{r})\}$ for a single quantum particle.³ The quantum numbers that describe a given Fock state are then the occupation numbers $\{n_j\}$ (non-negative integers) of these single-particle states. In other words, the Fock state

$$|\{n_j\}\rangle \equiv |n_1, n_2, \dots\rangle \quad (3.13)$$

is defined to be the (symmetrized) state where n_1 particles occupy state $\phi_1(\mathbf{r})$, n_2 particles occupy state $\phi_2(\mathbf{r})$, and so forth. These states are defined to be normalized, and they satisfy the orthonormality condition

$$\langle \{n'_j\} | \{n_j\} \rangle = \delta_{n_1, n'_1} \delta_{n_2, n'_2} \dots \quad (3.14)$$

Fock space is defined to be the span of all Fock states of the form (3.13). It is an enormous Hilbert space in which any number of particles can occupy any configuration. The Fock space itself, as defined, is then independent of the choice of $\{\phi_j(\mathbf{r})\}$. This is in the same sense that the Hilbert space for a single particle in free space exists independently of the basis in which we choose to represent vectors, be they momentum eigenstates or be they harmonic-oscillator wave functions. Of course, representing a Fock state in the form (3.13) presupposes a specific single-particle basis.

Given the discrete nature of occupation numbers in Fock space, it is useful to define raising and lowering operators. For a given single-particle basis $\{\phi_j(\mathbf{r})\}$, we can define a set of operators $\{\hat{a}_j\}$ and $\{\hat{a}_j^\dagger\}$ whose operation on a Fock state is

$$\begin{aligned} \hat{a}_i |n_1, n_2, \dots, n_i, \dots\rangle &= \sqrt{n_i} |n_1, n_2, \dots, n_i - 1, \dots\rangle \\ \hat{a}_i^\dagger |n_1, n_2, \dots, n_i, \dots\rangle &= \sqrt{n_i + 1} |n_1, n_2, \dots, n_i + 1, \dots\rangle \end{aligned} \quad (3.15)$$

in direct analogy with the operators that are defined in the one-body harmonic-oscillator problem.

³ These states could be momentum eigenstates, harmonic oscillator wave functions, or any other complete basis.

Bosonic symmetrization requires that these operators satisfy the commutation relation given by

$$\begin{aligned} [\hat{a}_j, \hat{a}_k^\dagger] &\equiv \hat{a}_j \hat{a}_k^\dagger - \hat{a}_k^\dagger \hat{a}_j = \delta_{j,k} \\ [\hat{a}_j, \hat{a}_k] &= [\hat{a}_j^\dagger, \hat{a}_k^\dagger] = 0 \end{aligned} \quad (3.16)$$

These operators can be used to construct number operators for each single-particle mode j via $\hat{n}_j \equiv \hat{a}_j^\dagger \hat{a}_j$, and the Fock states given by (3.13) serve as the eigenvectors of these operators with eigenvalue n_j . The state for which $n_j = 0$ for all j is called the particle “vacuum” $|0\rangle$, and Eq. (3.15) implies that $\hat{a}_j|0\rangle = 0$ for all j . It is possible to generate any Fock state from the vacuum by repeatedly acting on it with raising operators:

$$|n_j\rangle = \frac{1}{\sqrt{n_1! n_2! \dots}} \left(\hat{a}_1^\dagger\right)^{n_1} \left(\hat{a}_2^\dagger\right)^{n_2} \dots |0\rangle. \quad (3.17)$$

The operators \hat{a}_j^\dagger and \hat{a}_j are often called “creation” and “annihilation” operators, respectively, as they appear to create and annihilate particles in state j according to Eq. (3.15).

It is useful to define operators that create and annihilate particles at position \mathbf{r} . We can exploit the completeness of the arbitrary basis $\{\phi_j(\mathbf{r})\}$ to define the “quantum field operators”

$$\begin{aligned} \hat{\psi}(\mathbf{r}) &= \sum_j \hat{a}_j \phi_j(\mathbf{r}) \\ \hat{\psi}^\dagger(\mathbf{r}) &= \sum_j \hat{a}_j^\dagger \phi_j^*(\mathbf{r}) \end{aligned} \quad (3.18)$$

which must satisfy the commutation relations

$$\begin{aligned} [\hat{\psi}(\mathbf{r}), \hat{\psi}^\dagger(\mathbf{r}')] &= \delta^{(3)}(\mathbf{r} - \mathbf{r}') \\ [\hat{\psi}(\mathbf{r}), \hat{\psi}(\mathbf{r}')] &= [\hat{\psi}^\dagger(\mathbf{r}), \hat{\psi}^\dagger(\mathbf{r}')] = 0 \end{aligned} \quad (3.19)$$

One can use these fields to construct the particle number density operator

$$\hat{n}(\mathbf{r}) = \hat{\psi}^\dagger(\mathbf{r}) \hat{\psi}(\mathbf{r}). \quad (3.20)$$

It is significant that, in this formulation, the position \mathbf{r} appears as a parameter instead of as an operator. The familiar commutation relation from single-particle quantum mechanics $[\hat{\mathbf{r}}_i, \hat{\mathbf{p}}_j] = i\hbar\delta_{i,j}$, in which position and momentum are operators in the Hilbert space, is often referred to as

“first quantization”. The term “second quantization” refers to using operator-valued functions as quantized fields,⁴ in the sense of Eqs. (3.18)-(3.19).

In the representation of second quantization, the quantum field operators $\hat{\psi}$ and $\hat{\psi}^\dagger$ constitute useful building blocks for important theoretical quantities. For one thing, they provide a natural expression of the position-space wave function $\Psi(\mathbf{r}_1, \mathbf{r}_2, \dots, \mathbf{r}_N, t)$ in the abstract “ket” space:

$$|\Psi(t)\rangle = \frac{1}{\sqrt{N!}} \int d^3r_1 d^3r_2 \dots d^3r_N \Psi(\mathbf{r}_1, \mathbf{r}_2, \dots, \mathbf{r}_N, t) \hat{\psi}^\dagger(\mathbf{r}_1) \hat{\psi}^\dagger(\mathbf{r}_2) \dots \hat{\psi}^\dagger(\mathbf{r}_N) |0\rangle, \quad (3.21)$$

where the commutation of the $\hat{\psi}^\dagger$ operators according to Eq. (3.19) ensures that the state is symmetric under particle exchange. The Hamiltonian that governs the dynamics of $|\Psi(t)\rangle$ according to the Schrödinger equation (3.12) can be written as

$$\hat{H} = \int d^3r \hat{\psi}^\dagger(\mathbf{r}) \left[-\frac{\hbar^2}{2m} \nabla^2 + V_{\text{ext}}(\mathbf{r}) \right] \hat{\psi}(\mathbf{r}) + \frac{1}{2} \int d^3r d^3r' V_{\text{int}}(\mathbf{r} - \mathbf{r}') \hat{\psi}^\dagger(\mathbf{r}) \hat{\psi}^\dagger(\mathbf{r}') \hat{\psi}(\mathbf{r}') \hat{\psi}(\mathbf{r}). \quad (3.22)$$

It is worth pointing out that this representation of the Hamiltonian does not presuppose any specific particle number N ; it is valid for all particle numbers and can even be used for describing systems in which N is not fixed, such as the grand canonical ensemble [117].

It is often convenient to perform many-body calculations assuming a homogenous (untrapped) sample. This makes it easy to take the thermodynamic limit, where the particle number N and the volume V approach infinity with the number density n fixed. Momentum is also conserved in the absence of a trap, which simplifies ground state calculations by allowing us to work in the zero-momentum subspace. We therefore expand the quantum field operator $\hat{\psi}(\mathbf{r})$ in the basis of single-particle plane-wave states:

$$\hat{\psi}(\mathbf{r}) = \frac{1}{\sqrt{V}} \sum_{\mathbf{k}} \hat{a}_{\mathbf{k}} e^{i\mathbf{k}\cdot\mathbf{r}}, \quad (3.23)$$

where the operator $\hat{a}_{\mathbf{k}}$ annihilates a particle with momentum $\hbar\mathbf{k}$. The operators $\{\hat{a}_{\mathbf{k}}\}$ and $\{\hat{a}_{\mathbf{k}}^\dagger\}$ satisfy the discrete commutation relations given by Eq. (3.16), with momentum indices. In this basis, the Hamiltonian (3.22) takes the compact form

$$\hat{H} = \sum_{\mathbf{k}} \varepsilon_{\mathbf{k}} \hat{a}_{\mathbf{k}}^\dagger \hat{a}_{\mathbf{k}} + \frac{1}{2V} \sum_{\mathbf{k}, \mathbf{k}', \mathbf{q}} \tilde{V}_{\text{int}}(\mathbf{q}) \hat{a}_{\mathbf{k}+\mathbf{q}}^\dagger \hat{a}_{\mathbf{k}'-\mathbf{q}}^\dagger \hat{a}_{\mathbf{k}} \hat{a}_{\mathbf{k}'}, \quad (3.24)$$

⁴ For rigor, we should call them operator-valued distributions due to the singular nature of their commutators.

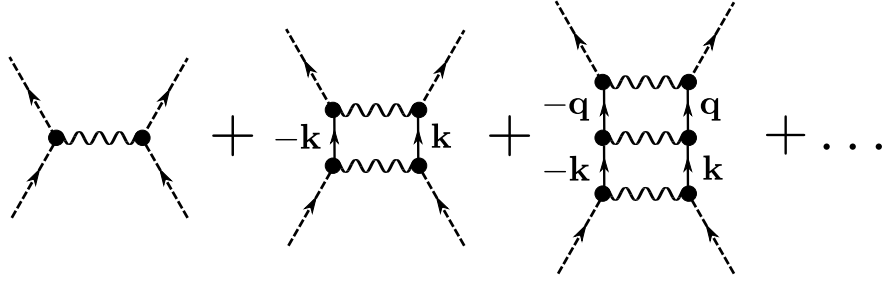


Figure 3.2: Diagrammatic representation of the Born series for interacting BEC particles. The dashed lines represent condensed atoms with zero momentum, the wiggly lines represent interactions via the potential \tilde{V}_{int} , and the straight solid lines represent intermediate scattering states with arbitrary momentum. Only the first two terms of this series can be generated by the Bogoliubov Hamiltonian (3.25).

where $\varepsilon_k = \frac{\hbar^2 k^2}{2m}$ is the kinetic energy of a particle, and $\tilde{V}_{\text{int}}(\mathbf{q})$ is the Fourier transform of the interaction potential.

3.3 Weakly Interacting BECs

It is notoriously difficult to solve the quantum many-body problem in the presence of non-trivial interactions. When these interactions are weak, however, progress can be made. We expect generally that the ground state of a weakly interacting BEC should still feature a sizeable condensate fraction, for example. This idea leads to the widely used Bogoliubov approximation [10], which treats the problem in a mean-field sense. In this section, we will focus on the case in which there are N atoms in a homogenous volume V , whose Hamiltonian is given by Eq. (3.24).

3.3.1 The Bogoliubov Approximation

The Bogoliubov theory of interacting BECs begins with the assumption that the condensate fraction is approximately equal to unity, with minimal uncertainty or fluctuation. Said another way, we assume that the ground state is dominated by configurations where the number of ground state atoms N_0 is nearly equal to the total number of atoms N . This suggests that, in the relevant part of the Hilbert space, the operators with the largest matrix elements are those that are composed of \hat{a}_0 and \hat{a}_0^\dagger , as these operators introduce factors of $\sqrt{N_0}$ and $\sqrt{N_0 + 1}$ according to Eq. (3.15). We

write the Bogoliubov Hamiltonian by discarding terms in the interaction that have fewer than two factors of either \hat{a}_0 or \hat{a}_0^\dagger :

$$\begin{aligned} \hat{H} \approx & \frac{\tilde{V}_{\text{int}}(0)}{2V} \hat{a}_0^\dagger \hat{a}_0^\dagger \hat{a}_0 \hat{a}_0 + \sum_{\mathbf{k}} \varepsilon_k \hat{a}_{\mathbf{k}}^\dagger \hat{a}_{\mathbf{k}} + \frac{1}{2V} \sum_{\mathbf{k} \neq 0} \tilde{V}_{\text{int}}(k) \left(2\hat{a}_0^\dagger \hat{a}_{\mathbf{k}}^\dagger \hat{a}_{\mathbf{k}} \hat{a}_0 + \hat{a}_{\mathbf{k}}^\dagger \hat{a}_{-\mathbf{k}}^\dagger \hat{a}_0 \hat{a}_0 + \hat{a}_0^\dagger \hat{a}_0^\dagger \hat{a}_{\mathbf{k}} \hat{a}_{-\mathbf{k}} \right) \\ & + \frac{\tilde{V}_{\text{int}}(0)}{V} \sum_{\mathbf{k} \neq 0} \hat{a}_0^\dagger \hat{a}_{\mathbf{k}}^\dagger \hat{a}_{\mathbf{k}} \hat{a}_0 \end{aligned} \quad (3.25)$$

The neglect of terms such as $\hat{a}_{\mathbf{q}}^\dagger \hat{a}_{-\mathbf{q}}^\dagger \hat{a}_{\mathbf{k}} \hat{a}_{-\mathbf{k}}$ has important consequences for the theory. This Hamiltonian can evidently excite a pair of atoms from the condensate (via $\hat{a}_{\mathbf{k}}^\dagger \hat{a}_{-\mathbf{k}}^\dagger \hat{a}_0 \hat{a}_0$), but these atoms cannot scatter multiple times before returning to the condensate (via $\hat{a}_0^\dagger \hat{a}_0^\dagger \hat{a}_{\mathbf{k}} \hat{a}_{-\mathbf{k}}$). In terms of Feynman diagrams, Eq. (3.25) only allows condensate atoms to scatter up to second order in the Born approximation, which are the first two terms shown in Fig. 3.2. We can expect this Hamiltonian, as written, to reproduce the correct physics only for cases in which the higher-order terms of the Born series are vanishingly small at low energies.

A good candidate for the interaction is the regularized contact potential given by Eqs. (2.28) and (2.31). This potential has the form

$$\tilde{V}_{\text{int}}(k) = U_\Lambda \Theta(\Lambda - k) = \frac{4\pi\hbar^2 a/m}{1 - \frac{2}{\pi}\Lambda a} \Theta(\Lambda - k). \quad (3.26)$$

In the limit that $\Lambda|a| \ll 1$, the first Born approximation [117] $f^{(1)} = -\frac{m}{4\pi\hbar^2} \tilde{V}_{\text{int}}(0)$ approximately reproduces the exact low-energy scattering amplitude $f = -a$; it can be shown that the higher-order terms of the Born series are smaller by successive powers of Λa at low energies. In this regime, the coupling constant U_Λ depends only weakly on the cutoff Λ , and it is convenient to simply write it as $U_0 = 4\pi\hbar^2 a/m$. It is worth noting that using an arbitrary short-range potential in (3.25), or even an effective potential (3.26) that violates $\Lambda|a| \ll 1$, leads to incorrect results due to the neglect of higher-order scattering in the sense of Fig. 3.2. At the same time, we must choose the range of the interaction Λ^{-1} to be small compared to the mean interparticle separation $\sim n^{-1/3}$ so that range effects remain negligible. These considerations constrain the cutoff Λ such that

$$n^{1/3} \ll \Lambda \ll |a|^{-1}. \quad (3.27)$$

We immediately see that these approximations, neglecting both higher-order scattering and range effects, can be consistent only for $n|a|^3 \ll 1$.

Besides neglecting certain terms in the interaction, the Bogoliubov approximation entails approximating \hat{a}_0 and \hat{a}_0^\dagger as $\sqrt{N_0}$. This is motivated by the fact that all relevant matrix elements that contain these operators introduce essentially that same factor. In this approximation, the Bogoliubov Hamiltonian can be written as

$$\begin{aligned} \hat{H}_{\text{Bog}} = & \frac{N_0^2 U_0}{2V} + \sum_{\mathbf{k} \neq 0}^{\Lambda} \varepsilon_k \hat{a}_{\mathbf{k}}^\dagger \hat{a}_{\mathbf{k}} + \frac{N_0 U_0}{2V} \sum_{\mathbf{k} \neq 0}^{\Lambda} \left(2\hat{a}_{\mathbf{k}}^\dagger \hat{a}_{\mathbf{k}} + \hat{a}_{\mathbf{k}}^\dagger \hat{a}_{-\mathbf{k}}^\dagger + \hat{a}_{\mathbf{k}} \hat{a}_{-\mathbf{k}} \right) \\ & + \frac{N_0 U_0}{V} \sum_{\mathbf{k} \neq 0}^{\Lambda} \hat{a}_{\mathbf{k}}^\dagger \hat{a}_{\mathbf{k}} \end{aligned} \quad (3.28)$$

where we have neglected high-energy modes $k > \Lambda$ that are not expected to be populated in a weakly interacting BEC.⁵ The first and last terms can be combined to yield

$$\begin{aligned} \frac{N_0^2 U_0}{2V} + \frac{N_0 U_0}{V} \sum_{\mathbf{k} \neq 0}^{\Lambda} \hat{a}_{\mathbf{k}}^\dagger \hat{a}_{\mathbf{k}} &= \frac{U_0}{2V} \left(N_0^2 + 2N_0 \sum_{\mathbf{k} \neq 0}^{\Lambda} \hat{a}_{\mathbf{k}}^\dagger \hat{a}_{\mathbf{k}} \right) \\ &\approx \frac{U_0}{2V} \left(N_0 + \sum_{\mathbf{k} \neq 0}^{\Lambda} \hat{a}_{\mathbf{k}}^\dagger \hat{a}_{\mathbf{k}} \right)^2 \\ &\approx \frac{N^2 U_0}{2V} \end{aligned} \quad (3.29)$$

according to number conservation. To this order of approximation, we can now set N_0/V and N/V to the number density n , and the Bogoliubov Hamiltonian becomes

$$\hat{H}_{\text{Bog}} = \frac{NnU_0}{2} + \sum_{\mathbf{k} \neq 0}^{\Lambda} \varepsilon_k \hat{a}_{\mathbf{k}}^\dagger \hat{a}_{\mathbf{k}} + \frac{nU_0}{2} \sum_{\mathbf{k} \neq 0}^{\Lambda} \left(2\hat{a}_{\mathbf{k}}^\dagger \hat{a}_{\mathbf{k}} + \hat{a}_{\mathbf{k}}^\dagger \hat{a}_{-\mathbf{k}}^\dagger + \hat{a}_{\mathbf{k}} \hat{a}_{-\mathbf{k}} \right). \quad (3.30)$$

⁵ It can be shown that these modes are approximately decoupled in the Bogoliubov ground-state calculation, which is reason enough to ignore them.

3.3.2 Solving the Problem

The Hamiltonian (3.30) can be diagonalized by a so-called Bogoliubov transformation.⁶ The trick is to define operators according to

$$\begin{aligned}\hat{a}_{\mathbf{k}} &= u_k \hat{\beta}_{\mathbf{k}} - v_k \hat{\beta}_{-\mathbf{k}}^\dagger, \\ \hat{a}_{\mathbf{k}}^\dagger &= u_k \hat{\beta}_{\mathbf{k}}^\dagger - v_k \hat{\beta}_{-\mathbf{k}}\end{aligned}\tag{3.31}$$

where u_k and v_k are undetermined parameters. It can be checked that $\hat{\beta}_{\mathbf{k}}$ and $\hat{\beta}_{\mathbf{k}}^\dagger$ satisfy the bosonic commutation relations

$$\begin{aligned}[\hat{\beta}_{\mathbf{k}}, \hat{\beta}_{\mathbf{k}'}^\dagger] &= \delta_{\mathbf{k}\mathbf{k}'} \\ [\hat{\beta}_{\mathbf{k}}, \hat{\beta}_{\mathbf{k}'}] &= [\hat{\beta}_{\mathbf{k}}^\dagger, \hat{\beta}_{\mathbf{k}'}^\dagger] = 0\end{aligned}\tag{3.32}$$

as long as

$$u_k^2 - v_k^2 = 1\tag{3.33}$$

for all $k > 0$. We can substitute (3.31) into (3.30), and we find that

$$\begin{aligned}\hat{H}_{\text{Bog}} &= \frac{NnU_0}{2} + \sum_{\mathbf{k} \neq 0}^{\Lambda} [v_k^2 (\varepsilon_k + nU_0) - u_k v_k nU_0] \\ &+ \sum_{\mathbf{k} \neq 0}^{\Lambda} \hat{\beta}_{\mathbf{k}}^\dagger \hat{\beta}_{\mathbf{k}} [(u_k^2 + v_k^2) (\varepsilon_k + nU_0) - 2u_k v_k nU_0] \\ &+ \frac{1}{2} \sum_{\mathbf{k} \neq 0}^{\Lambda} (\hat{\beta}_{\mathbf{k}'}^\dagger \hat{\beta}_{-\mathbf{k}}^\dagger + \hat{\beta}_{\mathbf{k}} \hat{\beta}_{-\mathbf{k}}) [(u_k^2 + v_k^2) nU_0 - 2u_k v_k (\varepsilon_k + nU_0)]\end{aligned}\tag{3.34}$$

We can choose the parameters u_k and v_k such that the last line of (3.34) vanishes:

$$\begin{aligned}u_k &= \sqrt{\frac{\varepsilon_k + nU_0}{2\hbar\omega_k} + \frac{1}{2}} \\ v_k &= \text{sgn}[U_0] \sqrt{\frac{\varepsilon_k + nU_0}{2\hbar\omega_k} - \frac{1}{2}}\end{aligned}\tag{3.35}$$

where we have defined

$$\hbar\omega_k = \sqrt{\varepsilon_k (\varepsilon_k + 2nU_0)}.\tag{3.36}$$

After some algebra, the Hamiltonian can be written as

$$\hat{H}_{\text{Bog}} = \frac{NnU_0}{2} + \frac{1}{2} \sum_{\mathbf{k} \neq 0}^{\Lambda} [\hbar\omega_k - \varepsilon_k - nU_0] + \sum_{\mathbf{k} \neq 0}^{\Lambda} \hat{\beta}_{\mathbf{k}}^\dagger \hat{\beta}_{\mathbf{k}} \hbar\omega_k.\tag{3.37}$$

⁶ Although Bogoliubov popularized the idea [10], it appeared in the literature several years earlier in the context of magnetic systems [82].

This form is diagonal in the sense that its operator component, the last term, has the form of a number operator. However, it is not counting particles, but rather a different form of excitation defined by Eqs. (3.31) and (3.35). These excitations, which are the approximate normal modes of the system, are often called “quasiparticles” [116] and their energies are given by $\hbar\omega_k$ in Eq. (3.36).

The excitation energies reveal important physics about interacting BECs. For $a < 0$, these energies are imaginary valued in the small- k limit, signifying that the assumed Bose-condensed state is dynamically unstable. For $a > 0$, they are real valued and behave asymptotically as

$$\hbar\omega_k \approx \begin{cases} \sqrt{\frac{4\pi\hbar^2na}{m^2}}\hbar k & \text{if } k\xi \ll 1 \\ \varepsilon_k + \frac{4\pi\hbar^2na}{m} & \text{if } k\xi \gg 1 \end{cases}, \quad (3.38)$$

where we have defined the length scale $\xi = 1/\sqrt{8\pi\hbar^2na}$, called the “healing length”. The linear dispersion for small k indicates that these modes are phonons with a sound speed given by $c = \sqrt{\frac{4\pi\hbar^2na}{m^2}}$. In this case, the sound speed c also serves as the superfluid critical velocity: impurities traveling slower than c (relative to the BEC) are energetically forbidden from exciting the BEC. This interesting result follows from energy-momentum conservation, as first discussed by Landau in the context of superfluid helium [103, 104]. It is worth pointing out that the critical velocity vanishes in the limit that $a \rightarrow 0$, and the BEC ceases to be a superfluid. Hence, interactions are crucial to the phenomenon of superfluidity.

3.3.3 The Ground State

The ground state of the system $|\Psi_0\rangle$ is defined by the absence of quasiparticle excitations. This means that it must satisfy $\hat{\beta}_{\mathbf{k}}|\Psi_0\rangle = 0$ for all $\mathbf{k} \neq 0$. We can use this feature, along with (3.31), to calculate the momentum distribution of excited particles. We find that

$$\begin{aligned} n_{\mathbf{k}} &= \langle \Psi_0 | \hat{a}_{\mathbf{k}}^\dagger \hat{a}_{\mathbf{k}} | \Psi_0 \rangle \\ &= \langle \Psi_0 | (u_k \hat{\beta}_{\mathbf{k}}^\dagger - v_k \hat{\beta}_{-\mathbf{k}}) (u_k \hat{\beta}_{\mathbf{k}} - v_k \hat{\beta}_{-\mathbf{k}}^\dagger) | \Psi_0 \rangle \\ &= v_k^2 \\ &= \frac{\varepsilon_k + nU_0}{2\hbar\omega_k} - \frac{1}{2} \end{aligned} \quad (3.39)$$

It can be shown that this distribution has a large- k tail that goes as C/k^4 , as anticipated in Sec. 2.3.

We can extract the contact C by noting that

$$\begin{aligned}
C &= \lim_{k \rightarrow \infty} k^4 \times \left[\frac{\varepsilon_k + nU_0}{2\sqrt{\varepsilon_k(\varepsilon_k + 2nU_0)}} - \frac{1}{2} \right] \\
&= \lim_{k \rightarrow \infty} k^4 \times \left[\frac{1 + \frac{nU_0}{\varepsilon_k}}{2\sqrt{1 + 2\frac{nU_0}{\varepsilon_k}}} - \frac{1}{2} \right], \\
&= \lim_{k \rightarrow \infty} k^4 \times \left[\frac{1}{4} \left(\frac{nU_0}{\varepsilon_k} \right)^2 + \mathcal{O} \left(\frac{nU_0}{\varepsilon_k} \right)^3 \right] \\
&= 16\pi^2 n^2 a^2
\end{aligned} \tag{3.40}$$

where we have used the definition of the quasiparticle energy (3.36).

We can sum Eq. (3.39) over $\mathbf{k} \neq 0$ to find the total fraction of excited particles. It is helpful to convert the sum to an integral via

$$\frac{N_{\text{ex}}}{N} = \frac{1}{N} \sum_{\mathbf{k} \neq 0}^{\Lambda} n_{\mathbf{k}} \approx \frac{1}{n} \int_{k < \Lambda} \frac{d^3 k}{(2\pi)^3} n_{\mathbf{k}}, \tag{3.41}$$

where we have made the usual replacement $\sum_{\mathbf{k} \neq 0} \rightarrow V \int \frac{d^3 k}{(2\pi)^3}$, and recalled that $n = N/V$. This convergent integral is approximately independent of the cutoff as long as $\Lambda\xi \gg 1$, which is consistent with the restrictions in Eq. (3.27) whenever $na^3 \ll 1$. We are therefore justified in extending the integration limits to infinity, and the excited fraction evaluates to

$$\frac{N_{\text{ex}}}{N} \approx \frac{8}{3} \sqrt{\frac{na^3}{\pi}}. \tag{3.42}$$

This verifies (after the fact, of course) that the BEC fraction is approximately unity in the limit that $na^3 \ll 1$. In contrast to the thermal depletion considered in Eq. (3.6), this depletion occurs purely as a result of interactions. It is often referred to as the ‘‘quantum depletion’’.

The ground state energy can almost be read off as the c-number contribution to the Bogoliubov Hamiltonian (3.37), which is

$$E_0 \rightarrow \frac{NnU_0}{2} + \frac{1}{2} \sum_{\mathbf{k} \neq 0}^{\Lambda} [\hbar\omega_{\mathbf{k}} - \varepsilon_{\mathbf{k}} - nU_0]. \tag{3.43}$$

This quantity, as written, grows linearly with Λ for $\Lambda\xi \gg 1$. This conundrum is rooted in the fact that we have ignored the weak cutoff dependence of the coupling constant U_{Λ} . If we restore this

cutoff dependence to (3.43), then the resulting energy is approximately cutoff independent. We can demonstrate this by expanding U_Λ to lowest order in $\Lambda a \ll 1$:

$$\begin{aligned} U_\Lambda &= \frac{4\pi\hbar^2 a}{m} \left[1 + \frac{2}{\pi}\Lambda a + \mathcal{O}(\Lambda a)^2 \right] \\ &= U_0 \left[1 + 4\pi a \int_{k<\Lambda} \frac{d^3k}{(2\pi)^3} \frac{1}{k^2} + \mathcal{O}(\Lambda a)^2 \right], \\ &= U_0 \left[1 + \frac{U_0}{V} \sum_{\mathbf{k}\neq 0} \frac{1}{2\varepsilon_k} + \mathcal{O}(\Lambda a)^2 \right] \end{aligned} \quad (3.44)$$

where we have exchanged an integral for a sum. Substituting this cutoff-dependent expression into Eq. (3.43) yields

$$E_0 = \left\{ \frac{NnU_0}{2} + \frac{1}{2} \sum_{\mathbf{k}\neq 0} \left[\hbar\omega_k - \varepsilon_k - nU_0 + \frac{n^2 U_0^2}{2\varepsilon_k} \right] \right\} [1 + \mathcal{O}(\Lambda a)] \quad (3.45)$$

after some algebra. This quantity is cutoff independent for $\xi^{-1} \ll \Lambda \ll a^{-1}$, where it evaluates to

$$E_0/N \approx \frac{2\pi\hbar^2 na}{m} \left(1 + \frac{128}{15} \sqrt{\frac{na^3}{\pi}} \right). \quad (3.46)$$

To lowest order, the energy per particle scales linearly with both the scattering length and the density, and it relates to the contact (3.40) in the way predicted by the Tan relations (2.33)-(2.35) if one ignores higher-order corrections.⁷ The small parameter na^3 , familiar from the depletion (3.42), appears in the next-order correction to the ground state energy. The expressions (3.42) and (3.46) were first derived in a seminal paper by Lee, Huang, and Yang [106].

Although our approach used a specific potential model, the results are valid more generally for weakly-interacting, dilute BECs satisfying $na^3 \ll 1$. Such can be proved rigorously using the diagrammatic methods of quantum field theory, as done by Beliaev in Refs. [7, 8]. Using the Bogoliubov method to treat the general case, however, requires altering the Bogoliubov Hamiltonian (3.25) at the first stage of the calculation. One must retroactively account for the neglected terms of the Born series in Fig. (3.2) by replacing the true potential $\tilde{V}_{\text{int}}(k)$ in (3.25) with the T-matrix, which is defined as the effective potential for which the first Born approximation gives the exact

⁷ The exact Tan relations are thus satisfied approximately by our inexact theory.

scattering behavior [21, 132]. In the language of quantum field theory, this is often referred to as “summing ladder diagrams”. It is worth noting that both the Bogoliubov and Beliaev approaches are ill suited to describing physics occurring uniquely at momentum scales larger than (or equal to) a^{-1} . This becomes a problem either when a is comparable to or larger than the length scales set by many-body physics (such as the particle separation $\sim n^{-1/3}$), or in nonequilibrium scenarios where the bound state may play a role in the dynamics. These situations will be discussed in the next two chapters.

Chapter 4

BEC Quenched to Unitarity

Many of the results presented in this chapter were published in Ref. [150].

4.1 Motivation

As shown in the previous chapter, the usual theoretical treatment of Bose-Einstein condensation is rooted in a perturbative inclusion of interaction effects. The starting assumption of Bogoliubov theory is that the condensate fraction remains close to unity despite interactions, and Eq. (3.42) indicates that this requirement is self-consistently fulfilled only in the limit that $na^3 \ll 1$. This condition is met in most BEC experiments, and thus Bogoliubov theory (with its Gross-Pitaevskii extension to confined systems [74, 75, 136]) has been enormously successful in quantitatively describing observations [162, 130, 81, 115, 126, 174]. In stark contrast, the strongly-interacting regime $na^3 \gg 1$ has remained theoretically elusive for decades, and the prospects for achieving it in a BEC experiment were bleak due to the a^4 scaling of three-body loss rates [63, 127, 167]. Even with the advent of magnetic Fano-Feshbach resonances in Alkali-atom experiments, whereby the scattering length a could be freely tuned, it seemed unlikely that one could create an equilibrium strongly-interacting BEC that would survive long enough for interesting physics to be observed.

It was soon realized that the strongly-interacting regime could be probed in an out-of-equilibrium scenario as long as the experimental timescale was short compared to the (already short) lifetime of the gas. One simple protocol for such an experiment is to rapidly change the

scattering length from an initial value a_i to a final value a_f by ramping the magnetic field near a Fano-Feshbach resonance, and then observe the response of the system. This sequence is often called an interaction “quench”. One early experiment [32] considered the response of a weakly-interacting BEC ($na_i^3 \ll 1$) of ^{85}Rb atoms that was quenched to $na_f^3 \lesssim 1$ over the course of $12.5 \mu\text{s}$, and it was observed that the condensate exhibited nontrivial decay dynamics over the course of about $100 \mu\text{s}$ that could not be explained simply by three-body loss. After more than a decade, these measurements still have not been explained quantitatively by theory [145].

More recently, experimenters boldly quenched a weakly-interacting ^{85}Rb BEC directly to the unitarity regime, where $a_f \rightarrow \infty$ [112]. In this case, the dynamical momentum distribution was measured by ballistically expanding the gas after various hold times at unitarity. It was observed, rather unexpectedly, that the populations of large-momentum modes saturated on timescales ($\lesssim 100 \mu\text{s}$) that were much shorter than the lifetime of the gas ($\sim 1 \text{ ms}$). This saturation suggested that the gas had reached a kind of metastable quasi-equilibrated state, despite the resonant interactions. Also significant was the fact that, when they repeated their measurements on a gas with a different density, there were indications of universality. That is, the saturation and loss dynamics for systems of different density were approximately identical as long as momenta and time were rescaled by $n^{1/3}$ and $n^{-2/3}$, respectively. These scalings can be derived trivially from dimensional analysis under the assumption that the particle spacing $\sim n^{-1/3}$ is the only physically relevant length scale for the system. This assumption makes some sense, given that the scattering length and thermal deBroglie wavelength are infinite and cannot be used for dimensional analysis. On the other hand, three-body Efimov physics [54, 55] can introduce another length scale to the problem, namely, the size of a three-body bound state. Discovering the role of this effect in the quenched BEC system, and how it might disrupt universality, is an area of active research. At the same time, it is useful to first consider the dynamical consequences of two-body physics in the quench to unitarity.

4.2 Many-Body Model

In our quest to understand the dynamics of a BEC quenched to unitarity, we consider a simplified system that is spatially uniform with density $n = N/V$ and whose atoms are initially noninteracting ($a_i = 0$). We adopt a time-dependent variational approach to solving the problem. Our variational wave function $|\Psi_{\text{var}}(t)\rangle$ is constructed to include the physics that should be most important at short times after the quench. For example, we expect that the jump to resonance does not instantaneously deplete the condensate, as the many-body wave function must evolve continuously from its initial condensed state. We also expect that the dominant process immediately following the quench should be that multiple pairs of condensate atoms scatter off each other with equal and opposite momentum, as required by momentum conservation. To incorporate these two notions, we use a time-dependent generalization of the ansatz used in Refs. [146, 67, 128]:

$$|\Psi_{\text{var}}(t)\rangle = \mathcal{A}(t) \exp \left\{ c_0(t) \hat{a}_0^\dagger + \frac{1}{2} \sum_{\mathbf{k} \neq 0} g_{\mathbf{k}}(t) \hat{a}_{\mathbf{k}}^\dagger \hat{a}_{-\mathbf{k}}^\dagger \right\} |0\rangle, \quad (4.1)$$

where $c_0(t)$ and $\{g_{\mathbf{k}}(t)\}$ are time-dependent variational parameters and

$$\mathcal{A}(t) = \exp \left\{ -|c_0(t)|^2 / 2 + \frac{1}{4} \sum_{\mathbf{k} \neq 0} \ln [1 - |g_{\mathbf{k}}(t)|^2] \right\} \quad (4.2)$$

is a normalization constant. The first term in the exponential in (4.1) represents the condensate as a coherent state [68]. The relation $\hat{a}_0 |\Psi_{\text{var}}(t)\rangle = c_0(t) |\Psi_{\text{var}}(t)\rangle$ essentially replaces the operator \hat{a}_0 by c_0 for all matrix elements in the restricted Hilbert space, in analogy with the Bogoliubov prescription described above Eq. (3.28). It therefore follows that the condensate population is given by $N_0(t) = |c_0(t)|^2$. The term involving $g_{\mathbf{k}}$, assumed to have reflection symmetry $g_{\mathbf{k}} = g_{-\mathbf{k}}$, generates correlated pairs of excited atoms. One can show that the dynamical momentum distribution is $n_{\mathbf{k}}(t) = \frac{|g_{\mathbf{k}}(t)|^2}{1 - |g_{\mathbf{k}}(t)|^2}$. As initial conditions for these parameters, we set $c_0(0) = \sqrt{N}$ and $g_{\mathbf{k}}(0) = 0$.

The Hamiltonian that governs the post-quench ($t > 0$) dynamics of the system is given by

Eq. (3.24), which reads

$$\hat{H} = \sum_{\mathbf{k}} \varepsilon_k \hat{a}_{\mathbf{k}}^\dagger \hat{a}_{\mathbf{k}} + \frac{1}{2V} \sum_{\mathbf{k}, \mathbf{k}', \mathbf{q}} \tilde{V}_{\text{int}}(\mathbf{q}) \hat{a}_{\mathbf{k}+\mathbf{q}}^\dagger \hat{a}_{\mathbf{k}'-\mathbf{q}}^\dagger \hat{a}_{\mathbf{k}} \hat{a}_{\mathbf{k}'}. \quad (4.3)$$

The interaction potential $\tilde{V}_{\text{int}}(k)$ must be chosen to yield resonant scattering ($a \rightarrow \pm\infty$). As discussed in Section 2.2, this can be accomplished by using an attractive short-range potential whose depth is chosen so that there is a two-body bound state at zero energy. It is expected that the dynamics, if computed correctly, should not depend on the particular model as long as the potential is short-ranged and resonant.¹ This idea will serve as a useful check of our solution method.

We derive the equations of motion for the parameters $c_0(t)$ and $\{g_{\mathbf{k}}(t)\}$ by minimizing the action for a suitably-defined Lagrangian that “knows” about quantum mechanics. Such a Lagrangian can be written as

$$\mathcal{L} = \frac{i\hbar}{2} \left(\langle \dot{\Psi}(t) | \dot{\Psi}(t) \rangle - \langle \dot{\Psi}(t) | \Psi(t) \rangle \right) - \langle \Psi(t) | \hat{H} | \Psi(t) \rangle, \quad (4.4)$$

where the dot denotes a time derivative. It can be checked that, for an unconstrained state $|\Psi\rangle$, the Euler-Lagrange equation of motion $\frac{\delta \mathcal{L}}{\delta \dot{\Psi}} - \frac{\delta \mathcal{L}}{\delta \Psi} = 0$ leads to the time-dependent Schrödinger equation [101]. In our case, the quantum state of the system is constrained to have the form (4.1), so it does not strictly satisfy the Schrödinger equation except in the least-action sense.² This should not be a problem at short times where the ansatz, by design, includes the dominant physics of the system.

In deriving the equations of motion, we evidently need to know the expectation value of \hat{H}

¹ Otherwise, we’d be stuck using the honest-to-goodness ⁸⁵Rb potentials, and even then, the result would only be relevant to a single atomic species.

² This is similar to how static variational calculations usually lead only to approximate solutions to the time-independent Schrödinger equation. In the dynamical case, we find the optimal solution by minimizing the action, instead of $\langle \hat{H} \rangle$.

in the variational state $|\Psi_{\text{var}}\rangle$. With a little bit of effort, one finds that [146]

$$\begin{aligned} \langle \Psi_{\text{var}} | \hat{H} | \Psi_{\text{var}} \rangle &= \sum_{\mathbf{k} \neq 0} \varepsilon_k \frac{|g_{\mathbf{k}}|^2}{1 - |g_{\mathbf{k}}|^2} + \frac{\tilde{V}_{\text{int}}(0)}{2V} |c_0|^4 + \frac{1}{V} \sum_{\mathbf{k} \neq 0} [\tilde{V}_{\text{int}}(\mathbf{k}) + \tilde{V}_{\text{int}}(0)] \frac{|g_{\mathbf{k}}|^2}{1 - |g_{\mathbf{k}}|^2} |c_0|^2 \\ &+ \frac{1}{2V} \sum_{\mathbf{k} \neq 0} \tilde{V}_{\text{int}}(\mathbf{k}) \frac{c_0^2 g_{\mathbf{k}}^* + c_0^{*2} g_{\mathbf{k}}}{1 - |g_{\mathbf{k}}|^2} + \frac{1}{2V} \sum_{\mathbf{k}, \mathbf{q} \neq 0} \tilde{V}_{\text{int}}(\mathbf{k} - \mathbf{q}) \left(\frac{g_{\mathbf{k}}^*}{1 - |g_{\mathbf{k}}|^2} \right) \left(\frac{g_{\mathbf{q}}}{1 - |g_{\mathbf{q}}|^2} \right) \\ &+ \frac{1}{2V} \sum_{\mathbf{k}, \mathbf{q} \neq 0} [\tilde{V}_{\text{int}}(\mathbf{k} - \mathbf{q}) + \tilde{V}_{\text{int}}(0)] \left(\frac{|g_{\mathbf{k}}|^2}{1 - |g_{\mathbf{k}}|^2} \right) \left(\frac{|g_{\mathbf{q}}|^2}{1 - |g_{\mathbf{q}}|^2} \right) \end{aligned} \quad (4.5)$$

Similarly, one can calculate that

$$\langle \Psi_{\text{var}} | \dot{\Psi}_{\text{var}} \rangle - \langle \dot{\Psi}_{\text{var}} | \Psi_{\text{var}} \rangle = c_0^* \dot{c}_0 - \dot{c}_0^* c_0 + \frac{1}{2} \sum_{\mathbf{k} \neq 0} \frac{g_{\mathbf{k}}^* \dot{g}_{\mathbf{k}} - \dot{g}_{\mathbf{k}}^* g_{\mathbf{k}}}{1 - |g_{\mathbf{k}}|^2}. \quad (4.6)$$

These ingredients allow us to find the Euler-Lagrange equations of motion

$$\frac{d}{dt} \left(\frac{\partial \mathcal{L}}{\partial \dot{\alpha}} \right) - \frac{\partial \mathcal{L}}{\partial \alpha} = 0, \quad (4.7)$$

where α is any variational parameter. When the smoke clears, we have

$$\begin{aligned} i\hbar \dot{c}_0 &= \frac{\partial \langle \hat{H} \rangle}{\partial c_0^*} \\ &= n \tilde{V}_{\text{int}}(0) c_0 + \frac{1}{V} \sum_{\mathbf{k} \neq 0} \tilde{V}_{\text{int}}(\mathbf{k}) \frac{c_0^* g_{\mathbf{k}} + c_0 |g_{\mathbf{k}}|^2}{1 - |g_{\mathbf{k}}|^2} \end{aligned} \quad (4.8)$$

and

$$\begin{aligned} i\hbar \dot{g}_{\mathbf{k}} &= (1 - |g_{\mathbf{k}}|^2)^2 \frac{\partial \langle \hat{H} \rangle}{\partial g_{\mathbf{k}}^*} \\ &= 2 \left(\varepsilon_k + n \tilde{V}_{\text{int}}(0) \right) g_{\mathbf{k}} + \frac{\tilde{V}_{\text{int}}(\mathbf{k})}{V} \left[c_0^2 + c_0^{*2} g_{\mathbf{k}}^2 + 2 |c_0|^2 g_{\mathbf{k}} \right] \\ &+ \frac{1}{V} \sum_{\mathbf{q} \neq 0} \tilde{V}_{\text{int}}(\mathbf{k} - \mathbf{q}) \frac{2 |g_{\mathbf{q}}|^2 g_{\mathbf{k}} + g_{\mathbf{q}} + g_{\mathbf{q}}^* g_{\mathbf{k}}^2}{1 - |g_{\mathbf{q}}|^2} \end{aligned} \quad (4.9)$$

In writing these equations of motion, we have used the fact that they conserve mean total particle number³ to make the replacement $\frac{1}{V} \left(|c_0|^2 + \sum_{\mathbf{k} \neq 0} \frac{|g_{\mathbf{k}}|^2}{1 - |g_{\mathbf{k}}|^2} \right) \rightarrow n$. We solve these coupled ODEs numerically, assuming that $g_{\mathbf{k}}(t)$ depends only on the magnitude of the momentum k .

It is interesting to note that our equations of motion (derived from an ansatz for the quantum state) map directly onto the time-dependent Hartree-Fock-Bogoliubov (HFB) formulation. In that

³ Proving this requires messy algebra.

case, one expands the Heisenberg-picture field operator as

$$\hat{\psi}(\mathbf{r}, t) \approx \Phi_0(t) + \frac{1}{\sqrt{V}} \sum_{\mathbf{k} \neq 0} e^{i\mathbf{k} \cdot \mathbf{r}} \left(u_{\mathbf{k}}(t) \hat{b}_{\mathbf{k}} + v_{\mathbf{k}}^*(t) \hat{b}_{-\mathbf{k}}^\dagger \right), \quad (4.10)$$

where Φ_0 is the condensate component and the $u_{\mathbf{k}}(t)$ and $v_{\mathbf{k}}(t)$ are quasiparticle amplitudes. After making certain mean-field approximations [72], one can write coupled equations of motion for $\Phi_0(t)$ and $\{u_{\mathbf{k}}(t), v_{\mathbf{k}}(t)\}$. It is then straightforward to show that our parameter $g_{\mathbf{k}}(t)$ and the HFB quantity $v_{\mathbf{k}}^*(t)/u_{\mathbf{k}}^*(t)$ satisfy exactly the same equations of motion. This equivalence between our variational calculation and the HFB formalism was suggested recently in Ref. [138]. Our variational treatment thus suffers from the same spurious low-energy gap as found in HFB; however, because this unphysical gap should manifest itself at longer time scales, this should not hinder our study of short-time behavior. This is a motivating reason why HFB was able to adequately simulate [99] the coherent atom-molecule oscillations observed a decade ago [48], the main results of which can be reproduced by our single-channel variational model. Our formalism also reduces to time-dependent Bogoliubov theory [125] once the usual approximations are made: replace the operators \hat{a}_0 and \hat{a}_0^\dagger by the constant $\sqrt{N_0}$, neglect quartic interaction terms of noncondensed particles in Eq. (4.3), and use a coupling constant $U_\Lambda \rightarrow U_0 = 4\pi\hbar^2 a_f/m$ as in Section 3.3.

4.3 Post-Quench Dynamics

We have solved the equations of motion (4.8)-(4.9) for densities and interaction ranges that are typical for Alkali-atom experiments. In particular, our simulations assumed a density of $n = 5 \times 10^{12} \text{ cm}^{-3}$, which approximately matches the average density probed in the JILA experiment [112]. One can use the density to define useful momentum and energy units as $k_F = (6\pi^2 n)^{1/3} \approx 1/(2800a_0)$ and $\hbar\omega_F = \frac{\hbar^2 k_F^2}{2m} \approx \hbar/(61 \mu\text{s})$, respectively. To test the robustness of our theory, we have employed three different models of resonant interactions: a square well, a Gaussian well, and

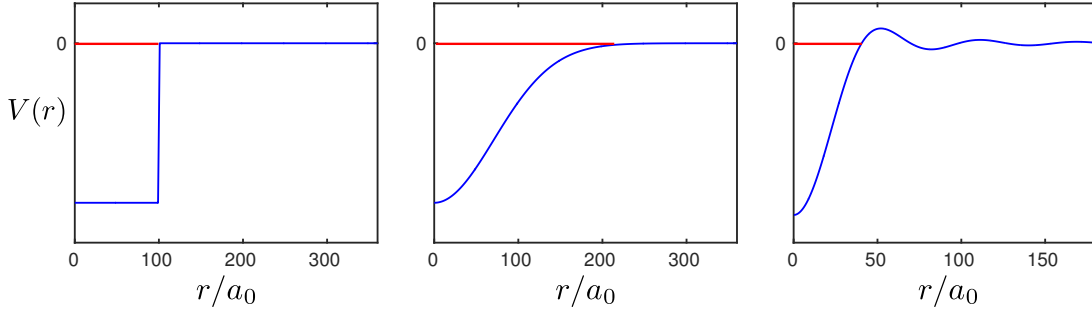


Figure 4.1: Three potential models for resonant interactions, as in Eq. (4.11). From left to right, we have the square well, Gaussian well, and the contact model. In each case, the depth of the well is chosen so that there is a two-body bound state with vanishing binding energy, depicted in red.

the contact model given by Eqs. (2.28) and (2.31). Their potentials are respectively given by

$$\begin{aligned}
 V_{\text{int}}(r) &= -\left(\frac{\pi}{2}\right)^2 \Theta(r_0 - r) \frac{\hbar^2}{mr_0^2} \\
 V_{\text{int}}(r) &= -2.68e^{-r^2/r_0^2} \frac{\hbar^2}{mr_0^2} \quad , \\
 \tilde{V}_{\text{int}}(k) &= -2\pi^2 \Theta(\Lambda - k) \frac{\hbar^2}{m\Lambda}
 \end{aligned} \tag{4.11}$$

where the depths have been chosen so that there is a two-body bound state of vanishing binding energy ($a \rightarrow \pm\infty$). We fixed the range to be $r_0 = 100a_0$ for the square and Gaussian wells, and we chose the momentum cutoff of the contact model to be $\Lambda = 100\pi k_F \approx 1/(9a_0)$ to get a better sense for the zero-range limit. These potentials are depicted in Fig. 4.1.

Our numerical solution of Eqs. (4.8)-(4.9) was performed with a 4th order Runge-Kutta scheme in MATLAB [143]. We replaced sums with integrals using the usual relation $\frac{1}{V} \sum_{\mathbf{k} \neq 0} \rightarrow \int \frac{d^3k}{(2\pi)^3}$. For the Gaussian-well calculations, we discretized momentum into 4095 evenly-spaced grid points up to a maximum of $5\pi/r_0$; for the square-well calculations, we used 16383 grid points up to the same maximum; for the contact model, we used 16383 grid points up to the cutoff Λ . The chosen grid sizes all have the form $2^m - 1$ for some integer m , as this optimizes the speed of discrete sine transforms in MATLAB. These sine transforms are helpful for spectrally evaluating the convolution integral in Eq. (4.9) via the convolution theorem [2]. It is worth pointing out that our discretizations are sufficient to resolve physics on both length scales appearing in the equations

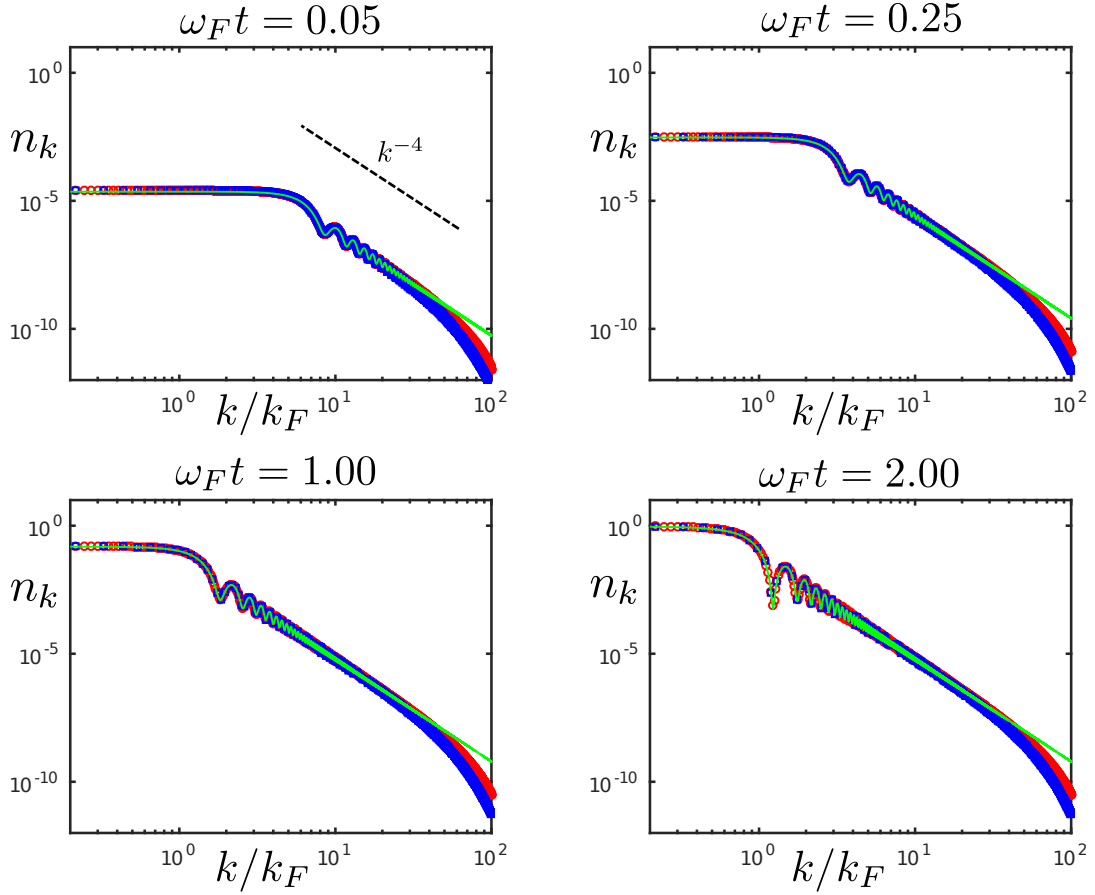


Figure 4.2: Dynamical momentum distribution of ^{85}Rb atoms at several times after quenching from noninteracting to unitarity, given a density of $n = 5 \times 10^{12} \text{ cm}^{-3}$. The red circles, blue squares, and solid green lines correspond respectively to the square well, Gaussian well, and contact interaction models, as in Eq. (4.11). In the first frame, the dashed line denotes generic k^{-4} scaling, for comparison.

of motion: the interaction range and the particle spacing.

The dynamical momentum distributions are plotted in Fig. 4.2 at several instants in time after the quench to unitarity. We can immediately observe that the three interaction models in Eq. (4.11) lead to the same dynamics over the range of momenta satisfying $k \ll r_0^{-1}$. At larger k , range effects predictably seep into the dynamics, as expected from the effective range expansion (2.3); nevertheless, these modes remain relatively unpopulated and thus contribute very little to the overall momentum distribution. The agreement between models shows that our solution method is robust against the arbitrariness of how we treat the short-range, resonant interactions. All calculations indicate that the system rapidly ($t \gtrsim mr_0^2/\hbar$) develops a k^{-4} tail in the large- k limit that first appears at large momenta and propagates into smaller momenta.⁴ We also observe subleading oscillatory structure. For the times shown, the low-momentum modes grow in approximate unison.

We reran our square-well simulations at the reduced density $n = 2 \times 10^{12} \text{ cm}^{-3}$ to see if our results displayed universality, as suggested in the experimental study [112]. Figure 4.3 compares these results against those of the previous density. The left-hand plot shows the dynamical distributions at the same instant in time and as a function of momentum in SI units; the results are quantitatively different. The right-hand plot shows the distributions after rescaling momenta and time by k_F and ω_F respectively, which are different for the two densities. (Note that we are now plotting the two sets of numerical data at different instants in time.) With this rescaling, the distributions agree quantitatively. We therefore infer that the dynamics of our variational model are universal. There is a sense in which this universality is mathematically equivalent to the model independence shown already in Fig. 4.2. If one writes the equations of motion in these density-derived units, then the only intrinsic parameter of the problem is $k_F r_0$. Thus, the two calculations discussed in this paragraph would appear to be identical except that they use resonant square wells of “different” range, due to their different values of $k_F r_0$. As evident in Fig. 4.2, the resulting dynamics should not depend on these details as long as this range remains small.

⁴ In analogy with Tan’s results (see Section 2.3), our invoking the “large- k limit” will always entail the stipulation $kr_0 \ll 1$.

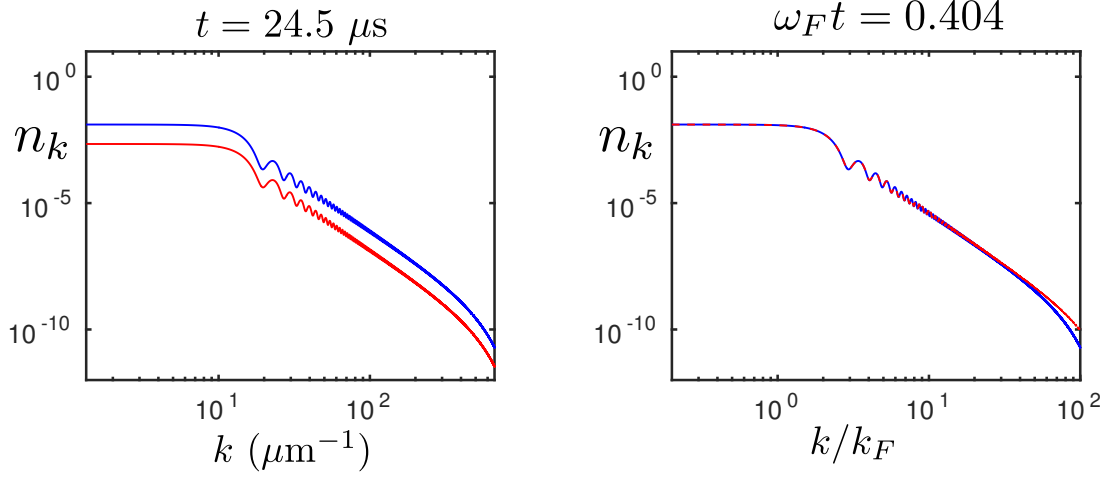


Figure 4.3: Dynamical momentum distribution of ^{85}Rb atoms after quenching from noninteracting to unitarity, for two different densities. The blue lines correspond to the density $n = 5 \times 10^{12} \text{ cm}^{-3}$, and the red lines correspond to the density $n = 2 \times 10^{12} \text{ cm}^{-3}$. Both distributions are calculated with the same attractive square well potential of range $r_0 = 100a_0$. On the left, we show these distributions as a function of momentum in fixed SI units at the same instant in time. On the right, we plot the computed distributions with time and momentum rescaled by the density units ω_F^{-1} and k_F , respectively.

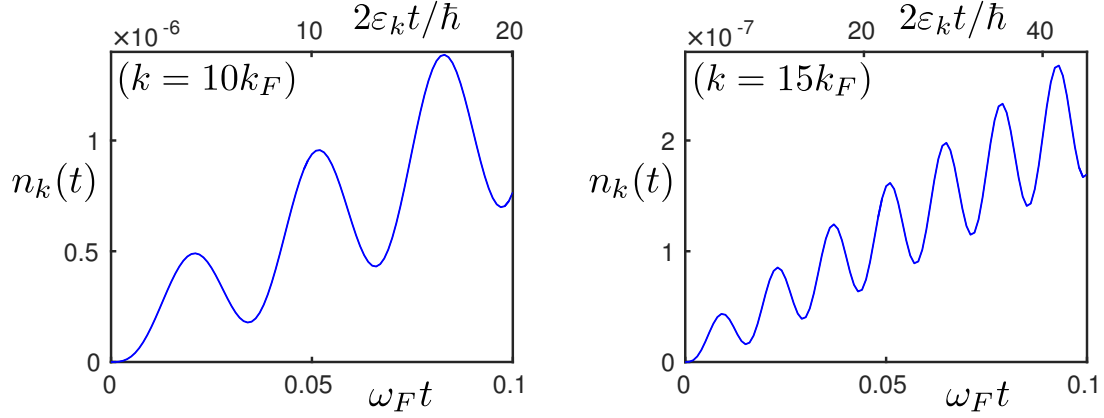


Figure 4.4: Population dynamics of a single mode immediately after the quench. On the left, we show the dynamics for the mode $k = 10k_F$. On the right, we show the dynamics for the mode $k = 15k_F$ over the same time interval. The bottom horizontal axis shows the time scaled by ω_F , and the top shows the time scaled by $2\varepsilon_k/\hbar$.

We now look more carefully at the oscillatory structure of the momentum distribution. These oscillations can be viewed more transparently in the population dynamics of a single mode. Figure 4.4 shows the time-dependent population of modes $k = 10k_F$ (left) and $k = 15k_F$ (right) shortly after the quench. Comparing the two populations, we find that the mode with larger k oscillates with a larger frequency and with a reduced amplitude relative to its (linearly-growing) offset. These oscillations occur with approximate frequency $2\varepsilon_k/\hbar$ in our simulations, as can be seen if one rescales time by this quantity (upper horizontal axis). Analyzing our numerics, we have found that the amplitude of these oscillations decays as k^{-5} in the large- k limit at all times after the quench. Similar oscillations have been observed in time-dependent Bogoliubov calculations for quenched systems [125, 85, 175], and Chapter 6 will demonstrate that they are the signature of ballistic correlation waves. We expect on physical grounds that quasiparticle collisions (which are mostly absent from our ansatz) will lead to damping, although it is difficult to model this quantitatively without introducing a certain amount of arbitrariness to the theory [137, 138, 92, 93, 94]. The general lack of oscillations in the JILA experiment [112] suggests that damping may play an important role in the late-time dynamics of the unitary Bose gas. In contrast, damping seemed less significant for the weakly-quenched BEC system described in Ref. [85].

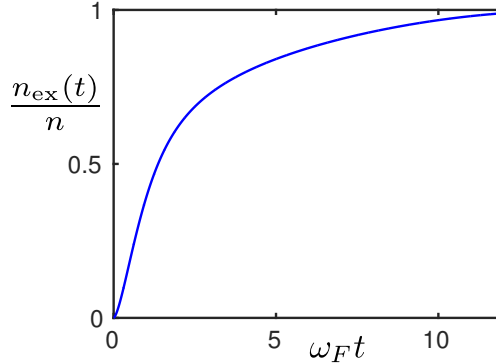


Figure 4.5: Depletion dynamics after the quench to unitarity, calculated using the square well model described in Eq. (4.11).

We calculate the total fraction of excited particles to get a sense for the speed at which resonant interactions deplete the BEC. This quantity is given by

$$\frac{n_{\text{ex}}(t)}{n} = \frac{1}{nV} \sum_{\mathbf{k} \neq 0} n_{\mathbf{k}}(t) = 1 - \frac{n_0(t)}{n}, \quad (4.12)$$

and we plot it in Fig. 4.5. Our numerics suggest that, immediately after the quench, the depletion fraction grows as $\sim 0.6 (\omega_F t)^{3/2}$. This should be contrasted with the predictions of time-dependent Bogoliubov theory, which suggest a scaling of \sqrt{t} after an interaction quench [125, 175, 89]. In our case, the depletion remains small shortly after the quench, and the heuristics motivating our ansatz (4.1) are self-consistently satisfied. This is no longer the case at late times, however. Our model predicts that all of the atoms are eventually expelled from the condensate. Hence, the main assumptions of our theory are only satisfied at relatively short times. It is worth mentioning, though, that the Hartree-Fock-Bogoliubov calculations of Ref. [99] gave a good description of atom-molecule coherence measurements [48] even when the depletion (4.12) was greater than 50%. This fact inspires hope that our theory might still capture relevant short-range physics, such as the contact dynamics, at intermediate times after the quench.

The dynamical contact can be computed by taking the large- k limit of the momentum distribution, similar to Eq. (3.40). As a practical matter, this limit is least ambiguous for the contact model with large Λ due to the relative lack of range effects in that case. The results are shown in

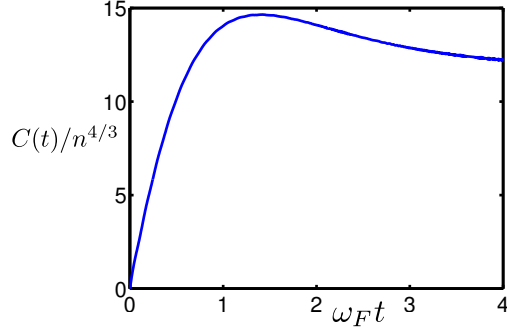


Figure 4.6: Contact dynamics after the quench to unitarity.

Fig. 4.6. As implied by the large- k dynamics in Fig. 4.4, the initial contact growth is linear:

$$C(t) \approx 26.9 n^{4/3} \omega_F t, \quad (4.13)$$

where the leading factor comes from a numerical fit. This linear growth is already qualitatively different from what one finds in time-dependent Bogoliubov theory, where the contact is mistakenly predicted to change discontinuously after a quench [125].⁵ We can extract the finite saturation timescale τ_C by fitting our numerical data to an exponential function $\Delta C(1 - e^{-t/\tau_C})$, exactly as in the experiment [112]. We find that the contact (and therefore all large- k modes) saturates in a time given by $\tau_C \approx 0.4\omega_F^{-1}$, which is consistent with the measured equilibration time of the largest momentum modes reported in Figure 5 of Ref. [112]. For $k > 2k_F$, the observed timescales are scattered within the range $\tau \in [0.1, 0.5]\omega_F^{-1}$.

At long times, we see that the contact saturates to a value of approximately $12n^{4/3}$. To give some context, predictions for C in the unitarity ground state can be found in Refs. [45, 149, 161, 36, 139], and they range from $9 - 32n^{4/3}$. The measured momentum distribution in the JILA experiment did not have enough signal-to-noise at large k to distinguish the contact. We should note, though, that our prediction is consistent with the measured late-time data shown in the inset of Figure 3 in Ref. [112]. Our model predicts that their plotted quantity, denoted as $\kappa^4 n(\kappa)$,⁶ should asymptote to $12/(6\pi^2)^{1/3} \approx 3$. This is consistent with the scatter in their data

⁵ The failure of time-dependent Bogoliubov theory to describe contact dynamics will be discussed in more detail in the next chapter.

⁶ They define $\kappa \equiv k/k_F$ and normalize $n(\kappa)$ such that $\int \frac{d^3\kappa}{(2\pi)^3} n(\kappa) = 1$.

at large momentum, which ranges from about 2 to 5 for $k > 2.5k_F$; unfortunately, there is not enough dynamic range to identify a clear asymptote. The authors of Ref. [144] separately analyzed the JILA data while making nontrivial assumptions about three-body universality violations,⁷ and they suggested that the late-time contact should be approximately $22n^{4/3}$. Perhaps a future version of the experiment will measure the contact directly. There are empirical and theoretical indications that the large-momentum modes saturate long before three-body loss kicks in, and one could perform RF spectroscopy [174] after this saturation occurs. Given the large separation in saturation and loss timescales, resolving the late-time contact should be possible even with relatively long RF pulses.

4.4 Summary and Discussion

Inspired by recent experimental results [112], we have used a time-dependent variational approach to explore the dynamics of a BEC that is quenched from noninteracting to unitarity. Our many-body model is based on the idea that the BEC depletes continuously after the quench, with pairs of condensate atoms scattering off each other with equal and opposite momentum. The calculation encodes two-body correlations while ignoring three-body effects, which are difficult to include in a many-body model. We have demonstrated that our approach is robust in the sense that the computed dynamics do not depend on the details of how we model the short-range, resonant interactions. We found that the dynamics scale universally with the appropriate density-dependent units, a result that seemed present in the published measurements but is still under experimental investigation. It is expected that any deviations from universality should be due to Efimov physics, which would be interesting to see in a nonequilibrium scenario.

We focused our attention on the evolution of the momentum distribution after the quench. We observed the rapid growth of a k^{-4} tail whose saturation time and value are consistent with the large-momentum measurements of Ref. [112]; however, further experimental work is necessary

⁷ These assumptions include the idea that the momentum distribution violates universality, while the two-body and three-body contacts do not. It is also assumed that the momentum range $k \in [1.5, 3]k_F$ is within the asymptotic regime where populations are governed by short-range correlations via the contact.

to identify the contact of the unitary Bose gas. In addition to the k^{-4} tail, we also saw subleading oscillations with frequency $\sim k^2$ and amplitude $\sim k^{-5}$ for large k . The total fraction of excited particles was found to scale as $t^{3/2}$ shortly after the quench, indicating that the BEC survives longer than Bogoliubov theory would suggest [175, 89].

About a year after we published this work [150], another theoretical development came along in the form of the Hyperbolic Bloch equations [92, 93, 94]. This new formulation is inspired by ideas from semiconductor physics [109], and it introduces phenomenological damping and dephasing to mean-field-like equations that are similar to the Hartree-Fock Bogoliubov framework. Like our variational model, this new formulation of the problem manifestly includes two-body correlations while ignoring Efimov physics. A major result of that study is that there exists an optimal choice of phenomenological parameters for which the theoretical momentum distribution agrees quite well with the experimental measurement, even at late times and small momentum. We have checked that, given the proposed free parameters, the model in Ref. [93] yields essentially the same short-time predictions for the contact and depletion growth as our variational model.⁸ In the next chapter, where we focus only on short-time quench dynamics at arbitrary scattering length, we employ our variational model.

⁸ The late-time predictions of the newer model depend quantitatively on the choice of phenomenological damping and dephasing parameters.

Chapter 5

Bound-State Signatures in Quenched BECs

Results presented in this chapter were published in Ref. [38].

5.1 Preliminaries

Rapid interaction quenches represent a possible pathway to creating exotic quantum states. This much is clear from the unitary BEC experiment [112] discussed in the previous chapter, which was able to explore the strongly-interacting regime that had been so elusive to both theory and experiment. The surprisingly-long lifetime of the gas in that setup has been attributed to the projective nature of the quench: The initial condition projects mainly onto long-lived states, thereby limiting inelastic loss [150]. Similar ideas play out in a 1D gas of hard-core bosons (a so-called “Tonks-Girardeau gas”) that is suddenly quenched to strong attraction. The resulting state, known as the “super-Tonks-Girardeau gas” [3], has a long lifetime despite the strong attractive interactions. This attraction would normally lead to rapid decay into a clustered state; however, the initial state is anti-clustered and does not project (much) onto eigenstates that are clustered, so minimal decay occurs. Experiments with quasi-1D BECs, in which radial motion is frozen out by tight confinement, have confirmed this prediction [76].

Interaction-quenched BECs have proven to be fascinating even outside of the the strongly-interacting regime. As mentioned in Section 3.3, homogeneous condensates are dynamically unstable for $a < 0$. In a trap, however, the nonzero kinetic energy can stabilize the system against collapse for small, negative a . In one experiment [49], a weakly-interacting BEC ($a_i > 0$) was

suddenly quenched across the stability threshold to a point where the gas was expected to be unstable. Violent collapse dynamics ensued, including an implosion followed by an explosion.¹ The sequence was artfully termed “bosonovae”. In another study [48], a multi-quench Ramsey sequence was used to put condensed atoms into a superposition of scattering and bound states. Such exotic states were found to occur in the dynamics even when the BEC was in the weakly-interacting regime, where $na^3 \ll 1$.

These exciting experimental developments have inspired a number of theoretical studies on the topic of nonequilibrium BECs near Fano-Feshbach resonances. Much of the early work a decade ago used two-channel resonance models embedded in a mean-field-like theory [159, 80, 99, 111, 97, 96, 120, 50, 51, 52, 70, 98, 145]. These models had sufficient flexibility to account for species-specific effective-range corrections to scattering and binding, which can be important either by narrow resonances or at large detunings away from a broad resonance. A common theme throughout these investigations was that bound-state physics can be important to the nonequilibrium dynamics of BECs, a fact that was underscored by the atom-molecule-coherence experiment described in Ref. [48]. This idea has been underappreciated in recent years, with many theories of quench phenomena being based on the time-dependent Bogoliubov (or Popov) formulation [25, 125, 175, 176, 89, 138], which lacks a bound state. These theories can be accurate only in the regime where quenches are adiabatic with respect to the bound state. Otherwise, pairs of atoms can project nontrivially onto the bound state of the new Hamiltonian.

In this chapter, we examine the effect of the bound state on the short-time, short-range correlations of a BEC that is quenched suddenly from one scattering length to another. Our focus is the dynamical response of Tan’s contact to the quench, and we find that it exhibits high-contrast oscillations occurring at a frequency $\omega_B = -E_B/\hbar$, where $E_B < 0$ is the binding energy of the Feshbach-molecular bound state. We first approach this phenomenon using the many-body variational model described in the previous chapter. The contact oscillations are shown to be

¹ The explosion was on an atomic scale, having only a few thousand atoms reaching “hot” temperatures of a few hundred nK.

significant for realistic quench times near the ^{85}Rb Fano-Feshbach resonance at 155 G. We then present exactly solvable two-body models that paint a simplified picture of the contact dynamics. We introduce an intuitive calibration scheme that unambiguously links these models to many-body physics; our prescription unifies the few-body predictions across a broad class of exactly-solvable models, while yielding analytic formulas that agree with the less-transparent, many-body numerics. Strikingly, we find that the dynamical correlations are larger than Bogoliubov theory would suggest, and a diabatic reduction of the scattering length is shown to increase pair correlations. This feature is surprising, considering that a smaller scattering length is often associated with “weaker” interactions. Our two-body models illustrate that these exciting results are a direct consequence of bound-state physics.

5.2 Many-body Phenomenon

We consider a homogeneous BEC of density $n = 10^{12} \text{ cm}^{-3}$ that is quenched from noninteracting ($a_i = 0$) to $a_f = 700a_0$. These values are reasonable for a hypothetical ^{85}Rb experiment. Within the zero-range approximation, this final scattering length corresponds to a binding energy of $\hbar\omega_B = \frac{\hbar^2}{ma_f^2} \approx \hbar/(2 \mu\text{s})$. The dynamics are computed using the time-dependent variational formulation presented in Section 4.2, with an interaction potential chosen to yield the desired scattering lengths. We showed in the previous chapter that the dynamics for modes $kr_0 \ll 1$ are independent of the choice of potential model;² hence, without loss of generality, we use the contact potential of Eqs. (2.28) and (2.31) as this gives us better access to the physics at large k . We account for the finite ramp rate of experimental quenches by letting the scattering length of our model be time dependent. We model these ramps using the scattering length profile of ^{85}Rb atoms near the resonance at $B_0 = 155.04 \text{ G}$:

$$a(t) = a_{\text{bg}} \left(1 - \frac{\Delta}{B(t) - B_0} \right), \quad (5.1)$$

² At finite scattering length, we find that this independence requires $a \gg r_0$ or $\Lambda a \gg 1$, where range effects do not change the binding energy appreciably.

where the resonance width is $\Delta = 10.7$ G and the background scattering length is $a_{\text{bg}} = -443a_0$ [33]. We assume linear ramps in the magnetic field. This results in a nonlinear evolution of $a(t)$ and $U_\Lambda(t)$ during the ramp. The equations of motion (4.8)-(4.9) are solved numerically with the same method as described in Section 4.3, except that we use a momentum grid of 8191 evenly-spaced points up to a cutoff of $\Lambda = 200\pi k_F \approx 1/(8a_0)$. At all instants in time, we find that there is a well-defined k^{-4} tail, which we use to extract the dynamical contact.

Figure 5.1 shows the time evolution of Tan's contact for several different quench speeds. We see that the contact oscillates at approximately the frequency of the bound state, ω_B , and the contrast of these oscillations is strikingly large even when we account for the finite ramp rate of $\dot{B}_{\text{exp}} = 1.6$ G/ μs reported in the JILA experiment [112]. The nature of the interference leading to these oscillations will become apparent in the careful two-body calculation of Section 5.3. We stress that these dynamics are quite different from those predicted by time-dependent Bogoliubov theory.

For the case of an instantaneous quench, it is difficult to define a contact in Bogoliubov theory because the momentum distribution does not have a well-defined k^{-4} tail [125]. However, such a tail exists as long as the ramp time t_R is nonzero, and it occurs at momenta such that $\hbar k^2 t_R / m \gg 1$. Large-momentum quasiparticles adiabatically follow the scattering length in this case, and the contact thus saturates quickly to a new equilibrium value [see Eq. (3.40)]

$$C_0 = 16\pi^2 n^2 a_f^2 \tag{5.2}$$

over the arbitrarily-small time scale of the quench, regardless of the initial scattering length. These trivial dynamics are plotted as the horizontal red line in Fig. 5.1, and they are in stark contrast to the strong oscillatory behavior predicted by our variational theory. The peak-to-trough oscillation amplitude remains as large as C_0 itself when the experimental ramp rate is decreased by a factor of 10. Further reducing the ramp rate eventually results in a quench that is adiabatic with respect to the bound state, in which case the variational and time-dependent Bogoliubov theories agree and give a nonoscillating contact.

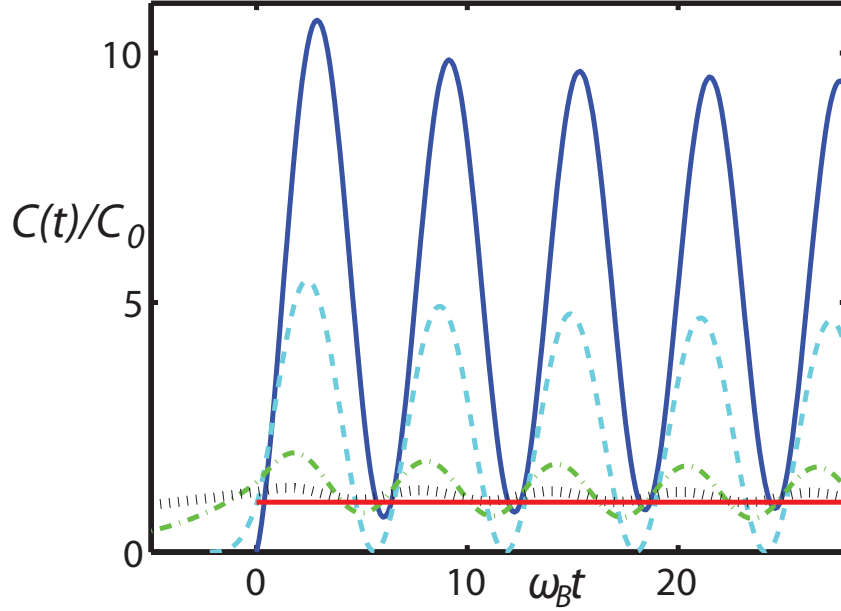


Figure 5.1: Contact dynamics following a quench from noninteracting to $700a_0$, for several ramp speeds near the ^{85}Rb Fano-Feshbach resonance at 155.04 G. We assume a density of 10^{12} cm^{-3} . As a reference, the red (horizontal) line represents the prediction from Bogoliubov theory, $C_0 = 16\pi^2 n^2 a_f^2$, which specifies the units of the plot. The blue (oscillating, solid) line is the many-body-variational prediction for a quench that is completely diabatic, the cyan (dashed) line is for the experimental ramp speed of $\dot{B}_{\text{exp}} = 1.6 \text{ G}/\mu\text{s}$ [112], the green (dot-dashed) line is for a ramp speed of $\dot{B}_{\text{exp}}/10$, and the black (dotted) line is for a ramp speed of $\dot{B}_{\text{exp}}/50$. In each case, the time $t = 0$ defines the end of the magnetic field ramp.

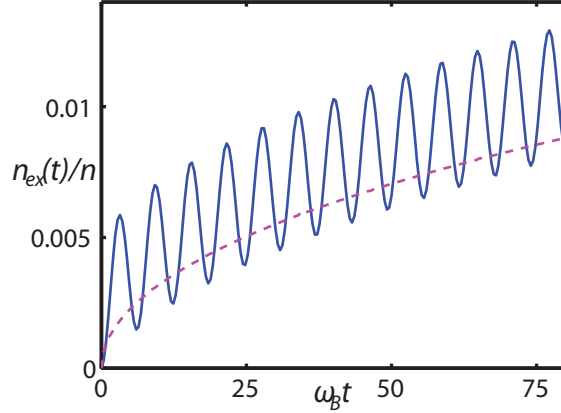


Figure 5.2: Excitation fraction following a diabatic quench from noninteracting to $700a_0$, for a BEC of density $n = 10^{12} \text{ cm}^{-3}$. The blue line is the prediction of our many-body-variational formulation. The magenta line is the prediction from Bogoliubov theory.

One can sense the limitations of the Bogoliubov description of diabatic quench experiments by considering momentum cutoffs heuristically. Recall from Section 3.3 that using the coupling constant $U_\Lambda \rightarrow 4\pi\hbar^2 a_f/m$ in the theory, as required within the Bogoliubov approximation, requires that the momentum cutoff satisfy $\Lambda a_f \ll 1$. There is no bound state in this limit, and any important physics occurring uniquely on the time scale ω_B^{-1} and length scale a_f of the bound state is therefore absent in time-dependent Bogoliubov theory [25, 125, 175, 176, 89, 138]. When the quench is adiabatic with respect to the bound state [105], the ramp time is at least consistent with the shortest timescale describable by the theory, where $t_R > (\hbar\Lambda^2/m)^{-1} \gg \omega_B^{-1}$. That is precisely the regime in which Bogoliubov theory correctly describes the contact dynamics, as shown in Fig. 5.1.

These bound-state oscillations also occur in the depletion of the condensate, defined by Eq. (4.12). Figure 5.2 shows the time evolution of this quantity after a sudden quench, computed both within the variational and Bogoliubov theories. As mentioned in the previous chapter, Bogoliubov theory predicts that the depletion grows as \sqrt{t} at short times [125]. This correctly captures the initial growth of the depletion except for the large-amplitude oscillations. The nonoscillatory contribution to this growth comes mainly from momenta that are too small to probe bound-state effects ($ka_f \ll 1$), whereas the oscillating component is due to the aforementioned contact dynamics (occurring at $ka_f \gtrsim 1$). Similar oscillations have been discussed previously in the theory literature

[159, 80, 50, 52], and they received only a brief mention in the experimental results of Ref. [48]. To date, there is no published data on the subject, although some preliminary observations of these condensate oscillations can be found in Ref. [31].

5.3 Two-Body Models

Two-body models afford another intuitive description of BEC quench dynamics. In some cases, they are exactly solvable [154, 22], and they can paint relatively transparent pictures of nonequilibrium physics [15, 70, 119, 13, 69] that are sometimes obscured by the mathematics of more sophisticated, many-body models. It was recently suggested that such models might even be made quantitatively accurate in their descriptions of short-time, large-momentum dynamics in quenched BEC systems [150], although an unambiguous, universal link to the many-body BEC problem has been absent in the literature. In this section, we establish such a link and derive analytic predictions for the contact dynamics following a diabatic quench of the scattering length near a broad Fano-Feshbach resonance.

5.3.1 Calibration

We consider the quantum dynamics of a pair of free-space atoms whose scattering length is quenched from an initial value $a_i \geq 0$ to a final value $a_f \geq 0$. Assuming zero momentum for the center of mass (as is the case for any pair of atoms that scatter out of a BEC), the post-quench dynamics are governed by the time-dependent Schrödinger equation

$$i\hbar \frac{\partial \psi(\mathbf{r}, t)}{\partial t} = -\frac{\hbar^2}{2\mu} \nabla^2 \psi(\mathbf{r}, t) + \frac{2\pi\hbar^2 a_f}{\mu} \delta(\mathbf{r}) \frac{\partial}{\partial r} [r\psi(\mathbf{r}, t)] \quad (5.3)$$

where $\psi(\mathbf{r}, t)$ is the wavefunction for the relative coordinate \mathbf{r} , $\mu = m/2$ is the reduced mass, and we model the short-range interactions of the system with the Fermi pseudopotential discussed in Section 2.2.2.

We can time-evolve an arbitrary spherically-symmetric initial condition by expanding in the basis of energy-normalized s -wave eigenfunctions of the Hamiltonian shown in Eq. (5.3). These

eigenfunctions are

$$\psi_k^{(S)}(r) = \frac{\sin(kr) - ka_f \cos(kr)}{r \sqrt{4\pi^2 \hbar^2 k (k^2 a_f^2 + 1)/m}} \quad , \quad E_k = \frac{\hbar^2 k^2}{m} \quad (5.4)$$

for the scattering states and

$$\psi_B(r) = \frac{e^{-r/a_f}}{r \sqrt{2\pi a_f}} \quad , \quad E_B = -\frac{\hbar^2}{ma_f^2} \quad (5.5)$$

for the bound state. Given an initial condition $\psi_0(r)$, the solution to Eq. (5.3) is [117]

$$\psi(r, t) = \int_0^\infty dE_{k'} e^{-iE_{k'}t/\hbar} \psi_{k'}^{(S)}(r) \int d^3r' \psi_{k'}^{(S)}(r') \psi_0(r') + e^{-iE_B t/\hbar} \psi_B(r) \int d^3r' \psi_B(r') \psi_0(r) \quad . \quad (5.6)$$

We then evaluate the momentum distribution by taking the Fourier transform of Eq. (5.6):

$$\tilde{\psi}(\mathbf{k}, t) = \int d^3r e^{-i\mathbf{k}\cdot\mathbf{r}} \psi(r, t). \quad (5.7)$$

Following our intuition from mean-field theory, we relate this two-body problem to the many-body system by considering the combined effect of a background, dilute BEC on the momentum distribution of a single particle. Assuming that this time-dependent, single-particle momentum distribution is normalized in the continuum via

$$1 = \int \frac{d^3k}{(2\pi)^3} |\tilde{\psi}(\mathbf{k}, t)|^2 \quad , \quad (5.8)$$

we compute the full momentum distribution by multiplying by the total density n [119, 70]. The combined effect of the dilute background gas is modeled by an appropriate choice of initial condition $\psi_0(r)$. Previous calculations of this type have placed the two-body system in a (fictitious) tight harmonic trap, whose frequency is chosen to reproduce either the total density n [13] or the approximate nearest-neighbor separation [150].³ Both of these prescriptions are limited in the sense that their quantitative predictions for short-distance dynamics depend strongly on the harmonic nature of the fictitious trap. In this sense, they are intrinsically semi-quantitative.

³ This reference estimated the mean nearest-neighbor spacing using the Wigner-Seitz radius $(4\pi n/3)^{-1/3}$, which is correct for an uncorrelated gas up to a factor of $\Gamma(4/3) \approx 0.89$. Including this factor in that model would change the prediction for the contact slope upon quenching to unitarity by a factor of $\Gamma^{-3}(4/3) \approx 1.4$. See Ref. [26] for an exact calculation of the nearest-neighbor distribution.

The new prescription that we propose is motivated by the fact that a quench of zero-range interactions signifies a quench of a log-derivative boundary condition at $r = 0$:

$$\lim_{r \rightarrow 0} \frac{\partial_r (r\psi(r))}{(r\psi(r))} = -\frac{1}{a}, \quad (5.9)$$

as discussed in Section 2.2.2. As a result, the contact dynamics immediately following a quench occurs entirely in the short range. The most important feature of an initial condition $\psi_0(r)$ is therefore its behavior as $r \rightarrow 0$. Our first requirement is that $\psi_0(r)$ satisfy Eq. (5.9) for the initial scattering length of the system, a_i . (All of the eigenstates in our post-quench expansion basis, Eqs. (5.4)-(5.5), satisfy this log-derivative condition for the final scattering length, a_f .) Importantly, this log-derivative condition does not fix the absolute magnitude of $\psi_0(r)$ for small r ; any such scaling cancels in Eq. (5.9). We propose that this absolute scaling of the short-range wavefunction be fixed by the many-body problem. The quantity $|\psi_0(r)|^2$ represents the probability density of finding a background particle a distance r from the particle of interest, and this is given by $ng^{(2)}(r)$ in the many body-problem, where $g^{(2)}(r)$ is the two-body correlation function [131]. For a pure, noninteracting BEC, there are no correlations and $g^{(2)}(r) = 1$. If the initial scattering length is nonzero, however, short-range correlations are determined exclusively by the contact via Eq. (2.32). We thus calibrate the short-range behavior of the two-body wavefunction as follows:

$$\lim_{r \rightarrow 0} |\psi_0(r)|^2 = n \quad (a_i = 0) \quad (5.10a)$$

$$|\psi_0(r)|^2 \rightarrow \frac{C_i}{16\pi^2 nr^2} + \mathcal{O}\left(\frac{1}{r}\right) \quad (a_i > 0) \quad (5.10b)$$

where $C_i = 16\pi^2 n^2 a_i^2$ is the contact for the initial BEC, as derived in Eq. (3.40). Equation (5.10) guarantees that the initial probability of finding another particle near the particle of interest (within our simple model) matches that same probability for the many-body system before the quench. We hypothesize that these probabilities remain approximately equal in the dynamics that occurs shortly after the quench.

We now choose a set of initial two-body wavefunctions to test the robustness of our calibration scheme. We have been able to analytically evaluate the integrals in Eqs. (5.6)-(5.7) for the initial

conditions

$$\psi_0(r) = \begin{cases} A_0(a_i, L_0) \left(1 - \frac{L_0 a_i}{(L_0 - a_i)r}\right) e^{-r/L_0} \\ A_1(a_i, L_1) \left(1 - \frac{a_i}{r}\right) e^{-r/L_1} \left[1 + \frac{r}{L_1}\right] \\ A_2(a_i, L_2) \left(1 - \frac{a_i}{r}\right) e^{-r/L_2} \left[1 + \frac{r}{L_2} + \frac{1}{2} \left(\frac{r}{L_2}\right)^2\right] \end{cases} \quad (5.11)$$

where L_j is a free parameter for each initial condition, and $A_j(a_i, L_j)$ is a constant chosen to give unit normalization. The leading factor in parentheses enforces the log-derivative boundary condition, and the bracketed polynomial factors have been chosen to add variety to our treatment of the long-range wavefunction. The calibration given by Eq. (5.10) then completely fixes the short-range behavior, along with the free parameter L_j . The necessary integrations in Eqs. (5.6)-(5.7) can be carried out with a combination of contour integration and symbolic mathematical software, such as Mathematica. Appendix A lays out the steps of the solution.

5.3.2 Revisiting the Quench to Unitarity

A useful figure of merit for nonequilibrium physics is the momentum distribution after a quench from noninteracting ($a_i = 0$) to unitarity ($a_f = \infty$). We computed this quantity in the previous chapter using a many-body variational formulation. For our two-body models, the formulae for the exact momentum-space wave functions $\tilde{\psi}(k, t)$ are too complicated to usefully write down. Here, we include only the simplest formula as an example. The first initial condition in Eq. (5.11) evolves as

$$\tilde{\psi}(k, t) = \frac{8\sqrt{L_0}}{k(1+k^2L_0^2)^2} \left\{ (1-k^2L_0^2) \text{DawsonF} \left[\sqrt{i\frac{\hbar k^2 t}{m}} \right] + (1+k^2L_0^2) \sqrt{i\frac{\hbar k^2 t}{m}} \right. \\ \left. + e^{i\frac{\hbar t}{mL_0^2}} \sqrt{\pi} \left(kL_0 - i(1+k^2L_0^2) \frac{\hbar kt}{mL_0} \right) \text{erfc} \left[\sqrt{i\frac{\hbar t}{mL_0^2}} \right] \right\}, \quad (5.12)$$

where the Dawson function is defined by

$$\text{DawsonF}(z) \equiv e^{-z^2} \int_0^z dy e^{y^2}. \quad (5.13)$$

This wave function evolves continuously from its initial condition.

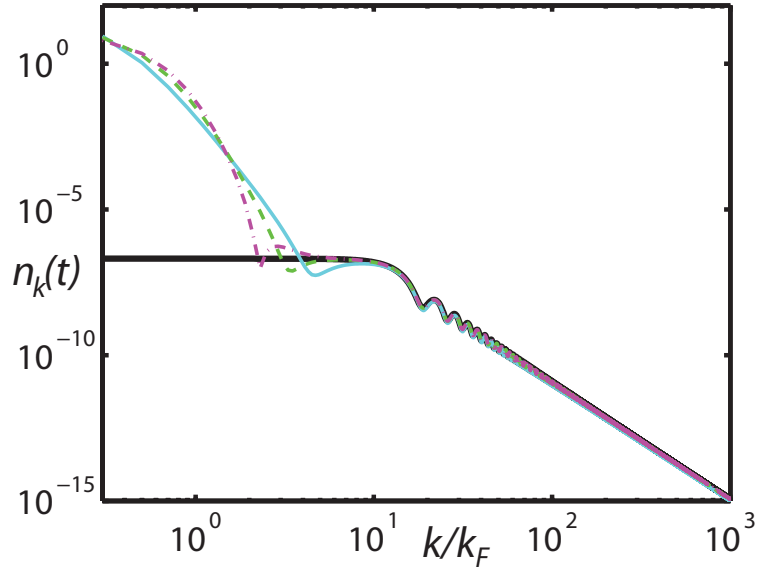


Figure 5.3: Momentum distributions at fixed time $\omega_F t = 0.01$ after a quench from noninteracting to unitarity. The thick black line is the numerical data from a many-body variational calculation at density $n = 5 \times 10^{12} \text{ cm}^{-3}$, using the contact interaction model. The thin lines are the analytically-computed two-body results. The cyan, green, and magenta lines respectively correspond to the properly-calibrated initial conditions in the order listed in Eq. (5.11).

The predicted momentum distributions from our two-body models are plotted in Fig. 5.3 at a fixed time shortly after the quench, and they are compared with the many-body numerics from Chapter 4. With the free parameter of each initial condition chosen in our prescribed manner, all results agree favorably at large momentum. Despite the various functional forms for the initial conditions in Eq. (5.11), all of our two-body wavefunctions predict that

$$C(t) = \frac{128\pi}{(6\pi^2)^{2/3}} n^{4/3} \omega_F t, \quad (5.14)$$

at short times, which agrees with the many-body variational prediction (4.13) to within less than two percent. Equation (5.14) also follows from applying our prescription to the Gaussian initial condition of Ref. [150], for which only the contact growth can be calculated analytically. The contact slope now appears to be independent of the arbitrary details of the two-body model.

We remark that the model independence of our large-momentum dynamics is nontrivial. If we had chosen each free parameter L_j by matching $\langle r \rangle$ to an estimate for the nearest-neighbor separation, the predicted slope of the contact would vary by almost an order of magnitude, depending on the chosen initial condition in Eq. (5.11).⁴ The approximate agreement between the two- and many-body models demonstrated in Ref. [150] is a result of the near-equivalence of the requirements that $\langle r \rangle \equiv (4\pi n/3)^{-1/3}$ and $|\psi_0(0)|^2 \equiv n$ for normalized Gaussian functions. As explained above, the latter requirement is more physically motivated, and it leads to improved agreement with the many-body results while unifying the large-momentum predictions of the various exactly-solvable two-body models. In the remainder of our discussion, we employ this calibration scheme.

Contact dynamics aside, our models also agree on the subleading oscillatory structure of the large-momentum dynamics, as shown in Fig. 5.3. As discussed in the previous chapter, these oscillations have phase $2\varepsilon_k t/\hbar$, where ε_k is the kinetic energy of a single particle of momentum k , and an amplitude that scales as k^{-5} . Each distribution shows distinct low-momentum behavior that is determined by the long-range characteristics of the initial conditions. We can infer from

⁴ This discrepancy is most pronounced for a Lorentzian initial condition $\psi_0(r) \sim 1/(r^2 + L^2)$, for which $\langle r \rangle$ is infinite and cannot be matched to the particle spacing. If this initial condition is calibrated as we propose, it yields Eq. (5.14).

Eq. (5.11) that these long-range features occur on a length scale that is set by the parameter L_j , which is of the order of the mean interparticle spacing for the gas. At such momentum scales, we expect many-body effects to determine the physics, and this limits the approximate validity of our two-body models to momenta $k \gg k_F$ and times $\omega_F t \ll 1$. These limits are implicit in all of the two-body results that follow.

5.3.3 Quenching to Finite Scattering Length

With our two-body models properly calibrated, we are well equipped to revisit and generalize the bound-state oscillations addressed in Sec. 5.2. We will see that the simple two-body approach illustrates the crucial role played by the bound state after a diabatic quench, while quantitatively describing the evolution of two-body correlations via the dynamical contact.

As a preliminary matter, our two-body approach leads to an intuitive understanding of bound-state oscillations. The basic structure of Eq. (5.6) suggests that the short range of the bound and scattering contributions may be compared to the two legs of a simple interferometer. The diabatic quench essentially projects the initial condition onto these two legs, and a different phase is acquired over each leg as time progresses, as evidenced by Eq. (5.6). The measured momentum distribution is always defined with respect to free-particle (noninteracting) momentum states, rather than the scattering states of Eq. (5.4); it is for this definition that the k^{-4} tail is meaningfully related to short-range density-density correlations via the contact [152, 147]. Hence, the two legs of the interferometer are recombined during a measurement of the momentum distribution, thereby projecting the quantum state onto the free-particle momentum basis as in Eq. (5.7). The phase evolution of the bound-state component leads to periodically-modulated interference that is most pronounced at the length scale of the bound state, $r \lesssim a_f$. As a result, the contact oscillates, along with certain other observables such as the condensate fraction (see Fig. 5.2).

As discussed previously, the various initial conditions of Eq. (5.11) lend themselves to analytical, time-dependent solutions for arbitrary initial and final scattering lengths. These formulae are

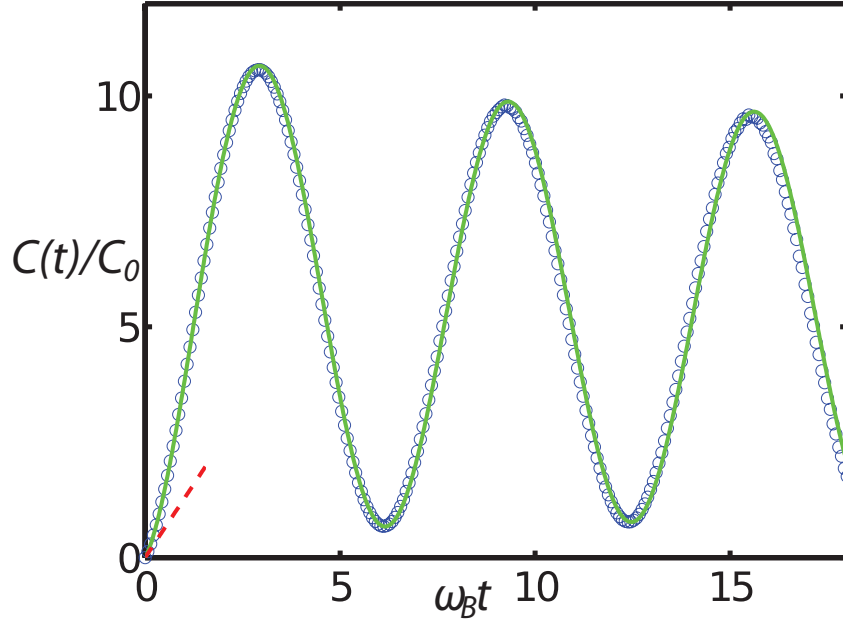


Figure 5.4: (Color online) Contact dynamics following a diabatic quench from noninteracting to $700a_0$, for a BEC of density $n = 10^{12} \text{ cm}^{-3}$. The circles represent the many-body-variational data computed with a momentum grid of 32767 evenly spaced points up to a cutoff $\Lambda = 2000\pi k_F$. (The cutoff is chosen to be large to make a better comparison with the zero-range theory assumed in the two-body model.) The green line represents the formula given in Eq. (5.15), and the red line represents the linear growth given in Eq. (5.14).

quite complicated in general, but, remarkably, they each predict the same behavior of the contact

$$C(t) = 16\pi^2 n^2 a_f^2 \left| 1 + \left(\frac{a_i}{a_f} - 1 \right) e^{i\omega_B t} \left(1 + \operatorname{erf} \left[\sqrt{i\omega_B t} \right] \right) \right|^2 \quad (5.15)$$

if we take the limits $na_i^3 \ll 1$ and $na_f^3 \ll 1$. Figure 5.4 plots this result against a many-body simulation for the diabatic quench considered already in Fig. 5.1. Apart from a slight offset in the oscillation frequency, the agreement is excellent. We believe that this small frequency deviation is due to the fact that our numerical solution of the many-body model is constrained to a finite (albeit large) momentum cutoff Λ , whereas our two-body models are truly zero-range. Any experimental realization of these oscillations would experience such an offset due to the finite range of true interatomic interactions. This was certainly the case in the Ramsey experiment of Ref. [48]. It is also possible that mean-field effects could shift the oscillation frequency [33], but this should not be significant in the small- na^3 limit that we are considering. Aside from the bound-state oscillations of the contact, the momentum distributions at small scattering length look essentially the same as in Fig. 5.3, including the subleading k^{-5} behavior mentioned previously.

It is useful to examine the general dynamics given by Eq. (5.15). At short times $\omega_B t \ll 1$, the contact evolves continuously from its initial value C_i as

$$C(t) = C_i + 32\pi^2 n^2 a_i (a_i - a_f) \sqrt{\frac{2}{\pi} \omega_B t} + \frac{128\pi}{(6\pi^2)^{2/3}} \left(\frac{a_i}{a_f} - 1 \right)^2 n^{4/3} \omega_B t + \mathcal{O}(t^{3/2}). \quad (5.16)$$

In the limit of vanishing initial scattering length, the contact first grows linearly according to Eq. (5.14) for all values of a_f . This is shown in Fig. 5.4 for the case of a quench to $a_f = 700a_0$. However, at nonzero initial scattering length, this linear growth is superseded by nonanalytic \sqrt{t} behavior. At later times $\omega_B t \gg 1$, the contact is oscillatory:

$$C(t) \approx 16\pi^2 n^2 a_f^2 \left[1 + 4 \left(\frac{a_i}{a_f} - 1 \right)^2 + 4 \left(\frac{a_i}{a_f} - 1 \right) \cos(\omega_B t) \right]. \quad (5.17)$$

For a diabatic quench upward ($a_f > a_i$), the time-averaged contact $\langle C(t) \rangle_t$ may be up to five times larger than the Bogoliubov prediction of $C_0 = 16\pi^2 n^2 a_f^2$, and the oscillation amplitude may be up

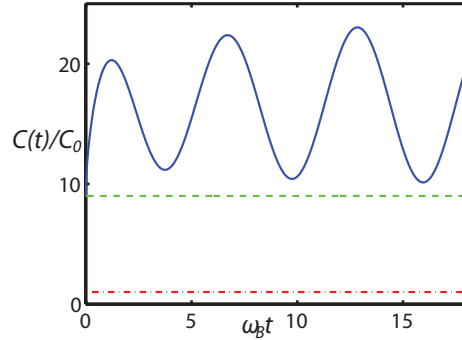


Figure 5.5: Contact dynamics following a diabatic quench downwards with $a_f = a_i/3$. For reference, the green line is the equilibrium contact C_i for the BEC at the initial scattering length a_i , and the red line is the contact C_0 for a ground state BEC at the final scattering length a_f .

to four times as large. Of course, in the limit of no quench ($a_f = a_i$), the contact is trivially time independent.

The case of a diabatic quench downward ($a_f < a_i$) reveals interesting physics. Depending on the ratio of initial and final scattering lengths, the time-averaged contact may be much larger than the Bogoliubov prediction C_0 , and larger even than the initial contact C_i . Figure 5.5 shows these dynamics for a quench to $a_f = a_i/3$, in which case $\langle C(t) \rangle_t$ is more than an order of magnitude larger than C_0 and almost twice as large as C_i . The peak-to-trough oscillation amplitude is also larger than both C_0 and C_i . This is in stark contrast to the Bogoliubov case, in which the contact relaxes to C_0 over the fast timescale of the diabatic quench. At least in the transient dynamics, a diabatic reduction in the scattering length can evidently increase local two-body correlations by up to a factor of four compared to the initial condition, as evidenced by Eq. (5.17). An important limitation, however, is that these dynamical correlations are most pronounced at and below the length scale of the bound state.

The heightened short-range correlations contained in $\langle C(t) \rangle_t$, beyond those already at the Bogoliubov level, come fundamentally from bound-state physics. For example, if we ignore the contribution of the bound state to the dynamics in Eq. (5.6), we find that the scattering states dephase in such a way that the dynamical contact asymptotes towards C_0 without any oscillations, regardless of the initial scattering length. This is in qualitative agreement with the Bogoliubov

prediction. Once the scattering states dephase, however, the bound state is left to dominate the short-range wavefunction except in the relatively trivial case where $a_f \sim a_i$. The excess short-range correlations, given by the second bracketed term in Eq. (5.17), are determined entirely by the original projection of the initial condition onto the bound state.

We can estimate the amplitude of the depletion oscillations by simply integrating over the relevant portion of the momentum distribution. From Eq. (5.17) and the fact that $n_k(t) \sim C(t)/k^4$ at large k , the part of the momentum distribution oscillating at the bound-state frequency behaves as

$$n_{k,\text{osc}}(t) \sim \frac{16\pi^2 n^2 a_f^2}{k^4} 4 \left(\frac{a_i}{a_f} - 1 \right) \cos(\omega_B t), \quad (5.18)$$

aside from the time-independent contribution to the k^{-4} tail. As mentioned previously, these oscillations occur at the momentum scale of the bound state, where $ka_f \gtrsim 1$. Integrating Eq. (5.18), we find that the oscillating part of the depletion fraction is approximately

$$\begin{aligned} \frac{n_{\text{ex,osc}}(t)}{n} &\sim \frac{1}{n} \int_{ka_f > 1} \frac{d^3 k}{(2\pi)^3} n_{k,\text{osc}}(t) \\ &\sim 32 (na_f^3) \left(\frac{a_i}{a_f} - 1 \right) \cos(\omega_B t) \end{aligned} \quad (5.19)$$

The oscillation amplitude given here agrees with the many-body data shown in Fig. 5.2 to within a factor of order unity, and we expect it to be a reasonable estimate as long as the diluteness parameter na^3 is small before and after the diabatic quench.

As a final aside, we note that our two-body analysis is able to generalize the short-time dynamics following a quench to unitarity. If we calibrate our initial wavefunction for $a_i \geq 0$ and then quench to unitarity, the initial contact dynamics are

$$C(t) = C_i - 32\pi^2 n^2 a_i \sqrt{\frac{2\hbar}{\pi m}} t + \frac{128\pi}{(6\pi^2)^{2/3}} n^{4/3} \omega_F t \quad (5.20)$$

to leading order in na_i^3 and $\omega_F t$. This represents a generalization of Eq. (5.14) for diabatic quenches from small initial scattering length. It is interesting that Eq. (5.20) is equal to the $a_f \rightarrow \infty$ limit of Eq. (5.16), despite the fact that Eq. (5.16) was derived for small final scattering length ($na_f^3 \ll 1$).

5.4 Summary

We have elucidated the important role of the bound state in determining the contact dynamics of a diabatically-quenched BEC. We first computed these dynamics using a variational many-body model, demonstrating that large-amplitude oscillations of the contact can be observed even with existing magnetic-field-ramp technology. Our calculations reinforce the idea that coherent, short-range physics can lead to measureable signatures even in the BEC fraction. This is the dominant physics of the quenched gas on short time scales, before many-body effects and loss become important.

We also developed a calibration scheme for two-body models that leads to an unambiguous, quantitative description of BEC contact dynamics following a sudden quench. Our prescription fixes both the log-derivative and absolute magnitude of the initial short-range, two-body wavefunction by matching to the many-body problem, and we are able to derive analytic formulae for the short-time evolution of the contact in the weakly-interacting and unitarity limits. Our dynamics are shown to be independent of the arbitrary features of the models, and they agree with many-body predictions. This two-body picture indicates that bound-state oscillations of the contact are analogous to interferometry. We expect that one can account for finite ramp speeds by numerically solving the two-body Schrödinger equation for a properly-calibrated model.

The dynamical contact can be measured using time-resolved RF spectroscopy, as done in Ref. [4]. Our analysis shows that even the time-averaged contact $\langle C(t) \rangle_t$ may be greatly magnified relative to the Bogoliubov prediction due to bound-state physics, and this could be observed with an RF pulse that is long compared to the bound-state oscillation period. Measuring the oscillations themselves necessarily requires using shorter pulses, and that may lead to inconvenient broadening of the central RF peak. In any event, the temporal constraints on time-resolved RF spectroscopy depend both on the atomic species and on the transition under consideration, and they are beyond the scope of the present study.

We reiterate that the bound-state dynamics that we have considered are a coherent, transient

effect. They encapsulate the response of a short-range wavefunction to an abrupt change in the scattering length or, equivalently, a log-derivative boundary condition. At longer time scales, we expect the oscillations to damp out as the system equilibrates. Similar damping was observed in the Ramsey experiment of Refs. [48, 33], and it was believed to be due to a combination of incoherent three-body loss and dephasing from magnetic-field inhomogeneities. Still, the coherence of large-momentum dynamics persisted for many oscillation periods before damping became significant. The engineering of quench apparatus has improved over the years, especially in creating ramps that are diabatic with respect to the bound state [112]. This opens the door for systematic experimental studies of bound-state signatures in quenched BECs.

Chapter 6

Quench-Induced Correlation Waves

Results presented in this chapter can be found in our recent preprint on the arXiv [39], which has been accepted for publication in Physical Review A.

6.1 Background

It is a generic property of wave mechanics that an abrupt change in a system's boundary condition generates waves that propagate outward from the boundary. The tap of a mallet excites phonons in a percussive chime; with a flick of the wrist, a lion tamer snaps his whip; electric pulses in an antenna generate a radio broadcast. If we think of short-range interactions in terms of a scattering-length-dependent boundary condition for the relative wave function, as in Eq. (2.17), then we should expect that a sudden change of the scattering length generates waves that propagate to nonzero particle separations. In contrast to previous chapters, which focused on short-range correlations via the dynamical contact, we now shift our focus to longer-range correlation waves that are generated by a quench.

One landmark experiment on this topic was performed recently at the University of Chicago [85]. A quasi-2D BEC was quenched between two different scattering lengths,¹ and the nonequilibrium density distribution was subsequently measured *in situ* after various hold times. The interfering phonons generated by the quench led to oscillatory pair correlations in the system. These waves, known as Sakharov oscillations [140], are similar in their acoustic nature to the observed

¹ The quench was adiabatic with respect to the bound state, so the results of the previous chapter do not apply to this experiment.

fluctuations of the cosmic microwave background [79]. Besides its intriguing relevance to cosmology, this experiment demonstrates how correlations can propagate from the short range (where the quench occurs) to the long range (where the fluctuations are measured) in a many-body system.

Dynamical waves that propagate in the pair correlation function in response to an interaction quench, hereafter referred to as “quench-induced correlation waves,” have been discussed at length in the context of several many-body models. For the case of 2D and 3D quenched Bose condensates, these correlations have been calculated in the Bogoliubov approximation [85, 25, 125] and with quantum kinetic theory [93]. Numerical results were presented for quenched 1D Bose gases in Refs. [73, 124, 178], with analytical results for the Tonks-Girardeau regime given in Ref. [100]. Other studies have calculated these waves in quenched single-band Hubbard models using matrix-product-state [5] and variational-Monte-Carlo [24] algorithms, where Lieb-Robinson bounds [108] can limit the spreading of correlations; these studies accompany recent experimental progress in that realm [27].

This chapter takes a different, but complementary, approach to correlation waves. Inspired by the results of the previous chapter, we reconsider the question: What does an interaction quench (alternatively, a quenched boundary condition) do to the relative wave function for a pair of particles? This question lies at the root of the many-body quench problem, where interactions are pairwise and three-body correlations are often negligible. Two-body models offer the advantage that they can be solved exactly and give direct access to the wave function [22]. Moreover, they are immediately relevant to few-body systems in optical tweezers [170, 179, 90] and deep optical lattices [148]. In many instances, they have given insight into understanding nonequilibrium many-body phenomena [15, 70, 119, 13, 69]. These models can moreover give a quantitative description of short-time short-range pair correlations in quenched systems, as demonstrated earlier in this thesis.

In this chapter, we show that two-body models give an intuitive description of the physics behind quench-induced correlation waves. Section 6.2 reviews ballistic expansion from the standpoint of a quench. Our phase-space analysis shows that the correlation waves propagate ballistically, i.e.,

as if they were free particles. We demonstrate that these waves, which are inherently nonlocal, can contribute to the k^{-4} tail of a dynamical momentum distribution. This result is unexpected considering that the ideas surrounding Tan's contact relate the k^{-4} tail exclusively to local correlations. In Section 6.3, we discuss the leading-order behavior of the momentum distribution for arbitrary interaction quenches. We find that there is generally a competition between short-range and ballistic physics in the large-momentum limit, an effect that is absent in equilibrium scenarios. Additionally, we find that the amplitude of the correlation wave is determined chiefly by the initial and final scattering lengths, and also by the initial amplitude of the wave function at vanishing particle separation. Section 6.4 outlines our solution of the two-body quench problem in the presence of an external lattice potential. We show that ballistic correlation waves can propagate even in deep lattices, and we present a simple semiclassical model that yields accurate estimates for the transport that occurs. Section 6.5 summarizes our results.

6.2 Ballistic waves

It is instructive to begin with the simplest case in which quench-induced correlation waves occur: a measurement of the momentum distribution of a strongly interacting ultracold gas. The general method is to rapidly turn off the external trap and interactions, thereby freezing the momentum distribution of the gas, and then to allow the sample to expand freely before imaging. After expansion, the image represents the column-integrated momentum distribution of the gas. Correlation waves are generated by this simple protocol, as we now demonstrate.

The above-described procedure constitutes an interaction quench in the sense that, trap effects aside, the scattering length is rapidly changed from some initial value (a_i) to some final value (a_f). The effect on the wave function can be seen in the ballistic expansion of a bound pair of interacting particles in 1D. In terms of the particle separation x and coupling constant g_{1D} , the short-range interaction potential is

$$V_{\text{int}}(x) = g_{1D}\delta(x). \tag{6.1}$$

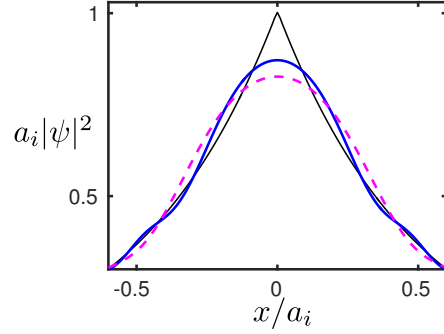


Figure 6.1: Ballistic expansion of a bound-state wave function. The black (thin) line represents the initial wave function. The blue (thick, solid) line represents the wave function at $\hbar t/2\mu a_i^2 = 0.008$, and the magenta (dashed) line is the wave function at $\hbar t/2\mu a_i^2 = 0.015$.

One can define a 1D scattering length via $a = -\hbar^2/\mu g_{1D}$, where μ is the reduced mass for the pair. The interactions are attractive (repulsive) for $a > 0$ ($a < 0$), and they vanish for $a = \pm\infty$.² For an initially bound pair of atoms, the relative wave function is

$$\psi(x, t = 0) = \frac{1}{\sqrt{a_i}} e^{-|x|/a_i}. \quad (6.2)$$

The solution, upon turning off interactions ($a_f \rightarrow \pm\infty$), is most compactly written in momentum space. In analogy with Eq. (2.25), we define the 1D Fourier transform as

$$\tilde{f}(k) \equiv \int dx e^{-ikx} f(x). \quad (6.3)$$

The time-dependent wave function is then given by

$$\tilde{\psi}(k, t) = \frac{2\sqrt{a_i}}{1 + k^2 a_i^2} e^{-iE_k t/\hbar}, \quad (6.4)$$

where $E_k = \hbar^2 k^2 / 2\mu$ is the relative kinetic energy. The short-time dynamics of the position-space wave function is shown in Fig. 6.1. At $t = 0$, the wave function has a kink at vanishing particle separation. This kink is absent for $t > 0$, where we see a correlation wave that propagates to larger particle separations.

The ballistic expansion dynamics can be easily visualized with a phase-space representation.

² This is a bit different from what one finds in 3D, although we will see shortly that the 1D scattering length still relates to a log-derivative boundary condition.

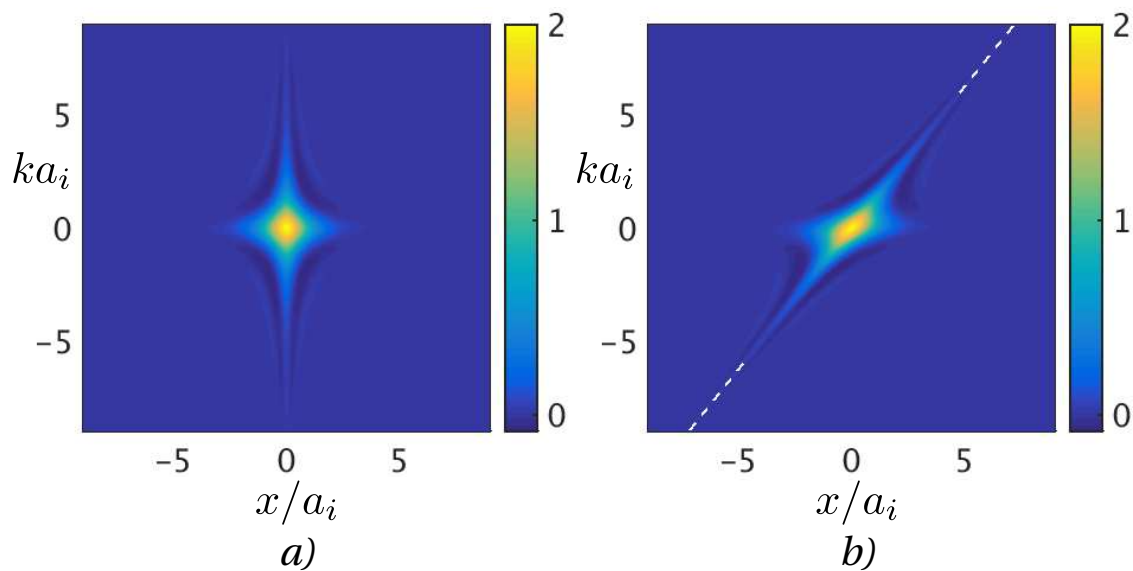


Figure 6.2: The Wigner distribution given by Eq. (6.5) for the ballistic expansion of a 1D bound-state wave function at (a) $t = 0$ and (b) $\hbar t/2\mu a_i^2 = 0.4$. The dashed white line in (b) represents the formula $x = 2\hbar kt/m$, which corresponds to the separation of two classical particles that start out on top of each other ($x = 0$) and then fly apart with momenta $\pm\hbar k$.

The Wigner function [173]

$$W(x, k, t) = \int dy e^{iky} \psi^* \left(x + \frac{y}{2}, t \right) \psi \left(x - \frac{y}{2}, t \right) \quad (6.5)$$

gives an approximate sense of the phase-space distribution of the instantaneous quantum state $\psi(x, t)$. The position and momentum distributions can be found by integrating:

$$\begin{aligned} |\psi(x, t)|^2 &= \int \frac{dk}{2\pi} W(x, k, t) \\ |\tilde{\psi}(k, t)|^2 &= \int dx W(x, k, t) \end{aligned} \quad (6.6)$$

Figure 6.2(a) shows the Wigner function of the bound state at $t = 0$. Initially, the k^{-2} tail of the momentum-space wave function is responsible for the kink in the position-space wave function at $x = 0$ (see Fig. 6.1). This is typical for wave functions of 1D systems with short-range interactions. It is generally understood that any state behaving as $\Psi(x) \approx \Psi(0)(1 - |x|/a)$ in the short range should have a contribution

$$\tilde{\Psi}(k) \sim \frac{2\Psi(0)}{ak^2} + \mathcal{O}\left(\frac{1}{k^3}\right) \quad (6.7)$$

to the large-momentum limit of the momentum-space wave function [129]. This momentum tail is analogous to what occurs in 3D: a wave function behaving as $\Psi(r) \approx (r\Psi)|_{r \rightarrow 0} \frac{1}{r}$ in the short range should have a momentum tail that goes as $\tilde{\Psi}(k) \sim (r\Psi)|_{r \rightarrow 0} \frac{4\pi}{k^2}$ at large k . The connection between short-range correlations and large-momentum asymptotics has led to the development of universal contact relations in 1D [129, 6], akin to Tan's work in 3D [152, 154, 153]. These ideas have also been extended to 2D systems [151, 35, 160, 172, 171].

Figure 6.2(b) shows that, after the interactions are turned off, the large-momentum components of the wave function propagate outwards to larger particle separations. Although the momentum distribution does not change during the dynamics [cf. Eq. (6.4)], the momentum components eventually separate spatially in a semiclassical sense, with the fastest modes moving the farthest. (In the figure, we see that the spatial wings of the phase-space distribution agree very well with the classical problem in which a pair of particles flies apart with momentum $\pm\hbar k$ (white dashed line), similar to the suggestion of Ref. [23].) This mechanism leads to the usual correspondence between the expanded spatial distribution and the initial momentum distribution, as probed

by ballistic expansion measurements of interacting systems. We point out that such a mapping would not occur if the interactions were turned off adiabatically or if they were left unchanged; it was necessary to quench the system.

It is interesting that ballistic expansion leads to a momentum distribution whose k^{-4} tail does not correspond to a kink in the short-range wave function. Rather, this tail is responsible for the correlation wave that propagates from the short range to the long range, as evidenced in Fig. 6.2. One can alternatively view this correlation wave, and hence the k^{-4} tail in the **dynamical** momentum distribution, to be the result of a rapidly disturbed boundary condition. It can be shown that the interaction potential in Eq. (6.1) enforces a log-derivative boundary condition

$$\left. \frac{\partial_x \psi}{\psi} \right|_{x \rightarrow 0^+} = -\frac{1}{a} \quad (6.8)$$

for symmetrized wave functions,³ similar to the Bethe-Peierls boundary condition (2.17) in 3D. The quench from $a_i > 0$ to $a_f = \pm\infty$ changes this boundary condition discontinuously, thereby generating a correlation wave. We expect intuitively that such a wave should be generated whenever the quench is diabatic and $a_f \neq a_i$. The strength of the wave should depend on the mismatch between the initial and final boundary conditions. For example, the generated wave should be weak when $a_f \approx a_i$, and it should be strong when a^{-1} changes drastically. We expect also that the large-momentum behavior of the wave function should contain both short-range and ballistic contributions, generalizing Eq. (6.7).

6.3 Arbitrary Quenches

We demonstrated in Chapter 5 that it is possible to find closed-form solutions to the two-body quench problem in 3D for a broad class of initial wave functions. The short-time, zero-range dynamics were found to depend on only three parameters: the initial scattering length a_i , the final scattering length a_f , and the initial zero-range behavior of the wave function $r\psi(r, 0)|_{r \rightarrow 0^+}$. It is natural to suppose that a similar universality should persist in the large-momentum content of the

³ This can be proved by integrating the Schrödinger equation in the vicinity of the interaction, as in Eq. (2.23).

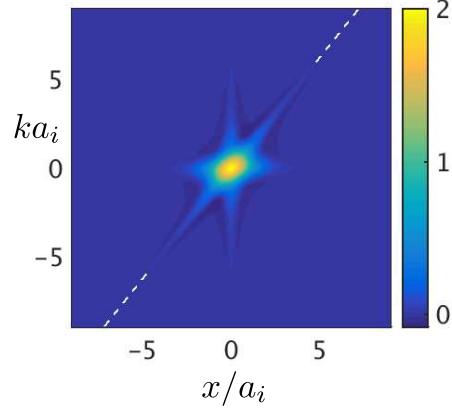


Figure 6.3: The Wigner distribution given by Eq. (6.5) for a 1D bound-state wave function quenched to $a_f = 2a_i$. The Wigner function is evaluated at the same time as in Fig. 6.2(b), and for the same initial scattering length a_i . The dashed white line represents the same classical model as shown previously.

quench-induced ballistic wave, as this wave originates in the short range and is a direct response to the change in boundary condition. We indeed find this to be the case in each dimensionality.

The derivation of the large-momentum limit of the 1D dynamical wave function is given in Appendix A. In short, one must project the initial wave function onto the complete basis of energy eigenstates satisfying the appropriate log-derivative boundary condition, Eq. (6.8), and then propagate in time.⁴ We find that the large-momentum limit of the wave function is

$$\tilde{\psi}(k, t) = \frac{2\psi(0, t)}{a_f k^2} + \left(\frac{a_f}{a_i} - 1\right) \frac{2\psi(0, 0)}{(k^2 a_f - i|k|)} e^{-iE_k t/\hbar} + \mathcal{O}\left(\frac{1}{k^3}\right) \quad (1D) \quad (6.9)$$

for $t > 0$. The first term shown here comes from the dynamical kink that appears in the short-range wave function for finite values of a_f , as in Eq. (6.7) and in accordance with our intuition about the contact [129]. The second term represents the ballistic wave that is generated by the quench, similar to Eq. (6.4). As a consistency check, it is easy to verify that Eq. (6.9) agrees with Eq. (6.4) in the $a_f \rightarrow \pm\infty$ limit. It is also immediately obvious that the ballistic contribution vanishes in the limit that no quench occurs (i.e., $a_f \rightarrow a_i$).

It is significant that, after the quench, the large-momentum limit of the wave function has two distinct components that are both $\mathcal{O}(k^{-2})$. This occurs whenever the final scattering length

⁴ This is the same approach we used to solve the 3D problem in Section 5.3.1.

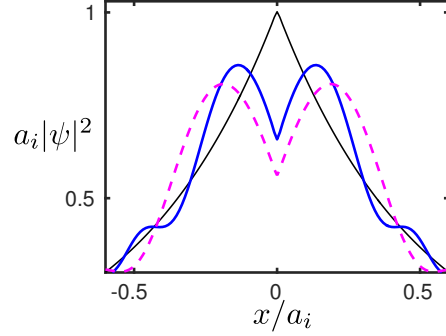


Figure 6.4: Quenching a bound state to $a_f = -a_i/2$. The black (thin) line represents the initial wave function. The blue (thick, solid) line represents the wave function at $\hbar t/2\mu a_i^2 = 0.008$, and the magenta (dashed) line is the wave function at $\hbar t/2\mu a_i^2 = 0.015$. Compare with Fig. 6.1, which depicts a quench to $a_f = \pm\infty$.

is finite. Figure 6.3 shows this behavior for the case in which an initial bound state at a scattering length $a_i > 0$ is quenched to a final scattering length $a_f = 2a_i$. Similar to Fig. 6.2(a), we see large-momentum content in the short range that is due to the residual kink in the wave function. Similar to Fig. 6.2(b), we see that the quench generates a ballistic correlation wave that rapidly propagates to large particle separations. This is in strong contrast to equilibrium systems, where only the short-range correlations contribute to the large-momentum asymptotics [129]. For this 1D quench problem, the k^{-4} tail of the one-body momentum distribution ($\sim |\tilde{\psi}(k, t)|^2$) does not correspond perfectly with the zero-range pair probability, indicating that one must exercise care when interpreting the 1D contact in a nonequilibrium context.

The amplitude of the ballistic correlation wave shown in Eq. (6.9) can be adjusted by changing the final scattering length a_f . Figure 6.4 shows the short-time position-space wave function for a bound state that is quenched to $a_f = -a_i/2$, evaluated at the same times as in Fig. 6.1. One can see that the quench from attraction ($a_i > 0$) to repulsion ($a_f < 0$) has increased the amplitude of the correlation wave when compared to the ballistic expansion case ($a_f = \pm\infty$). Equation (6.9) indicates that this enhancement is by approximately a factor of 3.

One may observe from Eq. (6.9) that quenches to the Tonks-Girardeau regime ($a_f \rightarrow 0^-$)

generate especially strong ballistic waves. In this limit, the wave function behaves as

$$\tilde{\psi}(k, t) = \frac{2\psi(0, 0)}{i|k|} e^{-iE_k t/\hbar} + \mathcal{O}\left(\frac{1}{k^2}\right) \quad (6.10)$$

for large k and $t > 0$, with the ballistic component dominating the short-range.⁵ One can intuit the k^{-1} tail by observing that the final energy of the system is determined by the expectation value of the post-quench Hamiltonian in the initial state; this energy must diverge as $g_f \sim -1/a_f \rightarrow \infty$. For $t > 0$, the interaction energy must vanish because $\psi(0, t) = 0$. Conservation of energy therefore requires that, after the quench, the kinetic energy diverge:

$$\int \frac{dk}{2\pi} \left| \tilde{\psi}(k, t) \right|^2 \frac{\hbar^2 k^2}{2\mu} \rightarrow \infty. \quad (6.11)$$

This was first pointed out by the authors of Ref. [100], who calculated analytically the dynamical density correlations for a many-body system of density n that is quenched from noninteracting to the Tonks-Girardeau regime. Our results connect smoothly with theirs in the short-time ($\hbar n^2 t/m \ll 1$), short-range ($nx \ll 1$) limit. In this limit, their dynamical pair correlations take the form of a relative wave function that behaves exactly as in Eq. (6.10) except that $\psi(0, 0) \rightarrow \sqrt{n}$. If we were to simulate the many-body problem with a two-body model, as done in the previous chapter, we would use this same prescription. This prescription also leads to quantitative agreement (at short times) with the numerical calculations of $g^{(2)}(0, t)$ in Ref. [178], which considered a broad range of $a_f < 0$. This reinforces our idea that properly calibrated few-body models can quantitatively describe short-time short-range correlation phenomena for quenched many-body systems.

The derivation given in Appendix A for quenched one-dimensional systems can be straightforwardly generalized to two and three dimensions. In direct analogy with Eq. (6.9), the results for $t > 0$ are

$$\tilde{\psi}(\mathbf{k}, t) = -\frac{2\pi \left(\frac{\psi(\rho, t)}{\ln(\rho/b)} \right) \Big|_{\rho \rightarrow 0^+}}{k^2} + \ln\left(\frac{a_i}{a_f}\right) \frac{2\pi \left(\frac{\psi(\rho, 0)}{\ln(\rho/b)} \right) \Big|_{\rho \rightarrow 0^+}}{k^2 (\ln(ka_f) - i\frac{\pi}{2})} e^{-iE_k t/\hbar} + \mathcal{O}\left(\frac{1}{k^3}\right) \quad (2D) \quad (6.12)$$

where $b > 0$ is an arbitrary length scale that makes the argument of the logarithm dimensionless,

⁵ The numerator and denominator of the first term in Eq. (6.9) both vanish in the $a_f \rightarrow 0^-$ limit. This subtlety can be treated along the lines presented in Appendix A.

and

$$\tilde{\psi}(\mathbf{k}, t) = \frac{4\pi (r\psi(r, t))|_{r \rightarrow 0^+}}{k^2} + \left(1 - \frac{a_f}{a_i}\right) \frac{4\pi (r\psi(r, 0))|_{r \rightarrow 0^+}}{k^2(1 + ik a_f)} e^{-iE_k t/\hbar} + \mathcal{O}\left(\frac{1}{k^4}\right) \quad (3D). \quad (6.13)$$

For the two-dimensional case, we define the scattering length with the convention that the bound state has energy $E_B = -\frac{\hbar^2}{2\mu a^2}$ [114].⁶ Both in 2D and in 3D, we see that the ballistic contribution (second term) vanishes when $a_f = a_i$. It can also be verified that both formulas reduce to the free-particle result when interactions are turned off ($a_f = \infty$ in 2D, and $a_f = 0$ in 3D).

The ballistic contribution in Eqs. (6.12) and (6.13) is subleading to the short range in the large- k limit, but it is nevertheless large compared to what one expects in equilibrium. The subleading terms of all equilibrium states are $\mathcal{O}(k^{-4})$ for both dimensionalities. In contrast, we see that the quench induces a new subleading structure, which is $\mathcal{O}(k^{-2} \ln^{-1}(k))$ in 2D and $\mathcal{O}(k^{-3})$ in 3D. This subleading behavior in 3D is responsible for the decaying oscillations that we observed in the BEC momentum distribution after quenching to unitarity, as shown in Figs. 4.2-4.4. Indeed, the cross term between the ballistic and short-range contributions to Eq. (6.13) oscillates with frequency $E_k/\hbar = 2\varepsilon_k/\hbar$ and decays as k^{-5} at all times, exactly as observed in the many-body numerics of Chapter 4. In that case, however, the nonlocal and ballistic origin of the effect was not obvious.

Despite the subleading nature of the ballistic terms in Eqs. (6.12) and (6.13) for finite a_f , one can generate leading-order $\mathcal{O}(k^{-2})$ behavior by turning off interactions. This is along the lines of the ballistic-expansion arguments presented in Sec. 6.2. If we then turn on interactions before the wave spreads appreciably, the wave function will develop a short-range singularity that will separately contribute a term of $\mathcal{O}(k^{-2})$ to $\tilde{\psi}(k, t)$. As was found for a single quench in 1D [Eq. (6.9)], the short-range and ballistic components can therefore occur at the same order in the large- k limit of the wave function. Again, we conclude that the considerations that relate the momentum tail exclusively to short-range correlations in equilibrium do not always hold outside of

⁶ We follow the scattering-length convention used in Ref. [114], which is slightly different from that used in Refs. [151, 35, 160, 172, 171]. They are related by $a'_{2D} = 2e^{-\gamma} a_{2D}$, where γ is Euler's constant, a_{2D} is the scattering length by our convention, and a'_{2D} is the scattering length in the other convention.

equilibrium.

We conclude this section by remarking on the limitations of our ballistic analysis. The zero-range approximation, wherein interactions are represented with boundary conditions at vanishing particle separation, has been enormously successful in describing ultracold quantum gases near broad Feshbach resonances [28]. This approximation is only valid for momenta satisfying $kr_0 \ll 1$, where r_0 is the range of the interaction. In experiments that use tight optical trapping to create quasi-low-dimensional geometries, the oscillator length of the tight trap represents another scale that bounds the “range” of the interaction in the reduced dimensionality. The immediate result is that the momentum tails discussed in the context of zero-range models do not extend out indefinitely to large k , although the point of breakdown ($kr_0 \sim 1$) might not be easily observable in typical signal to noise by a broad resonance (see Ref. [147]).

Our analysis also invoked the sudden approximation, wherein the scattering length (alternatively, the boundary condition) is assumed to change instantaneously. The consequence is that ballistic modes of arbitrarily large energy are generated by the quench, as shown in Eqs. (6.9)-(6.13). Any experimental realization of the quench protocol will occur over a finite timescale [32, 85, 112], and this will lead to an energy cutoff in the ballistic modes that can be generated. However, optical switching of interactions was demonstrated to be possible on timescales that are short compared to those set by the interaction range [30]. It follows that experimentally feasible quench times do not introduce any intrinsic constraint on the quench protocol beyond that already introduced by the range of interactions. We do expect, however, that slower quenches will produce weaker correlation waves; in the limit that interactions are changed adiabatically, no correlation waves are generated.

6.4 Lattice Transport

It makes sense to suppose that the ballistic nature of quench-induced correlation waves should allow for transport over potential-energy barriers. Semiclassically speaking, some part of the k^{-2} ballistic tail in Eq. (6.9) always has enough energy to cross a barrier of finite height, as suggested in Ref. [47]. We expect that the amount of transport can be tuned by adjusting the amplitude of the

wave and, therefore, the strength of the quench. In this section, we investigate the quench-induced dynamics that occurs for a pair of particles on a single site of a 1D optical lattice. We find that a semiclassical adaptation of our quantum description gives a good measure of the quench-induced transport.

Interaction-quench effects in an optical lattice were recently discussed in the numerical results of Refs. [121, 122]. There, the authors used the multi-layer multi-configuration time-dependent Hartree method for bosons (ML-MCTDHB) to investigate the dynamics of several interacting bosons in a few lattice sites. They found that a quench can trigger rapid transport between wells, as well as breathing and cradle modes within a given well. Such higher-band effects are ignored in typical Hubbard models that only include the lowest Wannier state in the formalism. Bound states, strong interactions, and/or strong quenches may distort the wave function considerably from the Wannier description, thereby necessitating models that encompass higher bands. The inclusion of higher bands, either in the ML-MCTDHB sense or in the spirit of a multi-band Hubbard model [53], makes it difficult to obtain numerically converged results for many-body systems on a lattice with strong interactions and strong quenches. Our two-body calculation should provide a useful benchmark in quantitatively understanding the rapid transport that takes place after an interaction quench.

The relative and center-of-mass coordinates do not separate for the case of an interacting pair of atoms in an optical lattice. We therefore resort to numerics to investigate the exact quantum dynamics. Without loss of generality, we consider identical bosons of mass m . The time-dependent Schrödinger equation for this system can then be written as

$$i\hbar \frac{\partial \Psi}{\partial t} = -\frac{\hbar^2}{2m} \frac{\partial^2 \Psi}{\partial x_1^2} - \frac{\hbar^2}{2m} \frac{\partial^2 \Psi}{\partial x_2^2} + V_{\text{lat}}(x_1)\Psi + V_{\text{lat}}(x_2)\Psi + V_{\text{int}}(x_1 - x_2)\Psi \quad (6.14)$$

where the interaction potential is given by Eq. (6.1), and the optical lattice potential of spacing ℓ and depth V_0 is given by

$$V_{\text{lat}}(x_j) = V_0 \sin^2 \left(\frac{\pi x_j}{\ell} \right). \quad (6.15)$$

It is customary to measure lattice depth in units of the recoil energy $E_R = \frac{\hbar^2}{8m\ell^2}$. Inasmuch as

the interaction quench directly excites relative momenta, it is convenient to work with the relative coordinate $x = x_1 - x_2$ and the center-of-mass coordinate $X = (x_1 + x_2)/2$. After changing variables and using a trig identity, one finds that

$$i\hbar \frac{\partial \Psi}{\partial t} = -\frac{\hbar^2}{m} \frac{\partial^2 \Psi}{\partial x^2} - \frac{\hbar^2}{4m} \frac{\partial^2 \Psi}{\partial X^2} + V_0 \left(1 - \cos\left(\frac{2\pi X}{\ell}\right) \cos\left(\frac{\pi x}{\ell}\right) \right) \Psi + V_{\text{int}}(x) \Psi \quad . \quad (6.16)$$

The energy eigenstates corresponding to Eqs. (6.14)-(6.16) were found numerically in Ref. [164] (see also Ref. [166] for the 3D analogue). Here, we instead solve for the dynamical wave function by time-evolving an initial condition with the widely-used split-operator method. This method is described in detail in Ref. [107].

In our numerics, we exploit bosonic symmetry [$\Psi(x, X) = \Psi(-x, X)$] by discretizing only for $x \geq 0$ and taking spectral transforms along this variable with the discrete cosine transform. We discretize the center-of-mass coordinate X for both positive and negative values, and we take spectral transforms along that variable using the fast Fourier transform. Our grid consists of 2^{13} equally spaced points for $x \in [0, 64\ell]$ meshed with 2^7 equally spaced points for $X \in [-4\ell, 4\ell]$. We model short-range interactions on the spatial grid by employing a potential that has support only at grid points where $x = 0$. We have found that representing $\delta(x) \rightarrow \delta_{x,0}/\Delta x$, where Δx is the grid spacing along the x direction, leads to the correct log-derivative boundary condition Eq. (6.8) in the limit that $\Delta x \ll |a|$. This condition is satisfied by all simulations discussed in this section.

Our study focuses on quenched systems for which the induced transport is expected to be the most significant. As indicated in Eq. (6.9) and alluded to in Ref. [47], the amplitude of the ballistic wave is proportional to the initial probability amplitude that the atoms are in the same position, $\psi(0, 0)$. This quantity is largest, in equilibrium, when the system is in a bound state. We therefore choose the initial condition for the transport problem Eq. (6.16) to be a bound state in a single lattice site. This configuration represents a subsystem of the state described by Ref. [163], which reported observing a single molecule per lattice site. For a deep lattice, the bottom of the well can be approximated as a harmonic-oscillator potential of frequency $\omega = 2\sqrt{V_0 E_R}/\hbar$ and width

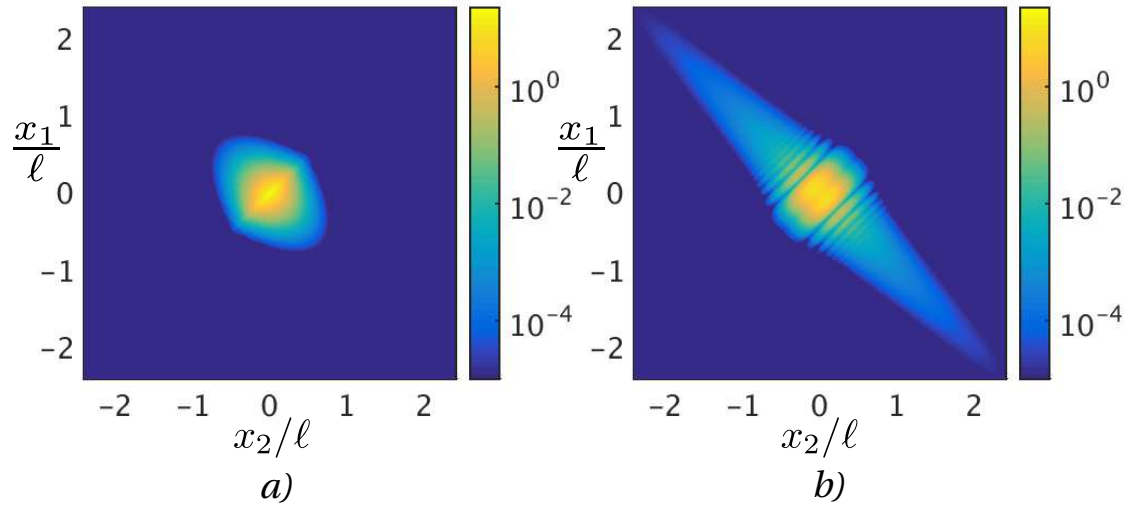


Figure 6.5: Quenching a bound state from $a_i = 0.2\ell$ to $a_f = -a_i$ on a single lattice site. The lattice is assumed to have a depth of $10E_R$. a) The initial two-body probability density $\ell^2|\Psi(x_1, x_2)|^2$ for a bound state on a lattice site ($t = 0$). b) The same quantity calculated at $\hbar t/m\ell^2 = 0.01$. Note the logarithmic color scale, whose lower limit is a cutoff.

$a_{\text{ho}} = \sqrt{\frac{\hbar}{m\omega}}$. One can write the approximate initial condition as

$$\Psi(x, X) = \psi_0(x)\phi_0(X), \quad (6.17)$$

where $\phi_0(X) = \left(\frac{2}{\pi a_{\text{ho}}^2}\right)^{1/4} e^{-X^2/a_{\text{ho}}^2}$ describes the center-of-mass degree of freedom, and $\psi_0(x)$ is the molecular state dressed by the oscillator [22]. For $a \ll a_{\text{ho}}$, one can show that ψ_0 approaches the ordinary bound state given by Eq. (6.2). For our simulations, we will consider an initial bound state of scattering length $a_i = 0.2\ell$ in a lattice of depth $V_0 = 10E_R$. The two-body probability density associated with this initial condition is shown in separate-particle coordinates in Fig. 6.5(a).

As discussed previously, we expect that an interaction quench will generate an energetic correlation wave that propagates over the potential barriers that separate individual lattice sites. This transport is shown in Fig. 6.5(b) a short time after quenching to $a_f = -a_i$. The wave has the same general structure as in Fig. 6.4, with spatially decaying oscillations and a cusp of reduced probability when both particles come together. Even after such a short time, we see that the wave already extends a couple of lattice sites in each direction.

It is instructive to quantify the amount of quench-induced transport that takes place. We can define a dynamical probability for the likelihood that both atoms remain in the central well:

$$P_{CC}(t) = \int_{|x_1| < \frac{\ell}{2}} dx_1 \int_{|x_2| < \frac{\ell}{2}} dx_2 |\Psi(x_1, x_2, t)|^2. \quad (6.18)$$

In like manner, we also define the probability that both atoms have tunneled,

$$P_{TT}(t) = \int_{|x_1| > \frac{\ell}{2}} dx_1 \int_{|x_2| > \frac{\ell}{2}} dx_2 |\Psi(x_1, x_2, t)|^2, \quad (6.19)$$

and the probability that a single atom has tunneled,

$$P_{TC}(t) = 2 \int_{|x_1| > \frac{\ell}{2}} dx_1 \int_{|x_2| < \frac{\ell}{2}} dx_2 |\Psi(x_1, x_2, t)|^2. \quad (6.20)$$

Here, we have exploited the symmetry of the bosonic wave function. The complementarity of the integration regions results in the identity $P_{CC} + P_{TT} + P_{TC} = 1$ at all times. These probabilities are plotted for $a_f = \pm\infty$ and $a_f = -a_i$ in Figs. 6.6(a) and 6.6(b), respectively. In both cases,

the atoms begin in the central well [$P_{CC}(0) \approx 1$]. After the quench, the transport probabilities smoothly saturate to values that depend on a_f . We note that the transport is substantial even though the lattice depth is of the order required for a typical Mott-insulating state in 1D [87, 180].

The ballistic description of the previous section leads to an intuitive, semiclassical model of transport. We can estimate the saturated values of P_{CC} , P_{TT} , and P_{TC} by considering the following question: What fraction of the momentum distribution describes ballistic atoms that are energetic enough to make it over the barrier?

The simplest analysis can be made for the case in which the interactions are turned off ($a_f = \pm\infty$). Short-range physics then does not contribute to the momentum distribution, and we can consider ballistic effects to stem entirely from the momentum-space version of the initial condition Eq. (6.17), similar to our analysis in Sec. 6.2. One can find the initial two-body wave function $\tilde{\Psi}(k_1, k_2, 0)$ from Eq. (6.17) via

$$\begin{aligned}\tilde{\Psi}(k_1, k_2, 0) &= \tilde{\psi}_0(k)\tilde{\phi}_0(K) \\ &= \tilde{\psi}_0(k_1 - k_2)\tilde{\phi}_0\left(\frac{k_1 + k_2}{2}\right)\end{aligned}\tag{6.21}$$

where we have changed to separate-particle momentum coordinates k_1 and k_2 from the relative and center-of-mass coordinates k and K . In a semiclassical sense, we expect that atoms with kinetic energy $\varepsilon_{k_i} < V_0$ don't make it over the barrier. Hence, we estimate that the probability for both atoms to stay in the central lattice site is given by

$$P_{CC} \rightarrow \int_{\varepsilon_{k_1} < V_0} \frac{dk_1}{2\pi} \int_{\varepsilon_{k_2} < V_0} \frac{dk_2}{2\pi} |\tilde{\Psi}(k_1, k_2, 0)|^2.\tag{6.22}$$

Similarly, we estimate the other transport probabilities to be

$$\begin{aligned}P_{TT} &\rightarrow \int_{\varepsilon_{k_1} > V_0} \frac{dk_1}{2\pi} \int_{\varepsilon_{k_2} > V_0} \frac{dk_2}{2\pi} |\tilde{\Psi}(k_1, k_2, 0)|^2 \\ P_{TC} &\rightarrow 2 \int_{\varepsilon_{k_1} > V_0} \frac{dk_1}{2\pi} \int_{\varepsilon_{k_2} < V_0} \frac{dk_2}{2\pi} |\tilde{\Psi}(k_1, k_2, 0)|^2.\end{aligned}\tag{6.23}$$

These probabilities are plotted as the horizontal dashed lines in Fig. 6.6(a), and they agree reasonably well with the saturation observed in the dynamics.

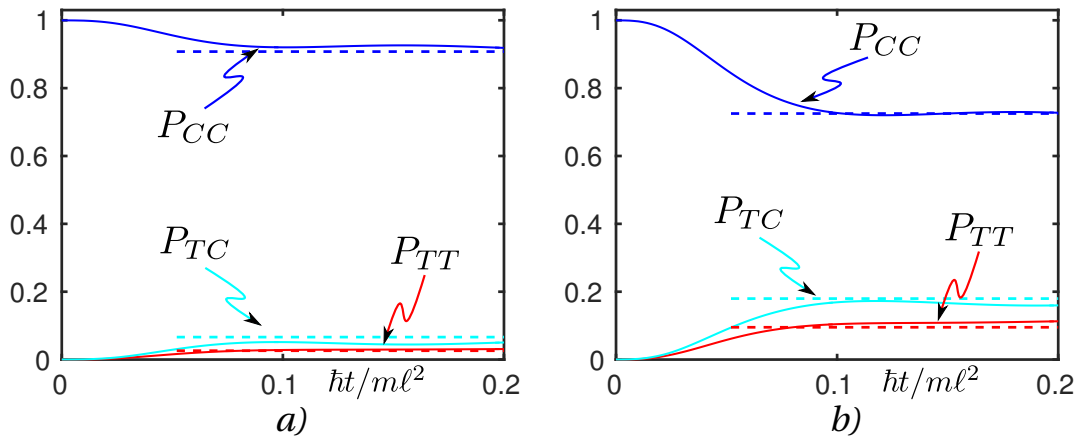


Figure 6.6: Lattice transport for a bound state that is quenched from $a_i = 0.2\ell$ to (a) $a_f = \pm\infty$ and (b) $a_f = -a_i$. The solid blue line denotes the dynamical probability of both atoms occupying the central well of the lattice, $P_{CC}(t)$; the solid cyan line is the probability of a single atom occupying the central well $P_{TC}(t)$; the solid red line is the probability that no atoms occupy the central lattice site, $P_{TT}(t)$. The horizontal dashed lines correspond to the semiclassical estimates for these probabilities.

When a_f is finite, the transport estimates should include only the ballistic contribution to the momentum distribution. This much is clear from the fact that, in the absence of a quench, the k^{-4} tail of the momentum distribution contributes to the short range instead of to transport. More generally, the momentum distribution has a mixture of short-range and ballistic effects, as shown in Eq. (6.9) to leading order. We have found that, in most cases, an accurate estimate of transport probabilities requires going beyond leading order so as to suitably include momenta $k \sim \sqrt{2mV_0}/\hbar$. In using Eqs. (6.21) and (6.23), we replace $\tilde{\psi}_0(k)$ with the full ballistic wave function $\tilde{\psi}_{\text{bal}}^{(S)}(k, t)$ derived in Appendix A and given by Eq. (A.14). For Eq. (6.22), we make this same replacement and also add in the probability that the atoms remain bound after the quench, since bound atoms will remain in the central well during the short timeframe of quench-induced transport.⁷ The resulting estimates for the case of $a_f = -a_i$ are plotted as dashed lines in Fig. 6.6(b). The increased transport that occurs for this quench is well described by the semiclassical estimate. This agreement owes itself to the fact that a wave of energy ε_k incident on a potential barrier of height V_0 has near unity transmission for $\varepsilon_k \gg V_0$. These waves dominate the integrals in Eq. (6.23) when the quench is strong.

It is interesting that the saturation timescale in Figs. 6.6(a)-(b) does not appear to depend on the final scattering length of the quench. We have found that the saturation time is well approximated by the time it takes an atom of momentum $k = \sqrt{2mV_0}/\hbar$ to travel one lattice spacing. This supports our semiclassical description of quench-induced transport. For the lattice depth used in our simulations, the saturation timescale is smaller than the lowest-band tunneling time by more than two orders of magnitude. The higher-band physics at play in this transport process comes from our use of strong interactions [95, 46] as well as from the quench itself [121, 122, 141].

6.5 Summary

In this chapter, we have taken a wave-function-based approach to describe the correlation waves induced by an interaction quench. Our calculations made use of the zero-range approxima-

⁷ Recall that this binding probability vanishes when the post-quench interactions are repulsive ($a_f < 0$).

tion for particle-particle interactions, represented here with a scattering-length-dependent boundary condition at vanishing particle separation. Within this approximation, the interaction quench disturbs the boundary and generates a wave that propagates ballistically to nonzero particle separations. We have derived the leading-order behavior of this wave in momentum space for one, two, and three spatial dimensions. These results are intuitive in that the amplitude of the correlation wave depends only on the initial amplitude at the boundary and the scattering length before and after the quench. In each dimensionality, the ballistic contribution to the wave function dominates the next-to-leading-order terms that occur in equilibrium systems. Particularly interesting is the fact that, in one dimension, the k^{-2} tail of the momentum-space wave function is generally determined by both short-range and ballistic effects. Similar results can occur in two and three dimensions, depending on the quench sequence. It is significant that a protocol as simple as a quench can surprise the intuition that usually associates large-momentum behavior exclusively with short-range physics. On this account, our two-body calculations indicate that one must exercise care when interpreting the contact out of equilibrium. We note that the contact dynamics we computed in the previous two chapters are well defined, as ballistic effects were subleading to the short range in those cases.

Our simulations reveal that quench-induced correlation waves can cause considerable transport in a 1D optical lattice. The amount of transport that takes place is readily tunable by altering the initial short-range pair probability of the state, as well as the strength of the quench. Our analytic two-body calculation makes possible a semiclassical framework within which both the transport and the saturation time can be estimated with surprising accuracy. We expect that similar results hold for optical-lattice systems in higher dimensionalities whose numerical calculations are more challenging. It would be interesting to see what role these ballistic dynamics might play in a quenched many-body system. For example, the system described in Ref. [163], which was essentially a Mott insulator of molecules in a lattice, might have phase coherence partially restored by the colliding ballistic waves that a quench might generate. One can expect generally that ballistic waves should be damped by collisions in a many-body system. This damping is dif-

difficult to model quantitatively without introducing a certain amount of arbitrariness to the theory [137, 138, 92, 94, 93]. At the same time, it is the crux of the question of how isolated quantum many-body systems equilibrate despite the high level of excitation provided by a quench. It may be possible to shed light on the matter by investigating how ballistic waves collide even at the few-body level. This remains for future work.

Chapter 7

Conclusion

The recurring theme of this thesis is that dynamically-tuned interactions can lead to interesting nonequilibrium phenomena. Our studies have focused on interaction quenches, where the scattering length a is suddenly changed and the system is allowed to evolve with the new interactions. When applied to Bose-condensed systems, this procedure has been used to create anti-clustered attractive states in 1D [76], generate time-dependent correlation waves in 2D [85], and probe the resonant limit ($a \rightarrow \infty$) of a Bose-Einstein condensate (BEC) in 3D [112]. These ground-breaking experiments, while advancing our understanding of quantum many-body physics, inspire further investigations of what an interaction quench does to a quantum state.

Our first results dealt with the short-time dynamics of a BEC that is quenched to unitarity. We studied this system using a time-dependent, many-body variational approach that encodes pair correlations. Although we incorporated the resonant interactions with several short-range model potentials, the time evolution of the momentum distribution was found to be essentially independent of the model, and it scaled universally with density-derived units. We also studied the evolution of short-range pair correlations via the dynamical contact, which grows and saturates in a way that is quantitatively consistent with the largest momentum modes measured in the ^{85}Rb experiment [112].

We then shifted gears to study the contact dynamics of BECs that are quenched to small scattering length. Although one might expect time-dependent Bogoliubov theory to be adequate in this regime, we found that this is not always the case. Fast quenches allow pairs of atoms to project

nontrivially onto the Feshbach-molecular bound state, and this can lead to short-range dynamics that are absent in Bogoliubov theory. Our many-body simulations revealed that the contact exhibits high-contrast oscillations at the frequency of the bound state, and this translates into oscillations of the condensate fraction. We then set up an intuitive two-body model that yielded a quantitatively accurate formula for the oscillatory contact, while highlighting the important role played by the bound state in the dynamics.

Our two-body framework was then applied to investigate the nonlocal correlation waves that are generated by a sudden quench. We were able to represent these waves analytically in momentum space for arbitrary initial and final scattering length. Our phase-space analysis revealed that they travel ballistically, ie. free-particle-like. One unexpected result was that these long-range correlation waves can contribute to the k^{-4} tail of the momentum distribution, depending on the quench protocol. This finding is at odds with the ideas surrounding Tan's contact, which relate the large- k asymptotics exclusively to short-range pair correlations. Our result, which came from an exact solution to the Schrödinger equation, provides a valuable demonstration of how equilibrium-based intuition about wave functions can break down in a nonequilibrium context. Our analytic calculation of correlation waves additionally lends itself to quantitative predictions for quench-induced transport over potential-energy barriers. A possible extension of this work would be to investigate how ballistic waves collide with each other at the few-body level, as such collisions are expected to occur in many-body systems and constitute the first steps towards equilibration.

It would be worthwhile to generalize the ideas of this thesis to include three-body effects related to Efimov physics. Several decades ago, Efimov showed that there is a ladder of three-body bound states that accumulates near the dissociation threshold at large scattering length [54, 55]. This effect has been shown to alter the Tan relations by introducing a three-body contact parameter to account for short-range triplet probabilities [18]. Attempts to measure the three-body contact in a weakly-interacting BEC yielded a value that was consistent with zero [174]. At large scattering length, however, one might expect the ladder of Efimov states to play a more significant role in the physics. In the same sense that we observed growth of the two-body contact after quenching

to unitarity, the three-body contact might also grow appreciably, albeit over a longer timescale. It should be possible to describe this growth at short times within a calibrated three-body calculation, similar to our approach in Chapter 5. Although it is unlikely that an analytical solution will be found for such a calculation, the problem could still be solved numerically by the methods described in Ref. [150].

Bibliography

- [1] M. H. Anderson, J. R. Ensher, M. R. Matthews, C. E. Wieman, and E. A. Cornell. Observation of bose-einstein condensation in a dilute atomic vapor. Science, 269:198, 1995.
- [2] George B. Arfken and Hans J. Weber. Mathematical Methods for Physicists, 6th Ed. Elsevier, 2005.
- [3] G. E. Astrakharchik, J. Boronat, J. Casulleras, and S. Giorgini. Beyond the tonks-girardeau gas: Strongly correlated regime in quasi-one-dimensional bose gases. Phys. Rev. Lett., 95:190407, Nov 2005.
- [4] A. B. Bardon, S. Beattie, C. Luciuk, W. Cairncross, D. Fine, N. S. Cheng, G. J. A. Edge, E. Taylor, S. Zhang, S. Trotzky, and J. H. Thywissen. Transverse demagnetization dynamics of a unitary fermi gas. Science, 344:722, 2014.
- [5] Peter Barmettler, Dario Poletti, Marc Cheneau, and Corinna Kollath. Propagation front of correlations in an interacting bose gas. Phys. Rev. A, 85:053625, May 2012.
- [6] M. Barth and W. Zwerger. Tan relations in one dimension. Ann. Phys., 326:2544, 2011.
- [7] S. Beliaev. Sov. Phys. JETP, 7:289, 1958.
- [8] S. Beliaev. Sov. Phys. JETP, 7:299, 1958.
- [9] H. Bethe and R. Peierls. Quantum theory of the dipton. Proc. R. Soc. A, 148:146, 1935.
- [10] N. Bogoliubov. On the theory of superfluidity. J. Phys. USSR, 11:23, 1947.
- [11] John L. Bohn and P. S. Julienne. Prospects for influencing scattering lengths with far-off-resonant light. Phys. Rev. A, 56:1486–1491, Aug 1997.
- [12] John L. Bohn and P. S. Julienne. Semianalytic theory of laser-assisted resonant cold collisions. Phys. Rev. A, 60:414–425, Jul 1999.
- [13] B. Borca, D. Blume, and C. H. Greene. A two-atom picture of coherent atom-molecule quantum beats. New J. Phys., 5:111, 2003.
- [14] Dmitry Borzov, Mohammad S. Mashayekhi, Shizhong Zhang, Jun-Liang Song, and Fei Zhou. Three-dimensional bose gas near a feshbach resonance. Phys. Rev. A, 85:023620, Feb 2012.

- [15] Cristian Degli Esposti Boschi, Elisa Ercolessi, Loris Ferrari, Piero Naldesi, Fabio Ortolani, and Luca Taddia. Bound states and expansion dynamics of interacting bosons on a one-dimensional lattice. Phys. Rev. A, 90:043606, 2014.
- [16] S. N. Bose. Z. Phys., 26:178, 1924.
- [17] Eric Braaten, H.-W. Hammer, and Thomas Mehen. Dilute bose-einstein condensate with large scattering length. Phys. Rev. Lett., 88:040401, Jan 2002.
- [18] Eric Braaten, Daekyoung Kang, and Lucas Platter. Universal relations for identical bosons from three-body physics. Phys. Rev. Lett., 106:153005, Apr 2011.
- [19] Eric Braaten and Agustin Nieto. Quantum corrections to the ground state of a trapped bose-einstein condensate. Phys. Rev. B, 56:14745–14765, 1997.
- [20] Eric Braaten and Lucas Platter. Exact relations for a strongly interacting fermi gas from the operator product expansion. Phys. Rev. Lett., 100:205301, May 2008.
- [21] K. A. Brueckner and K. Sawada. Bose-einstein gas with repulsive interactions: General theory. Phys. Rev., 106:1117–1127, Jun 1957.
- [22] T. Busch, B.-G. Englert, K. Rzazewski, and M. Wilkens. Two cold atoms in a harmonic trap. Found. Phys., 28:549, 1998.
- [23] Pasquale Calabrese and John Cardy. Time dependence of correlation functions following a quantum quench. Phys. Rev. Lett., 96:136801, Apr 2006.
- [24] Giuseppe Carleo, Federico Becca, Laurent Sanchez-Palencia, Sandro Sorella, and Michele Fabrizio. Light-cone effect and supersonic correlations in one- and two-dimensional bosonic superfluids. Phys. Rev. A, 89:031602, Mar 2014.
- [25] I. Carusotto, R. Balbinot, A. Fabbri, and A. Recati. Density correlations and dynamical casimir emission of bogoliubov phonons in modulated atomic bose-einstein condensates. Eur. Phys. J. D, 56:391, 2010.
- [26] S. Chandrasekhar. Stochastic problems in physics and astronomy. Rev. Mod. Phys., 15:1–89, 1943.
- [27] M. Cheneau, P. Barmettler, D. Poletti, M. Endres, P. Schauß, T. Fukuhara, C. Gross, I. Bloch, C. Kollath, , and S. Kuhr. Light-cone-like spreading of correlations in a quantum many-body system. Nature, 481:484, 2012.
- [28] C. Chin, R. Grimm, P. Julienne, and E. Tiesinga. Observation of low-field feshbach resonances in collisions of cesium atoms. Rev. Mod. Phys., 82:1225, 2010.
- [29] Steven Chu. Nobel lecture: The manipulation of neutral particles. Rev. Mod. Phys., 70:685–706, Jul 1998.
- [30] Logan W. Clark, Li-Chung Ha, Chen-Yu Xu, and Cheng Chin. Quantum dynamics with spatiotemporal control of interactions in a stable bose-einstein condensate. Phys. Rev. Lett., 115:155301, 2015.

- [31] N. R. Claussen. Dynamics of Bose-Einstein condensates near a Feshbach resonance in ^{85}Rb . PhD thesis, University of Colorado at Boulder, 2003.
- [32] N. R. Claussen, E. A. Donley, S. T. Thompson, and C. E. Wieman. Microscopic dynamics in a strongly interacting bose-einstein condensate. Phys. Rev. Lett., 89:010401, 2002.
- [33] N. R. Claussen, S. J. J. M. F. Kokkelmans, S. T. Thompson, E. A. Donley, E. Hodby, and C. E. Wieman. Very-high-precision bound-state spectroscopy near a ^{85}Rb feshbach resonance. Phys. Rev. A, 67:060701, 2003.
- [34] Claude N. Cohen-Tannoudji. Nobel lecture: Manipulating atoms with photons. Rev. Mod. Phys., 70:707–719, Jul 1998.
- [35] R. Combescot, F. Alzetto, and X. Leyronas. Particle distribution tail and related energy formula. Phys. Rev. A, 79:053640, May 2009.
- [36] Tommaso Comparin and Werner Krauth. Momentum distribution in the unitary bose gas from first principles. arXiv:1604.08870, 2016.
- [37] E. A. Cornell and C. E. Wieman. Nobel lecture: Bose-einstein condensation in a dilute gas, the first 70 years and some recent experiments. Rev. Mod. Phys., 74:875–893, Aug 2002.
- [38] John P. Corson and John L. Bohn. Bound-state signatures in quenched bose-einstein condensates. Phys. Rev. A, 91:013616, Jan 2015.
- [39] John P. Corson and John L. Bohn. Ballistic quench-induced correlation waves in ultracold gases. arXiv:1605.03169, 2016.
- [40] John P. Corson, Ryan M. Wilson, and John L. Bohn. Geometric stability spectra of dipolar bose gases in tunable optical lattices. Phys. Rev. A, 88:013614, Jul 2013.
- [41] John P. Corson, Ryan M. Wilson, and John L. Bohn. Stability spectroscopy of rotons in a dipolar bose gas. Phys. Rev. A, 87:051605, May 2013.
- [42] Ph. Courteille, R. S. Freeland, D. J. Heinzen, F. A. van Abeelen, and B. J. Verhaar. Observation of a feshbach resonance in cold atom scattering. Phys. Rev. Lett., 81:69, 1998.
- [43] S. Cowell, H. Heiselberg, I. E. Mazets, J. Morales, V. R. Pandharipande, and C. J. Pethick. Cold bose gases with large scattering lengths. Phys. Rev. Lett., 88:210403, May 2002.
- [44] K. B. Davis, M. O. Mewes, M. R. Andrews, N. J. van Druten, D. S. Durfee, D. M. Kurn, and W. Ketterle. Bose-einstein condensation in a gas of sodium atoms. Phys. Rev. Lett., 75:3969–3973, Nov 1995.
- [45] J. M. Diederix, T. C. F. van Heijst, and H. T. C. Stoof. Ground state of a resonantly interacting bose gas. Phys. Rev. A, 84:033618, Sep 2011.
- [46] Roberto B. Diener and Tin-Lun Ho. Fermions in optical lattices swept across feshbach resonances. Phys. Rev. Lett., 96:010402, Jan 2006.
- [47] Elmer V. H. Doggen and Jami J. Kinnunen. Quench-induced delocalization. New J. Phys., 16:113051, 2014.

- [48] E. A. Donley, N. R. Claussen, S. T. Thompson, and C. E. Wieman. Atom-molecule coherence in a bose-einstein condensate. Nature, 417:529, 2002.
- [49] Elizabeth A. Donley, Neil R. Claussen, Simon L. Cornish, Jacob L. Roberts, Eric. A. Cornell, and Carl E. Wieman. Dynamics of collapsing and exploding bose-einstein condensates. Nature, 412:295, 2001.
- [50] R. A. Duine and H. T. C. Stoof. Dynamics of a bose-einstein condensate near a feshbach resonance. Phys. Rev. A, 68:013602, 2003.
- [51] R. A. Duine and H. T. C. Stoof. Many-body aspects of coherent atom-molecule oscillations. Phys. Rev. Lett., 91:150405, 2003.
- [52] R. A. Duine and H. T. C. Stoof. Atom-molecule coherence in bose gases. Phys. Rep., 396:115, 2004.
- [53] O. Dutta, M. Gajda, P. Hauke, M. Lewenstein, D.-S. Lühmann, B. A. Malomed, T. Sowiński, and J. Zakrzewski. Non-standard hubbard models in optical lattices: a review. Rep. Prog. Phys., 78:066001, 2015.
- [54] V. Efimov. Energy levels arising from resonant two-body forces in a three-body system. Phys. Lett. B, 33:563, 1970.
- [55] V. Efimov. Weakly-bound states of three resonantly-interacting particles. Sov. J. Nuc. Phys., 12(5):589, 1971.
- [56] A. Einstein. Sitzber. Kgl. Preuss. Akad. Wiss., page 261, 1924.
- [57] A. Einstein. Sitzber. Kgl. Preuss. Akad. Wiss., page 3, 1925.
- [58] Daniel J. Eisenstein, Idit Zehavi, David W. Hogg, Roman Scoccimarro, Michael R. Blanton, Robert C. Nichol, Ryan Scranton, Hee-Jong Seo, Max Tegmark, and Zheng Zheng. Detection of the baryon acoustic peak in the large-scale correlation function of sdss luminous red galaxies. Ast. Phys. J., 633:560, 2005.
- [59] B. D. Esry, Chris H. Greene, and James P. Burke. Recombination of three atoms in the ultracold limit. Phys. Rev. Lett., 83:1751–1754, Aug 1999.
- [60] A. Antognini et al. Proton structure from the measurement of 2s-2p transition frequencies of muonic hydrogen. Science, 339:417, Jan 2013.
- [61] F. K. Fatemi, K. M. Jones, and P. D. Lett. Observation of optically induced feshbach resonances in collisions of cold atoms. Phys. Rev. Lett., 85:4462–4465, Nov 2000.
- [62] P. O. Fedichev, Yu. Kagan, G. V. Shlyapnikov, and J. T. M. Walraven. Influence of nearly resonant light on the scattering length in low-temperature atomic gases. Phys. Rev. Lett., 77:2913–2916, Sep 1996.
- [63] P. O. Fedichev, M. W. Reynolds, and G. V. Shlyapnikov. Three-body recombination of ultracold atoms to a weakly bound s level. Phys. Rev. Lett., 77:2921–2924, Sep 1996.
- [64] E. Fermi. Nuovo Cimento, 11:157, 1934.

- [65] E. Fermi. Motion of neutrons in hydrogenous substances. Ricerca Scientifica, 7:13, 1936.
- [66] V. V. Flambaum, G. F. Gribakin, and C. Harabati. Analytical calculation of cold-atom scattering. Phys. Rev. A, 59:1998–2005, Mar 1999.
- [67] M. Girardeau and R. Arnowitt. Theory of many-boson systems: Pair theory. Phys. Rev., 113:755–761, 1959.
- [68] Roy J. Glauber. Coherent and incoherent states of the radiation field. Phys. Rev., 131:2766–2788, Sep 1963.
- [69] K. Göral, T. Köhler, S. A. Gardiner, E. Tiesinga, , and P. S. Julienne. Adiabatic association of ultracold molecules via magnetic field tunable interactions. J. Phys. B, 37:3457, 2004.
- [70] Krzysztof Góral, Thorsten Köhler, and Keith Burnett. Ramsey interferometry with atoms and molecules: Two-body versus many-body phenomena. Phys. Rev. A, 71:023603, 2005.
- [71] G. F. Gribakin and V. V. Flambaum. Calculation of the scattering length in atomic collisions using the semiclassical approximation. Phys. Rev. A, 48:546–553, Jul 1993.
- [72] A. Griffin. Conserving and gapless approximations for an inhomogeneous bose gas at finite temperatures. Phys. Rev. B, 53:9341–9347, 1996.
- [73] Vladimir Gritsev, Timofei Rostunov, and Eugene Demler. Exact methods in the analysis of the non-equilibrium dynamics of integrable models: application to the study of correlation functions for non-equilibrium 1d bose gas. Journal of Statistical Mechanics: Theory and Experiment, 2010(05):P05012, 2010.
- [74] E. Gross. Ann. Phys., 4:57, 1958.
- [75] E. Gross. Il Nuovo Cimento, 20:3, 1961.
- [76] E. Haller, M. Gustavsson, M. J. Mark, J. G. Danzl, R. Hart, G. Pupillo, and H.-C. Nägerl. Realization of an excited, strongly correlated quantum gas phase. Science, 325:1224, 2009.
- [77] O. Hen, L. B. Weinstein, E. Piasezky, G. A. Miller, M. M. Sargsian, and Y. Sagi. Correlated fermions in nuclei and ultracold atomic gases. Phys. Rev. C, 92:045205, Oct 2015.
- [78] Harald F. Hess. Evaporative cooling of magnetically trapped and compressed spin-polarized hydrogen. Phys. Rev. B, 34:3476–3479, Sep 1986.
- [79] G. Hinshaw, J. L. Weiland, R. S. Hill, N. Odegard, D. Larson, C. L. Bennett, J. Dunkley, B. Gold, M. R. Greason, N. Jarosik, E. Komatsu, M. R. Nolta, L. Page, D. N. Spergel, E. Wollack, M. Halpern, A. Kogut, M. Limon, S. S. Meyer, G. S. Tucker, and E. L. Wright. Five-year wilkinson microwave anisotropy probe observations: Data processing, sky maps, and basic results. The Astrophysical Journal Supplement Series, 180(2):225, 2009.
- [80] M. Holland, J. Park, and R. Walser. Formation of pairing fields in resonantly coupled atomic and molecular bose-einstein condensates. Phys. Rev. Lett., 86:1915–1918, 2001.
- [81] M. J. Holland, D. S. Jin, M. L. Chiofalo, and J. Cooper. Emergence of interaction effects in bose-einstein condensation. Phys. Rev. Lett., 78:3801–3805, May 1997.

- [82] T. Holstein and H. Primakoff. Field dependence of the intrinsic domain magnetization of a ferromagnet. Phys. Rev., 58:1098–1113, Dec 1940.
- [83] M.-G. Hu, M. J. Van de Graaff, D. Kedar, J. P. Corson, E. A. Cornell, and D. S. Jin. Bose polarons in the strongly interacting regime. arXiv:1605.00729, 2016.
- [84] Kerson Huang and C. N. Yang. Quantum-mechanical many-body problem with hard-sphere interaction. Phys. Rev., 105:767–775, 1957.
- [85] C.-L. Hung, V. Gurarie, and C. Chin. From cosmology to cold atoms: Observation of sakharov oscillations in a quenched atomic superfluid. Science, 341:1213, 2013.
- [86] S. Inouye, M. R. Andrews, J. Stenger, H.-J. Miesner, D. M. Stamper-Kurn, and W. Ketterle. Observation of feshbach resonances in a bose-einstein condensate. Nature, 392:151, 1998.
- [87] D. Jaksch, C. Bruder, J. I. Cirac, C. W. Gardiner, and P. Zoller. Cold bosonic atoms in optical lattices. Phys. Rev. Lett., 81:3108–3111, Oct 1998.
- [88] L. M. Jensen, H. M. Nilsen, and Gentaro Watanabe. Bcs-bec crossover in atomic fermi gases with a narrow resonance. Phys. Rev. A, 74:043608, Oct 2006.
- [89] Ben Kain and Hong Y. Ling. Nonequilibrium states of a quenched bose gas. Phys. Rev. A, 90:063626, 2014.
- [90] A. M. Kaufman, B. J. Lester, C. M. Reynolds, M. L. Wall, M. Foss-Feig, K. R. A. Hazzard, A. M. Rey, and C. A. Regal. Two-particle quantum interference in tunnel-coupled optical tweezers. Science, 345:306, 2014.
- [91] Wolfgang Ketterle and N. J. Van Druten. Evaporative cooling of trapped atoms. Adv. At. Mol. Opt. Phys., 37:181, Nov 1996.
- [92] M. Kira. Excitation picture of an interacting bose gas. Ann. Phys., 351:200, 2014.
- [93] M. Kira. Coherent quantum depletion of an interacting atom condensate. Nat. Comm., 6:6624, 2015.
- [94] M. Kira. Hyperbolic bloch equations: atom-cluster kinetics of an interacting bose gas. Ann. Phys., 356:185, 2015.
- [95] Michael Köhl, Henning Moritz, Thilo Stöferle, Kenneth Günter, and Tilman Esslinger. Fermionic atoms in a three dimensional optical lattice: Observing fermi surfaces, dynamics, and interactions. Phys. Rev. Lett., 94:080403, Mar 2005.
- [96] T. Köhler, T. Gasenzer, P. S. Julienne, and K. Burnett. Long-range nature of feshbach molecules in bose-einstein condensates. Phys. Rev. Lett., 91:230401, 2003.
- [97] Thorsten Köhler and Keith Burnett. Microscopic quantum dynamics approach to the dilute condensed bose gas. Phys. Rev. A, 65:033601, 2002.
- [98] Thorsten Köhler, Krzysztof Góral, and Paul S. Julienne. Production of cold molecules via magnetically tunable feshbach resonances. Rev. Mod. Phys., 78:1311–1361, 2006.

- [99] S. J. J. M. F. Kokkelmans and M. J. Holland. Ramsey fringes in a bose-einstein condensate between atoms and molecules. Phys. Rev. Lett., 89:180401, 2002.
- [100] Márton Kormos, Mario Collura, and Pasquale Calabrese. Analytic results for a quantum quench from free to hard-core one-dimensional bosons. Phys. Rev. A, 89:013609, Jan 2014.
- [101] P. Kramer. A review of the time-dependent variational principle. J. Phys.: Conf. Ser., 99:012009, 2008.
- [102] Mark J. H. Ku, Ariel T. Sommer, Lawrence W. Cheuk, and Martin W. Zwierlein. Revealing the superfluid lambda transition in the universal thermodynamics of a unitary fermi gas. Science, 335:563, 2012.
- [103] L. Landau. Theory of the superfluidity of helium ii. Phys. Rev., 60:356–358, Aug 1941.
- [104] L. D. Landau. The theory of superfluidity of helium ii. J. Phys. USSR, 5:71, 1941.
- [105] C. K. Law, P. T. Leung, and M.-C. Chu. Dynamic depletion in a bose-einstein condensate via a sudden increase of the scattering length. Phys. Rev. A, 66:033605, 2002.
- [106] T. D. Lee, Kerson Huang, and C. N. Yang. Eigenvalues and eigenfunctions of a bose system of hard spheres and its low-temperature properties. Phys. Rev., 106:1135–1145, Jun 1957.
- [107] C. Leforestier, R. H. Bisseling, C. Cerjan, M. D. Feit, R. Friesner, A. Guldberg, A. Hammerich, G. Jolicard, W. Karrlein, H.-D. Meyer, N. Lipkin, O. Roncero, and R. Kosloff. A comparison of different propagation schemes for the time-dependent schrödinger equation. J. Comp. Phys., 94:59, 1991.
- [108] E. H. Lieb and D. W. Robinson. The finite group velocity of quantum spin systems. Comm. Math. Phys., 28:251, 1972.
- [109] M. Lindberg and S. W. Koch. Effective bloch equations for semiconductors. Phys. Rev. B, 38:3342–3350, Aug 1988.
- [110] R. V. E. Lovelace and T. J. Tommila. Theory of bose-einstein condensation of atomic hydrogen in a dynamic trap. Phys. Rev. A, 35:3597–3606, May 1987.
- [111] Matt Mackie, Kalle-Antti Suominen, and Juha Javanainen. Mean-field theory of feshbach-resonant interactions in ^{85}Rb condensates. Phys. Rev. Lett., 89:180403, 2002.
- [112] P. Makotyn, C. E. Klauss, D. L. Goldberger, E. A. Cornell, and D. S. Jin. Universal dynamics of a degenerate unitary bose gas. Nat. Phys., 10:116, 2014.
- [113] A. G. Martin, K. Helmerson, V. S. Bagnato, G. P. Lafyatis, and D. E. Pritchard. rf spectroscopy of trapped neutral atoms. Phys. Rev. Lett., 61:2431–2434, Nov 1988.
- [114] Mohammad S. Mashayekhi, Jean-Sébastien Bernier, Dmitry Borzov, Jun-Liang Song, and Fei Zhou. Two-dimensional bose gases near resonance: Competing two-body and three-body effects. Phys. Rev. Lett., 110:145301, Apr 2013.
- [115] M. R. Matthews, D. S. Hall, D. S. Jin, J. R. Ensher, C. E. Wieman, E. A. Cornell, F. Dalfovo, C. Minniti, and S. Stringari. Dynamical response of a bose-einstein condensate to a discontinuous change in internal state. Phys. Rev. Lett., 81:243–247, Jul 1998.

- [116] Richard D. Mattuck. A Guide to Feynman Diagrams in the Many-Body Problem, 2nd Ed. Dover, 1992.
- [117] E. Merzbacher. Quantum Mechanics, 2nd Ed. Wiley and Sons, 1998.
- [118] A. Messiah. Quantum Mechanics, Two Volumes Bound as One. Dover, 1999.
- [119] F. H. Mies, E. Tiesinga, and P. S. Julienne. Manipulation of feshbach resonances in ultracold atomic collisions using time-dependent magnetic fields. Phys. Rev. A, 61:022721, 2000.
- [120] J. N. Milstein, C. Menotti, and M. J. Holland. Long-range nature of feshbach molecules in bose-einstein condensates. New J. Phys., 5:52, 2003.
- [121] S. I. Mistakidis, L. Cao, and P. Schmelcher. Interaction quench induced multimode dynamics of finite atomic ensembles. J. Phys. B, 47:225303, 2014.
- [122] S. I. Mistakidis, L. Cao, and P. Schmelcher. Negative-quench-induced excitation dynamics for ultracold bosons in one-dimensional lattices. Phys. Rev. A, 91:033611, Mar 2015.
- [123] Philip M. Morse. Diatomic molecules according to the wave mechanics. ii. vibrational levels. Phys. Rev., 34:57–64, Jul 1929.
- [124] D. Muth, B. Schmidt, and M. Fleischhauer. Fermionization dynamics of a strongly interacting one-dimensional bose gas after and interaction quench. New J. Phys., 12:083065, 2010.
- [125] Stefan S. Natu and Erich J. Mueller. Dynamics of correlations in a dilute bose gas following an interaction quench. Phys. Rev. A, 87:053607, 2013.
- [126] Nir Navon, Swann Piatecki, Kenneth Günter, Benno Rem, Trong Canh Nguyen, Frédéric Chevy, Werner Krauth, and Christophe Salomon. Dynamics and thermodynamics of the low-temperature strongly interacting bose gas. Phys. Rev. Lett., 107:135301, Sep 2011.
- [127] Esben Nielsen and J. H. Macek. Low-energy recombination of identical bosons by three-body collisions. Phys. Rev. Lett., 83:1566–1569, Aug 1999.
- [128] P. Nozieres and D. Saint James. Particle vs. pair condensation in attractive bose liquids. J. Phys. (Paris), 43:1133, 1982.
- [129] Maxim Olshanii and Vanja Dunjko. Short-distance correlation properties of the lieb-liniger system and momentum distributions of trapped one-dimensional atomic gases. Phys. Rev. Lett., 91:090401, Aug 2003.
- [130] S. B. Papp, J. M. Pino, R. J. Wild, S. Ronen, C. E. Wieman, D. S. Jin, and E. A. Cornell. Bragg spectroscopy of a strongly interacting ⁸⁵Rb bose-einstein condensate. Phys. Rev. Lett., 101:135301, Sep 2008.
- [131] R. K. Pathria and P. D. Beale. Statistical Mechanics, 3rd Ed. Elsevier, 2011.
- [132] C. J. Pethick and H. Smith. Bose-Einstein Condensation in Dilute Gases, 2nd Ed. Cambridge University Press, 2008.
- [133] D. S. Petrov and G. V. Shlyapnikov. Interatomic collisions in a tightly confined bose gas. Phys. Rev. A, 64:012706, Jun 2001.

- [134] William D. Phillips. Nobel lecture: Laser cooling and trapping of neutral atoms. Rev. Mod. Phys., 70:721–741, Jul 1998.
- [135] R. Pires, M. Repp, J. Ulmanis, E. D. Kuhnle, M. Weidemüller, T. G. Tiecke, Chris H. Greene, Brandon P. Ruzic, John L. Bohn, and E. Tiemann. Analyzing feshbach resonances: A ${}^6\text{Li} - {}^{133}\text{Cs}$ case study. Phys. Rev. A, 90:012710, Jul 2014.
- [136] L. Pitaevskii. Sov. Phys. JETP, 13:451, 1961.
- [137] A. Rançon, Chen-Lung Hung, Cheng Chin, and K. Levin. Quench dynamics in bose-einstein condensates in the presence of a bath: Theory and experiment. Phys. Rev. A, 88:031601, 2013.
- [138] A. Rançon and K. Levin. Equilibrating dynamics in quenched bose gases: Characterizing multiple time regimes. Phys. Rev. A, 90:021602, 2014.
- [139] Maurizio Rossi, Luca Salasnich, Francesco Ancilotto, and Flavio Toigo. Monte carlo simulations of the unitary bose gas. Phys. Rev. A, 89:041602, Apr 2014.
- [140] A. D. Sakharov. The initial stage of an expanding universe and the appearance of a nonuniform distribution of matter. Sov. Phys. JETP, 49:345, 1966.
- [141] K. Sakmann, A. I. Streltsov, O. E. Alon, and L. S. Cederbaum. Optimal time-dependent lattice models for nonequilibrium dynamics. New J. Phys., 13:043003, 2011.
- [142] Daniel V. Schroeder. An Introduction to Thermal Physics. Addison Wesley Longman, 2000.
- [143] L. F. Shampine and M. W. Reichelt. The matlab ode suite. SIAM J. Sci. Comp., 18:1, 1997.
- [144] D. Hudson Smith, Eric Braaten, Daekyoung Kang, and Lucas Platter. Two-body and three-body contacts for identical bosons near unitarity. Phys. Rev. Lett., 112:110402, Mar 2014.
- [145] V. D. Snyder, S. J. J. M. F. Kokkelmans, and Lincoln D. Carr. Hartree-fock-bogoliubov model and simulation of attractive and repulsive bose-einstein condensates. Phys. Rev. A, 85:033616, 2012.
- [146] Jun Liang Song and Fei Zhou. Ground state properties of cold bosonic atoms at large scattering lengths. Phys. Rev. Lett., 103:025302, 2009.
- [147] J. T. Stewart, J. P. Gaebler, T. E. Drake, and D. S. Jin. Verification of universal relations in a strongly interacting fermi gas. Phys. Rev. Lett., 104:235301, 2010.
- [148] Thilo Stöferle, Henning Moritz, Kenneth Günter, Michael Köhl, and Tilman Esslinger. Molecules of fermionic atoms in an optical lattice. Phys. Rev. Lett., 96:030401, Jan 2006.
- [149] H. T. C. Stoof and J.J.R.M van Heugten. Resummation of infrared divergencies in the theory of atomic bose gases. J. Low Temp. Phys., 174:159, 2014.
- [150] A. G. Sykes, J. P. Corson, J. P. D’Incao, A. P. Koller, C. H. Greene, A. M. Rey, K. R. A. Hazzard, and J. L. Bohn. Quenching to unitarity: Quantum dynamics in a three-dimensional bose gas. Phys. Rev. A, 89:021601, 2014.

- [151] S. Tan. S-wave contact interaction problem: A simple description. [arXiv:cond-mat/0505615](https://arxiv.org/abs/cond-mat/0505615), 2005.
- [152] S. Tan. Energetics of a strongly correlated fermi gas. *Ann. Phys.*, 323:2952, 2008.
- [153] S. Tan. Generalized virial theorem and pressure relations for a strongly correlated fermi gas. *Ann. Phys.*, 323:2987, 2008.
- [154] S. Tan. Large momentum part of a strongly correlated fermi gas. *Ann. Phys.*, 323:2971, 2008.
- [155] John R. Taylor. *Scattering Theory*. John Wiley and Sons, 1972.
- [156] M. Theis, G. Thalhammer, K. Winkler, M. Hellwig, G. Ruff, R. Grimm, and J. Hecker Denschlag. Tuning the scattering length with an optically induced feshbach resonance. *Phys. Rev. Lett.*, 93:123001, Sep 2004.
- [157] M. Thgersen, D. V. Fedorov, and A. S. Jensen. N-body efimov states of trapped bosons. *EPL (Europhysics Letters)*, 83(3):30012, 2008.
- [158] E. Tiesinga, B. J. Verhaar, and H. T. C. Stoof. Theshold and resonance phenomena in ultracold ground-state collisions. *Phys. Rev. A*, 47:4114, 1993.
- [159] Eddy Timmermans, Paolo Tommasini, Robin Côté, Mahir Hussein, and Arthur Kerman. Rarified liquid properties of hybrid atomic-molecular bose-einstein condensates. *Phys. Rev. Lett.*, 83:2691–2694, 1999.
- [160] Manuel Valiente, Nikolaj T. Zinner, and Klaus Mølmer. Universal relations for the two-dimensional spin-1/2 fermi gas with contact interactions. *Phys. Rev. A*, 84:063626, Dec 2011.
- [161] J.J.R.M van Heugten and H. T. C. Stoof. Theory of unitary bose gases. [arXiv:1302.1792](https://arxiv.org/abs/1302.1792), 2013.
- [162] Lene Vestergaard Hau, B. D. Busch, Chien Liu, Zachary Dutton, Michael M. Burns, and J. A. Golovchenko. Near-resonant spatial images of confined bose-einstein condensates in a 4-dee magnetic bottle. *Phys. Rev. A*, 58:R54–R57, Jul 1998.
- [163] T. Volz, N. Syassen, D. M. Bauer, E. Hansis, S. Dürr, and G. Rempe. Preparation of a quantum state with one molecule at each site of an optical lattice. *Nat. Phys.*, 2:692, 2006.
- [164] Javier von Stecher, Victor Gurarie, Leo Radzihovsky, and Ana Maria Rey. Lattice-induced resonances in one-dimensional bosonic systems. *Phys. Rev. Lett.*, 106:235301, Jun 2011.
- [165] V. Vuletić, A. J. Kerman, C. Chin, and S. Chu. Observation of low-field feshbach resonances in collisions of cesium atoms. *Phys. Rev. Lett.*, 82:1406, 1999.
- [166] M. L. Wall and L. D. Carr. Microscopic model for feshbach interacting fermions in an optical lattice with arbitrary scattering length and resonance width. *Phys. Rev. Lett.*, 109:055302, Jul 2012.
- [167] Tino Weber, Jens Herbig, Michael Mark, Hanns-Christoph Nägerl, and Rudolf Grimm. Three-body recombination at large scattering lengths in an ultracold atomic gas. *Phys. Rev. Lett.*, 91:123201, Sep 2003.

- [168] Ronen Weiss, Betzalel Bazak, and Nir Barnea. Generalized nuclear contacts and momentum distributions. Phys. Rev. C, 92:054311, Nov 2015.
- [169] Ronen Weiss, Betzalel Bazak, and Nir Barnea. Nuclear neutron-proton contact and the photoabsorption cross section. Phys. Rev. Lett., 114:012501, Jan 2015.
- [170] A. N. Wenz, G. Zürn, S. Murmann, I. Brouzos, T. Lompe, and S. Jochim. Science, 342:457, 2013.
- [171] Félix Werner and Yvan Castin. General relations for quantum gases in two and three dimensions. ii. bosons and mixtures. Phys. Rev. A, 86:053633, Nov 2012.
- [172] Félix Werner and Yvan Castin. General relations for quantum gases in two and three dimensions: Two-component fermions. Phys. Rev. A, 86:013626, Jul 2012.
- [173] E. Wigner. On the quantum correction for thermodynamic equilibrium. Phys. Rev., 40:749–759, Jun 1932.
- [174] R. J. Wild, P. Makotyn, J. M. Pino, E. A. Cornell, and D. S. Jin. Measurements of tan’s contact in an atomic bose-einstein condensate. Phys. Rev. Lett., 108:145305, 2012.
- [175] Xiao Yin and Leo Radzihovsky. Quench dynamics of a strongly interacting resonant bose gas. Phys. Rev. A, 88:063611, 2013.
- [176] Xiao Yin and Leo Radzihovsky. Postquench dynamics and prethermalization in a resonant bose gas. Phys. Rev. A, 93:033653, 2016.
- [177] Fei Zhou and Mohammad S. Mashayekhi. Bose gases near resonance: Renormalized interactions in a condensate. Ann. Phys., 328:83, 2013.
- [178] Jan C. Zill, Tod M. Wright, Karén V. Kheruntsyan, Thomas Gasenzer, and Matthew J. Davis. Relaxation dynamics of the lieb-liniger gas following an interaction quench: A coordinate bethe-ansatz analysis. Phys. Rev. A, 91:023611, Feb 2015.
- [179] G. Zürn, A. N. Wenz, S. Murmann, A. Bergschneider, T. Lompe, and S. Jochim. Pairing in few-fermion systems with attractive interactions. Phys. Rev. Lett., 111:175302, Oct 2013.
- [180] W. Zwerger. Mott-hubbard transition of cold atoms in optical lattices. J. Opt. B, 5:S9, 2003.

Appendix A

Two-Body Solution after a Quench

Several results from Chapters 5 and 6 rely on an analytic solution to the two-body quench problem in momentum space. Dimensionality does not play a significant role in the strategy of the derivation. The general idea, already outlined at the beginning of Section 5.3.1, is to expand the wave function in the eigenstates of the zero-range model. One can always write down energy-normalized scattering states, and there is also a discrete bound-state solution for $a > 0$. The difficult part of the problem involves evaluating the integral that superposes the scattering solutions, but we will see that some methods from complex analysis can simplify the calculation. These ideas do not depend directly on the dimensionality of the problem; hence, without loss of generality, we will work through the details for the case of a quench in 1D. At the end of this Appendix, we will describe what alterations are necessary to solve the problem in 3D and 2D. We simplify expressions by scaling distances by an arbitrary length scale ξ and energies by $\frac{\hbar^2}{2\mu\xi^2}$, where μ is the reduced mass for the pair.

A.1 Solving the Problem in 1D

In free space, the time-dependent Schrödinger equation for the relative wave function $\psi(x, t)$ is

$$i\frac{\partial\psi(x, t)}{\partial t} = -\frac{\partial^2\psi(x, t)}{\partial x^2} - \frac{2}{a_f}\delta(x)\psi(x, t) \quad (\text{A.1})$$

where a_f is the 1D scattering length after the quench. Without loss of generality, we will consider symmetrized initial conditions, such that $\psi(x, 0) = \psi(-x, 0)$. This symmetry is preserved by the

Schrödinger equation whether or not the two particles are identical bosons. The overall effect of the interaction is to enforce the log-derivative boundary condition shown in Eq. (6.8), which is

$$\left. \frac{\partial_x \psi}{\psi} \right|_{x \rightarrow 0^+} = -\frac{1}{a}. \quad (\text{A.2})$$

This can be proved by integrating Eq. (A.1) over a vanishingly small interval $[-\epsilon, \epsilon]$ and assuming even symmetry.

We can propagate a given initial condition $\psi(x, 0)$ in time by expanding in the energy eigenstates that satisfy the post-quench log-derivative boundary condition. The scattering states are

$$\psi_{k'}^{(S)}(x) = A_{k'} [\sin(k'|x|) - k'a_f \cos(k'x)], \quad E_{k'} = k'^2, \quad (\text{A.3})$$

where

$$A_{k'} = \frac{1}{\sqrt{2\pi k'(1 + k'^2 a_f^2)}} \quad (\text{A.4})$$

is a constant that enforces energy normalization. These states are uniquely defined for $k' > 0$. For $a_f > 0$, the bound state solution is

$$\psi_B(x) = \frac{1}{\sqrt{a_f}} e^{-|x|/a_f}, \quad E_B = -\frac{1}{a_f^2}. \quad (\text{A.5})$$

It will be helpful to decompose the time-dependent wave function onto its scattering and bound contributions, which we will treat separately. Thus, we write [117]

$$\psi(x, t) = \psi^{(S)}(x, t) + \psi^{(B)}(x, t), \quad (\text{A.6})$$

where

$$\psi^{(S)}(x, t) \equiv \int_0^\infty dE_{k'} e^{-iE_{k'} t} \psi_{k'}^{(S)}(x) \langle \psi_{k'}^{(S)}(x') | \psi(x', 0) \rangle \quad (\text{A.7})$$

and

$$\psi^{(B)}(x, t) \equiv \Theta(a_f) e^{-iE_B t} \psi_B(x) \langle \psi_B(x') | \psi(x', 0) \rangle, \quad (\text{A.8})$$

and where $\langle \cdot | \cdot \rangle$ denotes a projection integral. The Heaviside function $\Theta(a_f)$ determines whether or not the bound state should be included in the dynamics. We will assume that $\psi(x, 0)$ is normalizable and smooth everywhere except possibly for a nontrivial log-derivative at $x = 0$.

It is most convenient to solve for the momentum-space wave function. This requires taking the Fourier transform of the energy eigenstates. For $a_f > 0$, the Fourier transform of the bound state can be inferred from Eq. (6.4)

$$\tilde{\psi}_B(k) = \frac{2\sqrt{a_f}}{1 + k^2 a_f^2}. \quad (\text{A.9})$$

The Fourier transform of the scattering states takes a more complicated form, but it can be written as

$$\tilde{\psi}_{k'}^{(S)}(k) = A_{k'} \left[-2k'\pi (i + k'a_f) \delta(k'^2 - k^2) + \frac{2k'}{k'^2 - k^2 - i\epsilon} \right], \quad (\text{A.10})$$

where we use the convention $\epsilon \rightarrow 0^+$. This formula can be verified by taking the inverse Fourier transform. The first term can be easily integrated due to the Dirac delta function, and the second term can be integrated by using the residue theorem [2]. One must close the contour in the upper half plane for $x > 0$, and the lower half plane for $x < 0$. The pole structure in (A.10) leads to the absolute-value dependence in the position-space scattering state (A.3). With these ingredients, we can rewrite the time-dependent wave function (A.6)-(A.8) in momentum space:

$$\tilde{\psi}(k, t) = \tilde{\psi}^{(S)}(k, t) + \tilde{\psi}^{(B)}(k, t), \quad (\text{A.11})$$

where

$$\tilde{\psi}^{(S)}(k, t) = \int_0^\infty dE_{k'} e^{-iE_{k'} t} \tilde{\psi}_{k'}^{(S)}(k) \langle \psi_{k'}^{(S)}(x') | \psi(x', 0) \rangle \quad (\text{A.12})$$

and

$$\tilde{\psi}^{(B)}(k, t) = \Theta(a_f) e^{-iE_B t} \tilde{\psi}_B(k) \langle \psi_B(x') | \psi(x', 0) \rangle. \quad (\text{A.13})$$

Having subdivided the scattering eigenstate as in (A.10), there are thus two parts that compose the scattering contribution $\tilde{\psi}^{(S)}(k, t)$ in Eq. (A.12). The first part can be evaluated trivially in momentum space by exploiting the delta function in Eq. (A.10). We write it as follows:

$$\tilde{\psi}_{\text{bal}}^{(S)}(k, t) \equiv -2\pi |k| A_{|k|} (i + |k|a_f) \langle \psi_{|k|}^{(S)}(x') | \psi(x', 0) \rangle e^{-iE_k t}. \quad (\text{A.14})$$

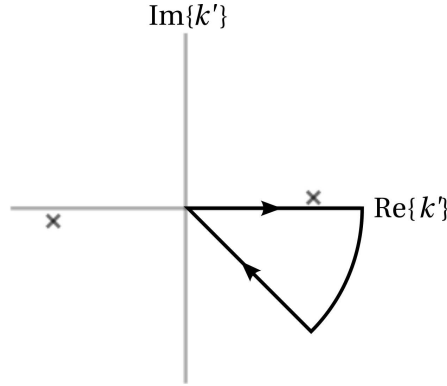


Figure A.1: Integration contour in the complex k' plane. The crosses denote the poles of the bracketed factor in Eq. (A.15). The final leg of the integral is along $\arg[k'] = -\pi/4$.

We call this the “ballistic” contribution to the wave function due to its free-particle-like $f(k)e^{-iE_k t}$ behavior, similar to Eq. (6.4). The second contribution can be written as

$$\tilde{\psi}_{\text{sr}}^{(S)}(k, t) = \int_0^{\infty} 2k' dk' e^{-ik'^2 t} \left[\frac{2k' A_{k'}}{k'^2 - k^2 - i\epsilon} \right] \langle \psi_{k'}^{(S)}(x') | \psi(x', 0) \rangle, \quad (\text{A.15})$$

and we will see that it generally contributes to the short-range part of the wave function. In sum, we can write

$$\tilde{\psi}(k, t) = \tilde{\psi}_{\text{bal}}^{(S)}(k, t) + \tilde{\psi}_{\text{sr}}^{(S)}(k, t) + \tilde{\psi}^{(B)}(k, t). \quad (\text{A.16})$$

for the full momentum-space wave function.

One can make progress with Eq. (A.15) by exploiting the residue theorem. The integration, as written, is along the positive real k' axis. If we close the contour as shown in Fig. A.1, the contribution from the $|k'| \rightarrow \infty$ arc vanishes. The only poles that can contribute residues must come from the analytic continuation of the scattering projection inside the integration loop. We have found empirically that, if $\psi(x, 0)$ decays smoothly and without oscillation (such as for a bound state, a ground-state Busch wave function [22], or forms analogous to Eq. (5.11)), the integrand is analytic inside the closed contour and the integral vanishes.¹ The two straight legs of the integral

¹ More generally, the residues from any poles inside the contour can be absorbed into the definition of $\tilde{\psi}_{\text{bal}}^{(S)}(k, t)$. This occurs, for example, if $\psi(x, 0)$ already has a ballistic component. We will ignore such exotic initial conditions in our analysis.

then cancel, and we can rewrite Eq. (A.15) as an integral along $k' = ze^{-i\frac{\pi}{4}}$ for real, nonnegative z :

$$\begin{aligned}\tilde{\psi}_{\text{sr}}^{(S)}(k, t) &= -4ie^{-i\frac{\pi}{4}} \int_0^\infty dz e^{-z^2 t} \frac{z^2}{-iz^2 - k^2} \left[A_{k'} \langle \psi_{k'}^{(S)}(x') | \psi(x', 0) \rangle \right]_{k' \rightarrow ze^{-i\frac{\pi}{4}}} \\ &= \frac{4ie^{-i\frac{\pi}{4}}}{k^2} \int_0^\infty dz \frac{e^{-z^2 t}}{1 + iz^2/k^2} z^2 \left[A_{k'} \langle \psi_{k'}^{(S)}(x') | \psi(x', 0) \rangle \right]_{k' \rightarrow ze^{-i\frac{\pi}{4}}}\end{aligned}\quad (\text{A.17})$$

where the factor in brackets has been analytically continued. Mathematica can evaluate this quantity in closed form for several interesting cases, including where $\psi(x, 0)$ takes a form similar to Eq. (5.11) or is a bound state. Unfortunately, the expressions are usually too lengthy to usefully write down.

The physical significance of $\tilde{\psi}_{\text{sr}}^{(S)}(k, t)$ can be seen if one compares it with the zero-range contribution to the scattered wave function, $\psi^{(S)}(0, t)$. Using Eq. (A.3), we can write the result as

$$\begin{aligned}\psi^{(S)}(0, t) &= \int_0^\infty dE_{k'} e^{-iE_{k'} t} \psi_{k'}^{(S)}(0) \langle \psi_{k'}^{(S)}(x') | \psi(x', 0) \rangle \\ &= -a_f \int_0^\infty dE_{k'} e^{-iE_{k'} t} k' A_{k'} \langle \psi_{k'}^{(S)}(x') | \psi(x', 0) \rangle \\ &= 2ia_f e^{-i\frac{\pi}{4}} \int_0^\infty dz e^{-z^2 t} z^2 \left[A_{k'} \langle \psi_{k'}^{(S)}(x') | \psi(x', 0) \rangle \right]_{k' \rightarrow ze^{-i\frac{\pi}{4}}}\end{aligned}\quad (\text{A.18})$$

where we have again exploited the integration contour in Fig. A.1. A direct comparison of Eq. (A.17) and Eq. (A.18) indicates that

$$\tilde{\psi}_{\text{sr}}^{(S)}(k, t) = \frac{2\psi^{(S)}(0, t)}{a_f k^2} + \mathcal{O}\left(\frac{1}{k^4}\right)\quad (\text{A.19})$$

for large k satisfying $k^2 t \gg 1$. This verifies our claim that $\tilde{\psi}_{\text{sr}}^{(S)}$ generally encodes the short-range behavior of the scattered wave. The Gaussian suppression in Eqs. (A.17)-(A.18) indicates that this contribution to the wave function vanishes in the $t \rightarrow \infty$ limit. This is as expected for an unconfined wave packet composed entirely of scattering states, which must spread out in space as time passes. With significantly less work, one can combine (A.5) and (A.9) to show that

$$\tilde{\psi}^{(B)}(k, t) = \frac{2\psi^{(B)}(0, t)}{a_f k^2} + \mathcal{O}\left(\frac{1}{k^4}\right)\quad (\text{A.20})$$

for the bound-state contribution to the dynamical wave function.

We now examine the large-momentum behavior of the ballistic contribution to the wave function, given by Eq. (A.14). This requires finding the asymptotics of the projection integral

$$\int_{-\infty}^{\infty} dx [\sin(k|x|) - ka_f \cos(kx)] \psi(x, 0) \quad (\text{A.21})$$

for a symmetric wave function whose short range behaves as $\psi(x, 0) \approx \psi(0, 0)(1 - |x|/a_i)$, and whose long range is regular and smooth. The second part of this integral is reminiscent of Eq. (6.7), and evaluates to

$$\begin{aligned} -ka_f \int_{-\infty}^{\infty} dx \cos(kx) \psi(x, 0) &= -ka_f \int_{-\infty}^{\infty} dx e^{ikx} \psi(x, 0) \\ &= -ka_f \left[\frac{2\psi(0, 0)}{a_i k^2} + \mathcal{O}\left(\frac{1}{k^3}\right) \right] \end{aligned} \quad (\text{A.22})$$

as discussed in Ref. [129]. The first part of the integral can be understood as we integrate by parts

$$\begin{aligned} \int_{-\infty}^{\infty} dx \sin(k|x|) \psi(x, 0) &= 2 \int_0^{\infty} dx \sin(kx) \psi(x, 0) \\ &= 2 \left(-\frac{\cos(kx)}{k} \right) \psi(x, 0) \Big|_0^{\infty} - 2 \int_0^{\infty} dx \left(-\frac{\cos(kx)}{k} \right) \psi'(x, 0), \\ &= \frac{2\psi(0, 0)}{k} + \frac{2}{k} \int_0^{\infty} dx \cos(kx) \psi'(x, 0) \\ &= \frac{2\psi(0, 0)}{k} + \mathcal{O}\left(\frac{1}{k^2}\right) \end{aligned} \quad (\text{A.23})$$

where we have assumed that $\psi(x, 0)$ vanishes in the $x \rightarrow \infty$ limit, and that $\psi'(x, 0)$ is smooth and decays at large x . Combining (A.22) and (A.23), we find that

$$\int_{-\infty}^{\infty} dx [\sin(k|x|) - ka_f \cos(kx)] \psi(x, 0) = \frac{2\psi(0, 0)}{k} \left(1 - \frac{a_f}{a_i} \right) + \mathcal{O}\left(\frac{1}{k^2}\right) \quad (\text{A.24})$$

for the projection asymptotics. This leading-order behavior encodes the mismatch between the initial and final boundary conditions of the quench. Inserting this result into Eq. (A.14), we find that

$$\tilde{\psi}_{\text{bal}}^{(S)}(k, t) = \left(\frac{a_f}{a_i} - 1 \right) \frac{2\psi(0, 0)}{(k^2 a_f - i|k|)} e^{-iE_k t} + \mathcal{O}\left(\frac{1}{k^3}\right) \quad (\text{A.25})$$

after some algebra. Combining Eqs. (A.19), (A.20), and (A.25), we arrive at Eq. (6.9).

A.2 Generalizing to 3D

The solution described in the previous section generalizes naturally to three dimensions. The reason for this is that the 1D wave function $\psi_{1D}(x, t)$ and the 3D wave function $r\psi_{3D}(r, t)$ satisfy the same equations of motion and log-derivative boundary conditions. One can compare the 3D eigenstates in Eqs. (5.4)-(5.5) to those in 1D, given by Eqs. (A.3)-(A.5). The main difference is in the definition of the Fourier transform in 3D, which leads to slightly different expressions for the bound and scattering states in momentum space:

$$\tilde{\psi}_B(k) = \frac{\sqrt{8\pi a_f^3}}{1 + k^2 a_f^2} \quad (\text{A.26a})$$

$$\tilde{\psi}_{k'}^{(S)}(k) = B_{k'} \left[\frac{2\pi^2}{k} (1 - ika_f) \delta(k - k') + \frac{4\pi k' a_f}{k'^2 - k^2 - i\epsilon} \right] \quad (\text{A.26b})$$

where the normalization constant is given by

$$B_{k'} = \frac{1}{\sqrt{4\pi^2 k' (1 + k^2 a_f^2)}}. \quad (\text{A.27})$$

Otherwise, the solution proceeds as outlined in Section A.1. The results of Chapter 5 can be found by following the steps of the derivation up to Eq. (A.17) and performing the necessary integrals with the initial conditions given in Eq. (5.11). To derive the large- k asymptotics shown in Eq. (6.13), one finds from the contour integration that

$$\tilde{\psi}_{\text{sr}}^{(S)}(k, t) = \frac{4\pi (r\psi^{(S)}(r, t))|_{r \rightarrow 0^+}}{k^2} + \mathcal{O}\left(\frac{1}{k^4}\right) \quad (\text{A.28a})$$

$$\tilde{\psi}^{(B)}(k, t) = \frac{4\pi (r\psi^{(B)}(r, t))|_{r \rightarrow 0^+}}{k^2} + \mathcal{O}\left(\frac{1}{k^4}\right) \quad (\text{A.28b})$$

in analogy with Eqs. (A.19)-(A.20).

A.3 Generalizing to 2D

The generalization to two dimensions is more subtle. First, the scattering and bound wave functions are defined in terms of Bessel functions, so there is no immediate functional connection

between the 2D and 1D eigenstates. As an added complication, there are a couple different conventions in the literature for defining the 2D scattering length for zero-range interactions. We choose to follow the convention of Ref. [114], in which the bound state has energy $E_B = -\frac{\hbar^2}{2\mu a_f^2}$. Within this framework, the bound state can be written as

$$\psi_B(\rho) = \frac{1}{\sqrt{\pi a_f^2}} K_0\left(\frac{\rho}{a_f}\right), \quad (\text{A.29})$$

and the scattering states can be written as

$$\psi_{k'}^{(S)}(\rho) = D_{k'} \left[J_0(k'\rho) - \frac{\pi/2}{\ln(k'a_f)} N_0(k'\rho) \right], \quad (\text{A.30})$$

where

$$D_{k'} = \left[4\pi \left(1 + \left[\frac{\pi/2}{\ln(k'a_f)} \right]^2 \right) \right]^{-1/2} \quad (\text{A.31})$$

enforces energy normalization.² We write them as

$$\tilde{\psi}_B(k) = \frac{\sqrt{4\pi a_f^2}}{1 + k^2 a_f^2} \quad (\text{A.32a})$$

$$\tilde{\psi}_{k'}^{(S)}(k) = D_{k'} \frac{2\pi}{\ln(k'a_f)} \left[\frac{\delta(k - k')}{k} \left(\ln(k'a_f) + i\frac{\pi}{2} \right) - \frac{1}{k'^2 - k^2 - i\epsilon} \right] \quad (\text{A.32b})$$

in momentum space. These transforms can be verified with the aid of Mathematica. The solution of the quench problem then proceeds as in Section A.1. To derive the large- k asymptotics shown in Eq. (6.12), the contour integration in Fig. A.1 reveals that

$$\tilde{\psi}_{\text{sr}}^{(S)}(k, t) = -\frac{2\pi \left(\frac{\psi^{(S)}(\rho, t)}{\ln(\rho/b)} \right) \Big|_{\rho \rightarrow 0^+}}{k^2} + \mathcal{O}\left(\frac{1}{k^4}\right) \quad (\text{A.33a})$$

$$\tilde{\psi}^{(B)}(k, t) = -\frac{2\pi \left(\frac{\psi^{(B)}(\rho, t)}{\ln(\rho/b)} \right) \Big|_{\rho \rightarrow 0^+}}{k^2} + \mathcal{O}\left(\frac{1}{k^4}\right) \quad (\text{A.33b})$$

where $b > 0$ is an arbitrary length scale that makes the argument of the logarithm dimensionless. These relations are analogous to Eqs. (A.19)-(A.20).

² For small ρ , these states behave as $\psi(\rho) \propto \ln\left[\frac{\rho e^\gamma}{2a_f}\right] + \mathcal{O}(\rho)$. The logarithms that appear in 2D constrain the scattering length to be strictly nonnegative. See, for example, Ref. [133].